AN INFRARED OPTICAL PHASE MODULATOR IN GaAs AND THE QCSE IN $Al_xGa_{1-x}As$-GaAs QUANTUM WELLS

AN INFRARED OPTICAL PHASE MODULATOR IN GaAs AND THE QCSE IN $Al_xGa_{1-x}As$-GaAs QUANTUM WELLS

by

MICHAEL GEORGE DALY, B.Sc. (ENG.)

A Thesis
Submitted to the School of Graduate Studies
in Partial Fulfilment of the Requirements
for the Degree
Master of Engineering

McMaster University
October 1990

MASTER OF ENGINEERING (1990) McMASTER UNIVERSITY

(Engineering Physics) Hamilton, Ontario

TITLE: AN INFRARED OPTICAL PHASE MODULATOR IN GaAs AND THE QCSE IN $Al_xGa_{1-x}As$-GaAs QUANTUM WELLS

AUTHOR: Michael George Daly, B.Sc. (Eng.) (Queen's University)

SUPERVISORS: P.E. Jessop and P.M. Smith

NUMBER OF PAGES: xvi, 169.

ABSTRACT

This thesis describes the design, fabrication and characterisation of an infrared optical waveguide phase modulator. The modulator was fabricated in GaAs utilizing a carrier-concentration-reduction rib waveguide structure with a Schottky diode contact to allow the application of an electric field across the waveguide region. Measurements of the phase modulation are presented with results agreeing with the theoretical predictions of an electrooptic coefficient of 1.2×10^{-12} m/V at 1.15 μm. Fabrication techniques and problems are thoroughly discussed.

The second part of this thesis consists of measurements of the quantum confined stark shift in an AlGaAs-GaAs multiple quantum well p-i-n diode structure. The results show useful changes in absorption with applied electric field. Transmission measurements as a function of applied field are presented for TE polarized light in a waveguiding geometry as well as photocurrent measurements in the same geometry and with light incident perpendicular to the MQW layers.

Reasonable agreements for the relative field induced shifts of the excitonic feature are found but the absolute position of the feature is blue shifted by 7 meV with respect to the theoretically predicted position.

ACKNOWLEDGEMENTS

I would like to thank my supervisors, Dr. Paul Jessop and Dr. Peter Smith, for their guidance during this work. I also would like to thank all of my friends who have contributed to this work with their many conversations and who have helped to make the time spent at McMaster enjoyable. Appreciation also goes to the Government of Ontario who have supported me through the Ontario Graduate Scholarship Program.

My parents deserve thanks for their help and encouragement which instilled in me the wish to pursue my education. Lastly, and most importantly, I would like to thank my wife, Ruth, who has put up with the eccentricities of a student.

TABLE OF CONTENTS

CHAPTER ONE

INTRODUCTION

CHAPTER TWO

PHASE MODULATION AND THE ELECTROOPTIC EFFECT

CHAPTER THREE

DESIGN AND FABRICATION OF THE PHASE MODULATOR

CHAPTER FOUR

EXPERIMENTAL OBSERVATION OF THE ELECTROOPTIC EFFECT

CHAPTER FIVE

SUMMARY OF PHASE MODULATOR RESULTS

CHAPTER SIX

INTRODUCTION TO QUANTUM WELLS AND DEVICES

CHAPTER SEVEN

EXCITON THEORY

CHAPTER EIGHT

CALCULATION OF THE EXCITON RESONANCE SHIFT

CHAPTER NINE

MEASUREMENT OF THE FIELD INDUCED EXCITON SHIFT

CHAPTER TEN

SUMMARY OF QCSE RESULTS

APPENDIX A

COMPARISON OF CALCULATIONS FROM PROGRAM EXCITON AND THOSE OF LENGYEL et al.[34]

APPENDIX B

APPENDIX C

SAMPLE OUTPUT FROM PROGRAM EXCITON

LIST OF FIGURES

LIST OF TABLES

CHAPTER ONE

INTRODUCTION

1.1 Historical Background

Interest in semiconductor materials for optoelectronic integrated circuits (OEIC) is growing yearly. Optical communication over long distances in fibre-optic cable has become the norm due to advantages such as high bandwidth, low attenuation and good noise characteristics due to the absence of electrical problems such as cross-talk. These advantages as well as the wish for complete integrated optical systems without the need for multiple conversions from optical signals to electrical signals and back again are the impetus for research in this field[1].

Integrated optics has been studied in many materials and may be loosely defined as the production, manipulation, and detection of light. These processes may take place using either monolithic or hybrid integration. Interest has been primarily in the wavelength range between 0.1 μm and 10.0 μm and has been further limited to discrete wavelengths within this range as determined by the available laser sources.

In recent years the primary activity in integrated optics has been in the III-V compound semiconductors. The reasons for this are their good electrical as well as optical characteristics which make them prime candidates for optoelectronic integration.

Before large scale OEIC's may be produced, the individual components which will make up these circuits must be clearly understood. These include lasers, light-emitting diodes, modulators, waveguide interconnects, and detectors. This thesis describes two such devices.

The first part of this thesis describes the design, fabrication and measurement of a GaAs phase modulator which operates at a wavelength of 1.15μm. After this project was completed a multiple quantum well material became available. The second part of this thesis deals with the examination and modelling of this material as pertains to band edge electroabsorption modulators.

1.2 Phase Modulators

Phase modulators are one particular type of component that has uses as intensity modulators in interferometric configurations where band edge electroabsorption modulators may not be practical. Other applications where adjustment of the phase of one beam relative to another is necessary also exist. Fibre-optic gyros[2], interferometric sensors and coherent communication systems are such applications.

A phase modulator is simply a device which allows a variation in the optical path length of a propagating light beam. This can be done by physically changing the path length in free space by the use of mirrors and translators or by actually changing the propagation medium's characteristics. It is the second of these methods which is of interest for optical integrated circuits.

Phase modulation can be accomplished by a number of effects such as the electrooptic effect[3], carrier concentration effects[4] and infrared transitions in MQW materials[5]. The simplest of these methods is the electrooptic effect. This type of modulator has been extensively investigated but is very important due to the presence of large electrooptic coefficients in III-V semiconductors which, if not the useful effect behind a device, can be important for its detrimental effects.

1.3 Purpose of Phase Modulator Project

The purpose of this project was to design and fabricate a simple, single-mode, waveguide electrooptic modulator in GaAs. The primary reasons for attempting a project such as this were to increase the knowledge of semiconductor waveguide fabrication in III-V materials at McMaster as well as to investigate the electrooptic effect in this material. The project, although simple conceptually, has many of the attributes necessary for more complex fabrications. These include the fabrication of single-mode waveguides by wet chemical etching and the control of the guiding light by electrical means.

CHAPTER TWO

PHASE MODULATION AND THE ELECTROOPTIC EFFECT

2.1 Chapter Introduction

This chapter will deal with the basic theory of the electrooptic effect in Gallium Arsenide. Phase modulation will be defined in the context of the electrooptic effect. The concept of the index ellipsoid will be then be introduced and used to derive the expression for phase modulation using a transverse electric field in GaAs.

2.2 Optical Phase Modulation

An optical phase modulator can simply be thought of as a material with an electrically changeable index of refraction. This can be accomplished in many materials by the application of an electric field. The electric field causes the change in the index of refraction by the electrooptic effect. The change in the index results in a change in the effective optical path length of a beam which traverses the material. This results in the lightwave having a different phase when exiting the material than it would have had in the absence of an electric field.

The linear electrooptic effect (Pockels effect) is present in crystals which do not have an inversion centre. Gallium arsenide is in the $\bar{4}3m$ or T_d crystal symmetry class and does not have such a centre. A non-linear effect (Kerr effect) can also be present but in Gallium Arsenide, the specific material to be discussed here, the Kerr effect is small and is negligible to first order.

2.2 The Linear Electrooptic Effect

The linear electrooptic effect can be described by an index ellipsoid (sometimes called an optical indicatrix). If the crystal axes are chosen as the principle axes the index ellipsoid is

$$\frac{x^2}{n_x^2} + \frac{y^2}{n_y^2} + \frac{z^2}{n_z^2} = 1 \qquad \textbf{(2.1)}$$

where n_x is the index for a wave polarized in the x direction. The index for a wave travelling in the any arbitrary direction is found by taking a section of the ellipsoid perpendicular to the propagation direction and through the origin. This will, in general, yield an ellipse which has a major and a minor axis. These two axes represent the indices for two orthogonal plane waves.

If an electric field is now applied the index ellipsoid is changed to the form

$$\left(\frac{1}{n^2}\right)_1 x^2+\left(\frac{1}{n^2}\right)_2 y^2+\left(\frac{1}{n^2}\right)_3 z^2+2\left(\frac{1}{n^2}\right)_4 yz+2\left(\frac{1}{n^2}\right)_5 xz+2\left(\frac{1}{n^2}\right)_6 xy=1 \tag{2.2}$$

where

$$\left.\left(\frac{1}{n^2}\right)_1\right|_{E=0}=\frac{1}{n_x^2}\ ,\quad \left.\left(\frac{1}{n^2}\right)_2\right|_{E=0}=\frac{1}{n_y^2}\ ,\quad \left.\left(\frac{1}{n^2}\right)_3\right|_{E=0}=\frac{1}{n_z^2} \tag{2.3}$$

and

$$\left.\left(\frac{1}{n^2}\right)_4\right|_{E=0}=\left.\left(\frac{1}{n^2}\right)_5\right|_{E=0}=\left.\left(\frac{1}{n^2}\right)_6\right|_{E=0}=0\ . \tag{2.4}$$

The differences in the coefficients can be written in tensor form as

$$\Delta\left(\frac{1}{n^2}\right)_i=\sum_{j=1}^{3} r_{ij}E_j \tag{2.5}$$

with the r_{ij} matrix being the electrooptic tensor. This expression can be expanded in matrix form as

$$\begin{bmatrix} \Delta\left(\frac{1}{n^2}\right)_1 \\ \Delta\left(\frac{1}{n^2}\right)_2 \\ \Delta\left(\frac{1}{n^2}\right)_3 \\ \Delta\left(\frac{1}{n^2}\right)_4 \\ \Delta\left(\frac{1}{n^2}\right)_5 \\ \Delta\left(\frac{1}{n^2}\right)_6 \end{bmatrix} = \begin{bmatrix} r_{11} & r_{12} & r_{13} \\ r_{21} & r_{22} & r_{23} \\ r_{31} & r_{32} & r_{33} \\ r_{41} & r_{42} & r_{43} \\ r_{51} & r_{52} & r_{53} \\ r_{61} & r_{62} & r_{63} \end{bmatrix} \begin{bmatrix} E_1 \\ E_2 \\ E_3 \end{bmatrix} . \tag{2.6}$$

Due to the symmetry of the GaAs crystal, as discussed earlier, the electro-optic matrix for GaAs is

$$\boldsymbol{r} = \begin{bmatrix} 0 & 0 & 0 \\ 0 & 0 & 0 \\ 0 & 0 & 0 \\ r_{41} & 0 & 0 \\ 0 & r_{41} & 0 \\ 0 & 0 & r_{41} \end{bmatrix} . \tag{2.7}$$

Therefore one need only refer to one electro-optic coefficient for GaAs.

Phase modulation using the electro-optic effect can be achieved in GaAs by having the waveguide region in the intrinsic region of a pin diode or in the depletion region of a schottky diode. If we apply a field in the y direction

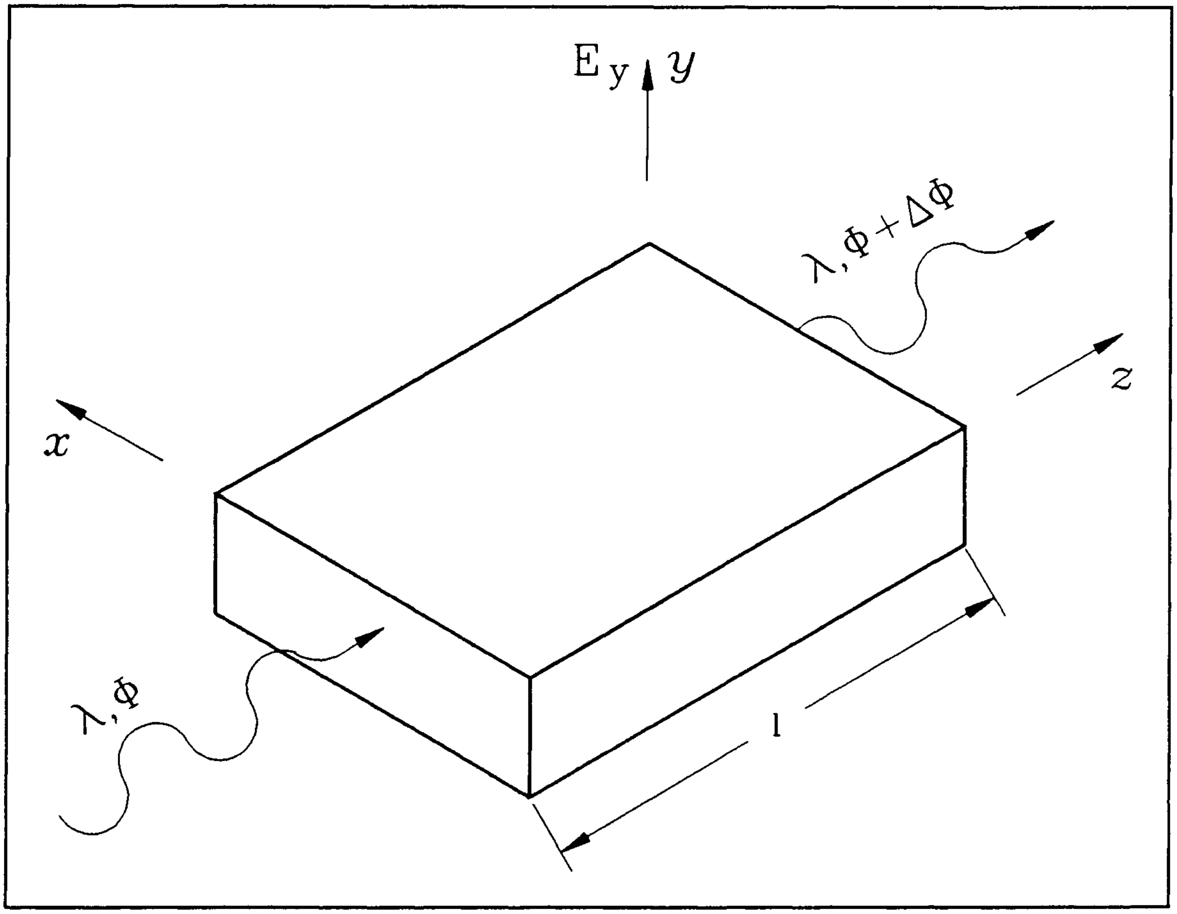

Figure 2.1 The geometry used to describe the electrooptic effect in the text.

while the lightwave travels in the z direction and is polarized in the x direction (Figure 2.1) we have

$$E = E_y \hat{j} \ . \tag{2.8}$$

GaAs is optically isotropic in the absence of an applied field therefore

$$\left(\frac{1}{n^2}\right)_1 = \left(\frac{1}{n^2}\right)_2 = \left(\frac{1}{n^2}\right)_3 = \frac{1}{n_0^2} \qquad (2.9)$$

so the optical indicatrix becomes

$$\frac{x^2+y^2+z^2}{n_0^2} + 2r_{41}E_y xz = 1 \quad . \qquad (2.10)$$

The application of an electric field changes the principle axes of the index ellipsoid. A change of variables to

$$\begin{aligned} x' &= \frac{1}{\sqrt{2}}x + \frac{1}{\sqrt{2}}z \\ z' &= \frac{1}{\sqrt{2}}z - \frac{1}{\sqrt{2}}x \\ y' &= y \end{aligned} \qquad (2.11)$$

changes the index ellipsoid to

$$x'^2\left(\frac{1}{n_0^2} + r_{41}E_y\right) + z'^2\left(\frac{1}{n_0^2} - r_{41}E_y\right) + y'^2\left(\frac{1}{n_0^2}\right) = 1 \ . \qquad (2.12)$$

Assuming the index change is small and given

$$dn = -\left(\frac{n^3}{2}\right)d\left(\frac{1}{n^2}\right) \qquad (2.13)$$

gives

$$\begin{aligned} n_{x'} &= n_0 - \frac{n_0^3}{2} r_{41} E \\ n_{z'} &= n_0 + \frac{n_0^3}{2} r_{41} E \\ n_{y'} &= n_0 \; . \end{aligned} \tag{2.14}$$

The relevant change in the refractive index is that for the x polarization. The phase shift is given by

$$\Delta \phi = \frac{\omega l}{c} \left(\frac{n_0^3}{2} r_{41} E_y \right) \tag{2.15}$$

or if the voltage is dropped across a width d

$$\Delta \phi = \frac{\pi l}{\lambda d} n_0^3 r_{41} V \tag{2.16}$$

where l is the field interaction length, ω is the optical frequency and c is the speed of light. A figure of merit for phase modulators is the voltage required to produce a π phase shift. For this type of modulator this voltage is given by

$$V_\pi = \frac{\lambda d}{l n_0^3 r_{41}} \; . \tag{2.17}$$

Typically V_π is of the order of 10 or 20 V/cm. This voltage is high for large scale integration due to the small interaction lengths which are sought but is low enough for discrete and small scale integration projects to make use of this effect. The speed of this effect has been demonstrated into the GHz range which also makes it attractive for communications purposes.

CHAPTER THREE

DESIGN AND FABRICATION OF THE PHASE MODULATOR

3.1 Chapter Introduction

This chapter will outline the materials parameters of the Gallium Arsenide epilayer material which was chosen for this project. Using these parameters, constraints will be placed on the waveguide fabrication. Finally, the fabrication steps will be discussed.

3.2 Wafer Structure and Materials Parameters

The phase modulator was fabricated in GaAs from a wafer which consisted of a n-type substrate with a dopant concentration of 1.93 x 10^{18} per cm^3. On the substrate was a GaAs epilayer which was 4.791 μm thick and had a dopant concentration of 2.76 x 10^{15} cm^{-3}. The wafer was a product of Sumitomo Electric Inc.

The index of refraction of GaAs at 1.15μm and with no doping was calculated using the Sellmeier equation[6]

$$n^2 = 10.906 + \frac{0.97501}{\lambda_0^2 - 0.27969} - 0.002467\,\lambda_0^2 \tag{3.1}$$

where λ_0 is the free space wavelength in microns. At a wavelength of 1.15 μm the Sellmeier equation yields $n_0 = 3.405$. The higher doping in the substrate provides the difference in the refractive indices necessary for an optical waveguide. Free carriers cause a reduction in the refractive index and can form what is called a carrier-concentration-reduction waveguide. The change due to free carriers is due to a plasma effect. The index change can be calculated in the same manner as for a free carrier plasma but the band effective mass must be used. The expression is[7]

$$\Delta n = -\frac{N\lambda_0^2 e^2}{\varepsilon_0 n\, 8\,\pi^2 m^* c^2} \tag{3.2}$$

where m^* is the band effective mass, N is the carrier concentration, λ_0 is the free space wavelength of light, e is the electronic charge, ε_0 is the permittivity of free space, and c is the speed of light.

The correct parameters for this material are given below:

$m^* = 0.082$

$\varepsilon_0 = 8.854 \times 10^{-12}$ F/m

$m_0 = 9.109 \times 10^{-31}$ kg

$c = 2.998 \times 10^{8}$ m/s

e = 1.602×10^{-19} C

n = 3.405

N = 1.93×10^{18} /cm^3

The resulting index change due to free carrier effects for the material is $\Delta n = -0.004$.

The value of the index of refraction for aluminum at 1.15μm is 1.203 + i11.452[8].

3.3 Waveguide Calculations

The largest constraint placed upon the design of the phase modulator is the need for the modulator to be single mode. This is required since in multiple mode waveguides each mode has a different propagation constant which would result in the phase of each mode being different upon exiting the material. This would make interferometric measurement techniques very difficult and is, in any case, not practical from a device point of view.

The epilayer thickness is such that the slab guide it forms is single mode. To have a true, single mode, confining rib guide, the rib must be fabricated such that the guide is single mode in the lateral direction also. If this is not done multiple modes would exist which would each have a slightly different propagation constant and a slightly different optical path length. A further reason for attempting single mode guides is to test the limits of the fabrication facilities at McMaster.

Due to the above constraint it was necessary to calculate the allowable rib widths and depths to insure single mode operation. The calculations were accomplished by using the effective index method[9,10], which will be described below.

The effective index method consists of examining the slab waveguide solutions in one dimension and using these results to refine the problem in the second dimension. It is more complicated than other, more simplistic, methods such as that of Marcatili[11] but has proven to give better results.

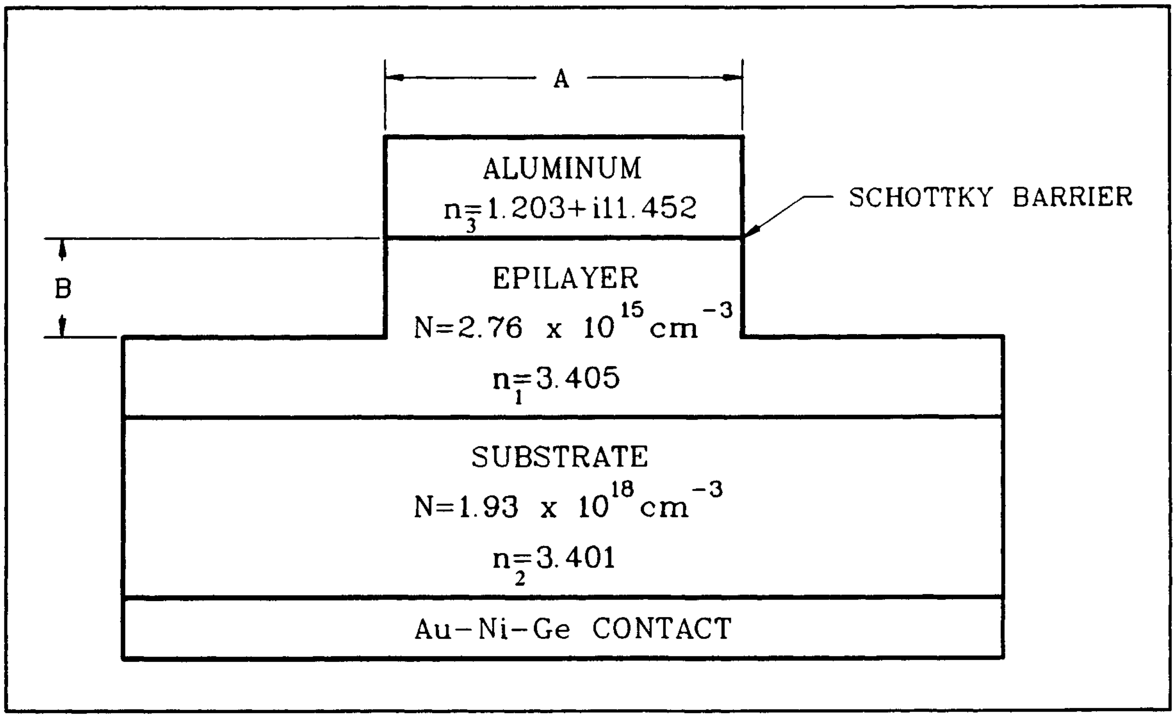

Figure 3.1 The rib waveguide structure of the electrooptic modulator.

The rib waveguide modulator structure is shown in Figure 3.1. The relationship between the parameters A and B must be determined. A is the rib width while B is the etch depth. In general, a wider rib width will necessitate a smaller etch depth for single mode operation. The first step in solving this problem by the effective index method is to solve two asymmetric metal clad waveguides. The two different thicknesses of the epilayer region (4.791 μm and 4.791 - B μm) constitute the two slab waveguide problems to be solved.

The eigenvalue equation for such a waveguide is given by Adams[12] as

$$4aq = 2\tan^{-1}\left(\eta_{12}\frac{p}{q}\right) + 2\tan^{-1}\left(\eta_{13}\frac{r}{q}\right) + 2N\pi \qquad (N = 0,1,2,\ldots) \tag{3.3}$$

where

$$\begin{aligned} p^2 &= \beta^2 - n_2^2k^2 \\ q^2 &= n_1^2k^2 - \beta^2 \\ r^2 &= \beta^2 - \varepsilon_3 k^2 \end{aligned} \tag{3.4}$$

and

$$\eta_{12} = \begin{cases} 1, & \textit{for TE modes} \\ \left(\dfrac{n_1}{n_2}\right)^2, & \textit{for TM modes} \end{cases}$$
$$\eta_{13} = \begin{cases} 1, & \textit{for TE modes} \\ \dfrac{n_1^2}{\varepsilon_3}, & \textit{for TM modes.} \end{cases} \tag{3.5}$$

If the metal cladding satisfies

$$\begin{gathered} n_1 - n_2 < n_1 \\ k\left|\eta_{13}\sqrt{n_1^2 - \varepsilon_3}\right| > Re(q) \end{gathered} \tag{3.6}$$

then an approximation due to Garmire and Stoll[13] may be used although a complete solution is possible and has been done by Kaminow et al[14]. Using the Garmire and Stoll approximation the eigenvalue equation may be reduced to

$$\frac{p}{q} \approx \tan\left[2aq - \left(N + \frac{1}{2}\right)\pi\right] \qquad (N = 0,1,2,...) \tag{3.7}$$

which can be again rewritten as

$$v = \frac{u_r(-1)^N}{\sin 2u_r} \qquad (N = 0,1,2,...) \tag{3.8}$$

where u is the transverse propagation constant given by

$$u \equiv u_r + iu_i = aq \ , \tag{3.9}$$

v is the normalized frequency given by

$$v = ak\sqrt{n_1^2 - n_2^2} \tag{3.10}$$

and assuming that $u_r \gg u_i$ which is true if the field does not penetrate deeply into the metal.

The solution for the propagation constants for both the thin and the thick regions allow the definition of effective indices which define a new problem in the perpendicular direction. The effective index, in each region, is given by

$$n_{eff}^2 = n_1^2 - \left(\frac{k_x}{k}\right)^2 \tag{3.11}$$

and Figure 3.2 shows its dependence on etch depth for this structure. The correct effective index for each region (slab waveguide) can now be read off the graph for any etch depth up to 2 μm. The problem is now reduced to a symmetric waveguide problem solutions to which can be found in any elementary optical waveguide book[15]. Figure 3 shows the maximum waveguide width for a particular etch depth to have single lateral mode operation in this material.

An interesting problem occurs with metal clad optical waveguides. Due

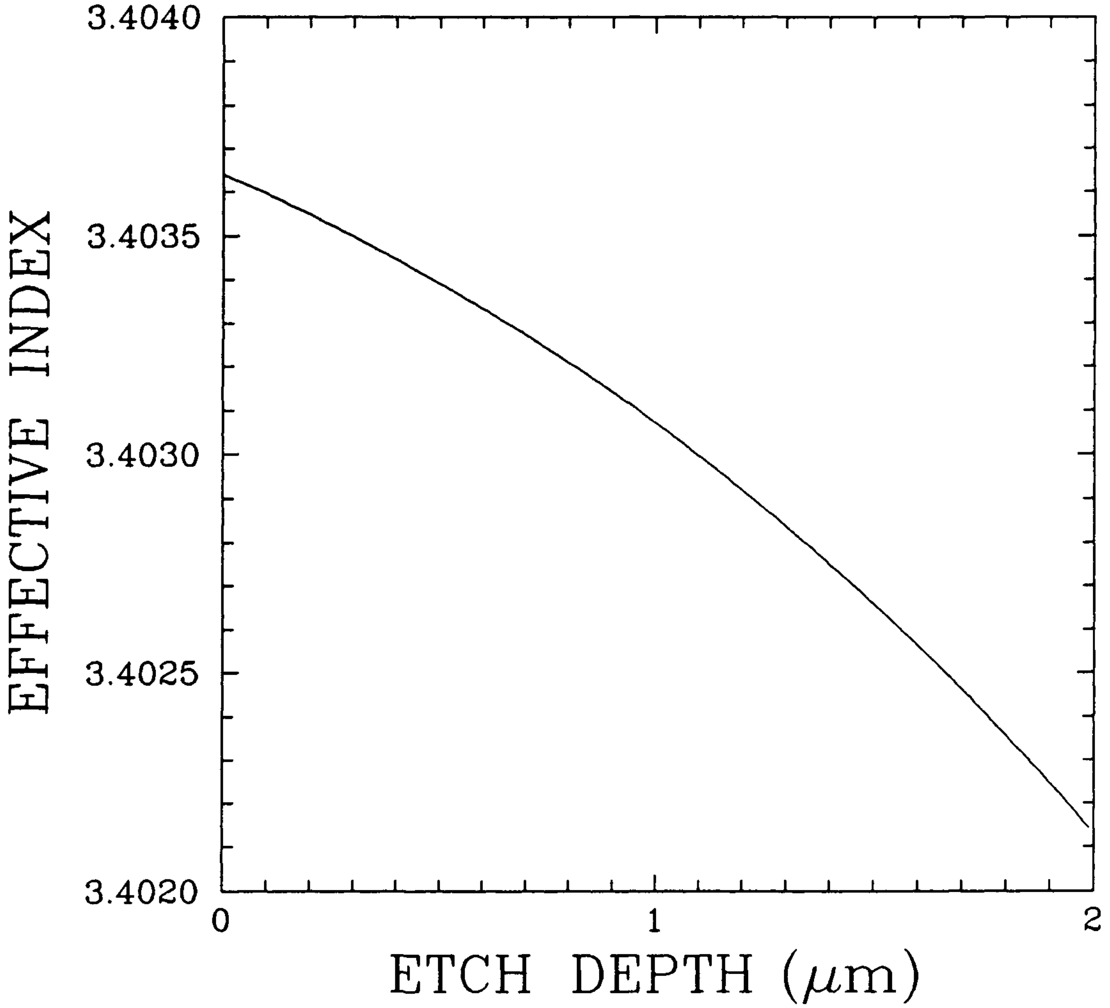

Figure 3.2 The effective index as a function of etch depth. The etch depth is given by B in Figure 3.1.

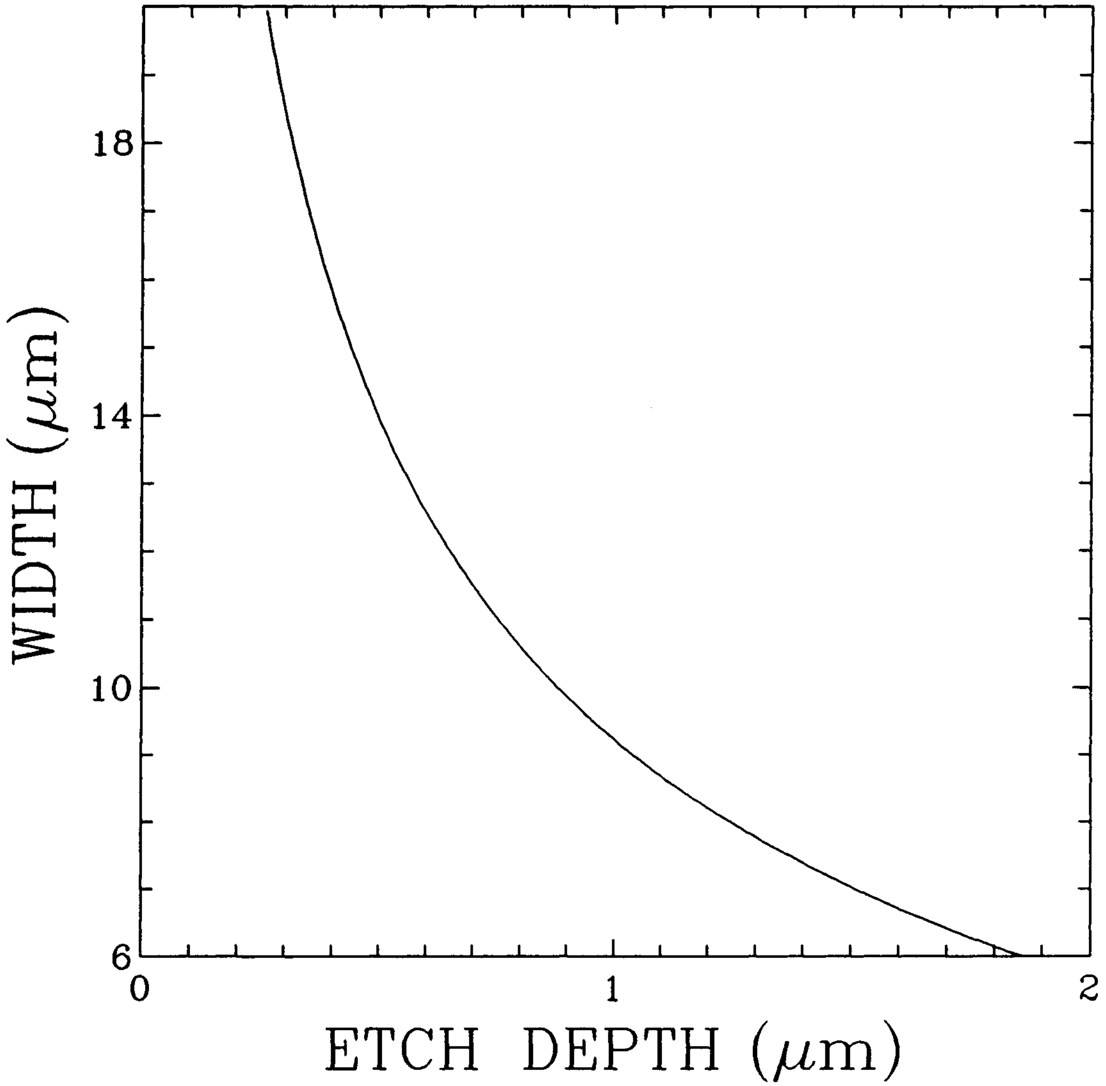

Figure 3.3 The maximum width for single mode operation as a function of etch depth.

to the metal's complex permittivity an evanescent wave in the metal will be absorbed. The magnitude of this absorption can be quite important for a device such as this especially considering that the electrooptic effect is weak and devices must be long. The approximations made by Garmire and Stoll made it possible for them to produce an expression for the attenuation coefficient of a waveguide such as this. Their expression is derived from a ray model approach and considers the power reflection coefficients at the two interfaces.

The expression for the attenuation coefficient (α) is[13]

$$\alpha = \frac{-2u_r^3}{a^3k^2(2u_r - \tan 2u_r)} \, Im\left(\frac{1}{\eta_{13}\sqrt{n_1^2-\varepsilon_3}}\right) . \tag{3.12}$$

The aluminum clad waveguide here gives an attenuation of approximately 0.3 dB/cm for the TE polarization. This number has also been verified by the more correct method of Kaminow et al[14].

The possibility of a TM polarization has been neglected for two main reasons. The primary reason being the high attenuation of TM modes in metal clad waveguides[14]. This fact was qualitatively examined experimentally and verified. The second reason is that TE polarization is much more common in

OEIC's due to the semiconductor diode laser's production of TE polarized light. It should be noted that if the TM mode was able to be transmitted a much simpler method of determining the phase modulation using crossed polarizers is possible[16].

3.4 Fabrication Procedure A: General Methods

The GaAs etch initially chosen for this project was the Bromine-Methanol system[17]. It was chosen because its diffusion limited etching character produced a smoothing effect which is desirable for waveguides because it tends to reduce scattering losses. This etching system has two disadvantages. The first being the extreme pungency of bromine which requires good ventilation. The second disadvantage is the caustic nature of bromine. This is a major disadvantage since the use of photo-resist or metals for masks is in general not possible due to the caustic nature of this etch. Dielectric masks must generally be used. Since a reliable CVD-SiO_2 deposition system was not available a spin-on glass from Emulsitone was used.

Aluminum was chosen as the Schottky barrier metal for three reasons. The first of these is the ease at which Aluminum forms a Schottky barrier on n-type GaAs. The second reason is that it is quite stable as a Schottky metal even to high temperatures. Lastly aluminum exhibits good adhesion to GaAs.

The disadvantages of aluminum include a high reactivity and a conductivity less than that of gold.

The waveguide masking patterns were formed by photographing a line drawing produced by computer. The mask plate was of the photographic emulsion type and the 20x reduction from the line drawing to the mask plate was accomplished in one step. A section of the mask used in Fabrication Procedure A is shown in Figure 3.4. The waveguide patterns were nominally 9 μm wide.

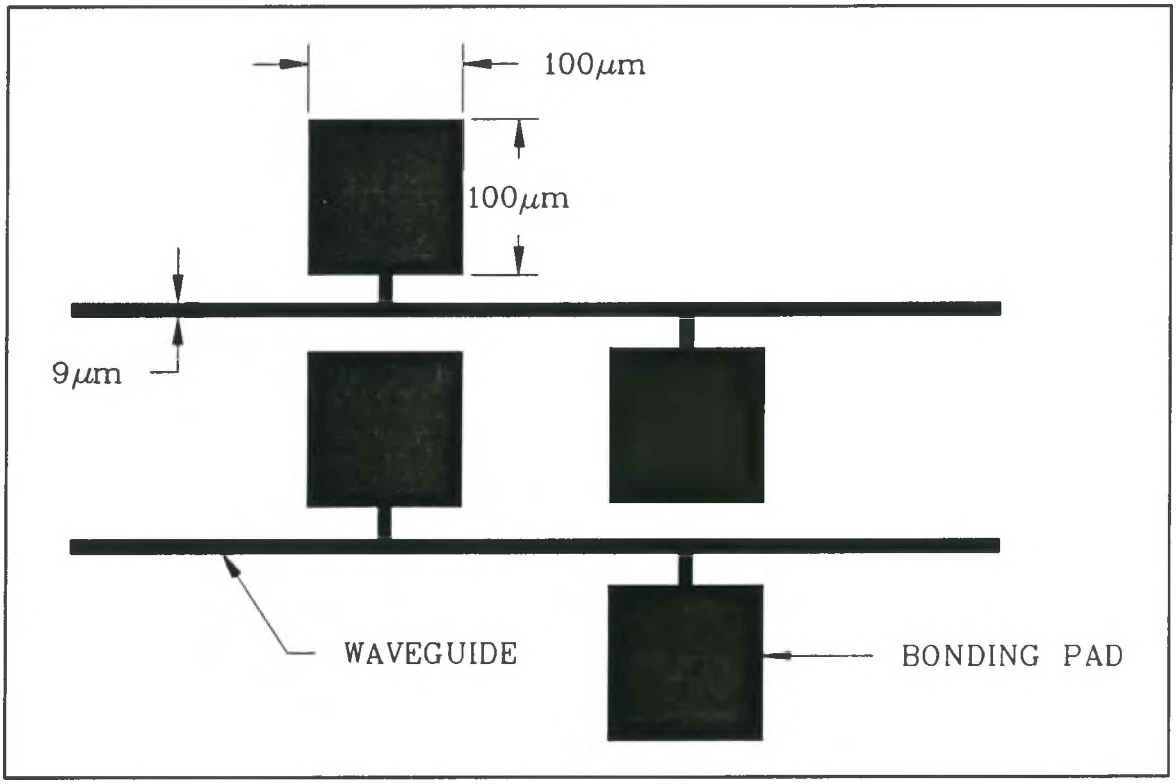

Figure 3.4 Waveguide mask A.

3.5 Fabrication Procedure A: Steps

The following list details the steps used in fabrication procedure A.

1. Thin wafer to less than 200μm (facilitates cleaving).
2. Clean wafer in: a) Trichloroethylene
   b) Acetone
   c) Methanol
   d) De-ionized water.
3. Dry with nitrogen.
4. Place in the UV-ozone cleaner for 30s.
5. Clean wafer in: a) Buffered HF for 30s
   b) De-ionized water.
6. Dry with flowing nitrogen.
7. Spin-on Emulsitone 209 glass at 3000 rpm for 20s.
8. Bake in air at 150°C for 1 hour.
9. Slowly ramp temperature to 400°C (slow ramping is necessary to prevent cracking due to different thermal expansion coefficients of glass and GaAs).
10. Bake at 400°C for 1 hour to densify glass.
11. Slowly ramp temperature down to room level.
12. Spin on Photo-resist (Shipley Microposit® Photo Resist 1400-27) at 4000 rpm for 30s.

13. Softbake in air at 110°C for 30min.
14. Expose for 6s using mask A.
15. Develop in (Shipley Microposit® Developer 351) 6 H_2O : 1 developer.
16. Dry.
17. Hardbake in air at 175°C for 2 hours.
18. Etch in buffered HF until SiO_2 is removed from open areas.
19. Remove photo-resist (Shipley Microposit® Remover 1165).
20. Dehydrate bake at 150°C for 30 min.
21. Etch in 1% bromine : 99% methanol for 1 min. (approximately 0.67μ/min.).
22. Etch away SiO_2 film in buffered HF.
23. Deposit 800 - 1000Å of aluminum for a schottky barrier.
24. Spin-on photo-resist at 4000 rpm for 30s.
25. Soft bake in air at 110°C for 30min.
26. Expose for 6s using mask A.
27. Develop in 6 H_2O : 1 developer.
28. Hard bake in air at 175°C for 2 hours.
29. Etch Aluminum in 1 HCl : 4 H_2O at 80°C.
30. Remove Photo-resist.

31. Deposit ohmic contact on the backside: 250Å Nickel
500Å Germanium
1000Å Gold.

32. Rapid thermal anneal in a carbon boat at 450°C for 30s to anneal the ohmic contact.

33. Cleave devices to the required length.

3.6 Fabrication Procedure A: Evaluation

The above fabrication procedure had some problems. The first of these was the unpredictability of the bromine-methanol etch. It was very difficult to maintain a consistency in the etch rate. It is believed that this is due to the sensitivity of the etch to agitation. This etch has a predictable etch rate in the absence of agitation when it is basically a diffusion limited etch but agitation makes the etch reaction-rate limited by removing the protective layer of reacted species. One possible way to help this situation is to dilute the etch and etch over a much longer time scale. The problem with this procedure is the increased likelihood of the spin-on glass layer lifting off.

A second problem encountered was the difficulty in coupling light into the waveguides. This was believed to be due to two factors. The first being the poor confinement due to the very shallow etching (approximately 15% of

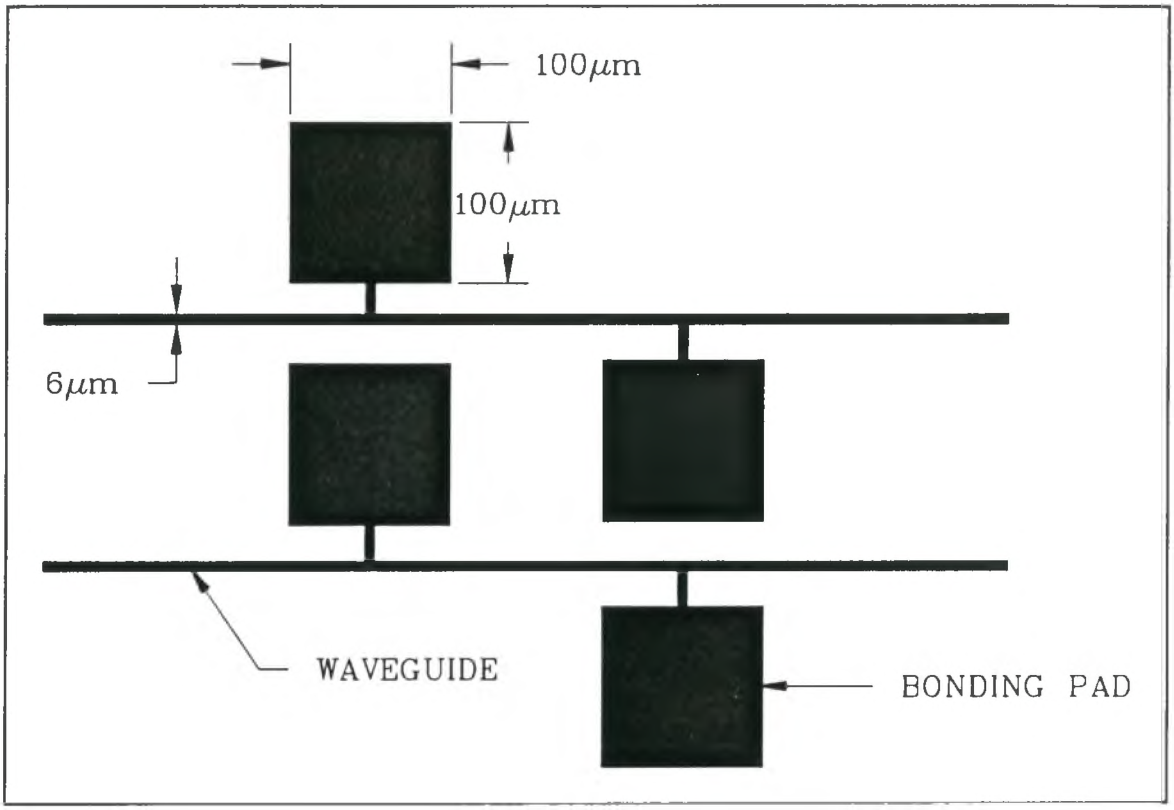

Figure 3.5 Waveguide mask B.

the epilayer thickness). The way that this can be changed is to make narrower waveguides which would allow deeper etching while maintaining single mode operation. A further problem was a strange light channelling effect along one side of the waveguide. This was traced to an absence of aluminum at the edge of the guide[18] which was due to alignment difficulties. The solution to this problem was a wider deposition of aluminum and it will be discussed below.

New masks were fabricated. Mask B (Figure 3.5) was identical to Mask A but had a width of approximately 6 μm. This is the approximate limit of the

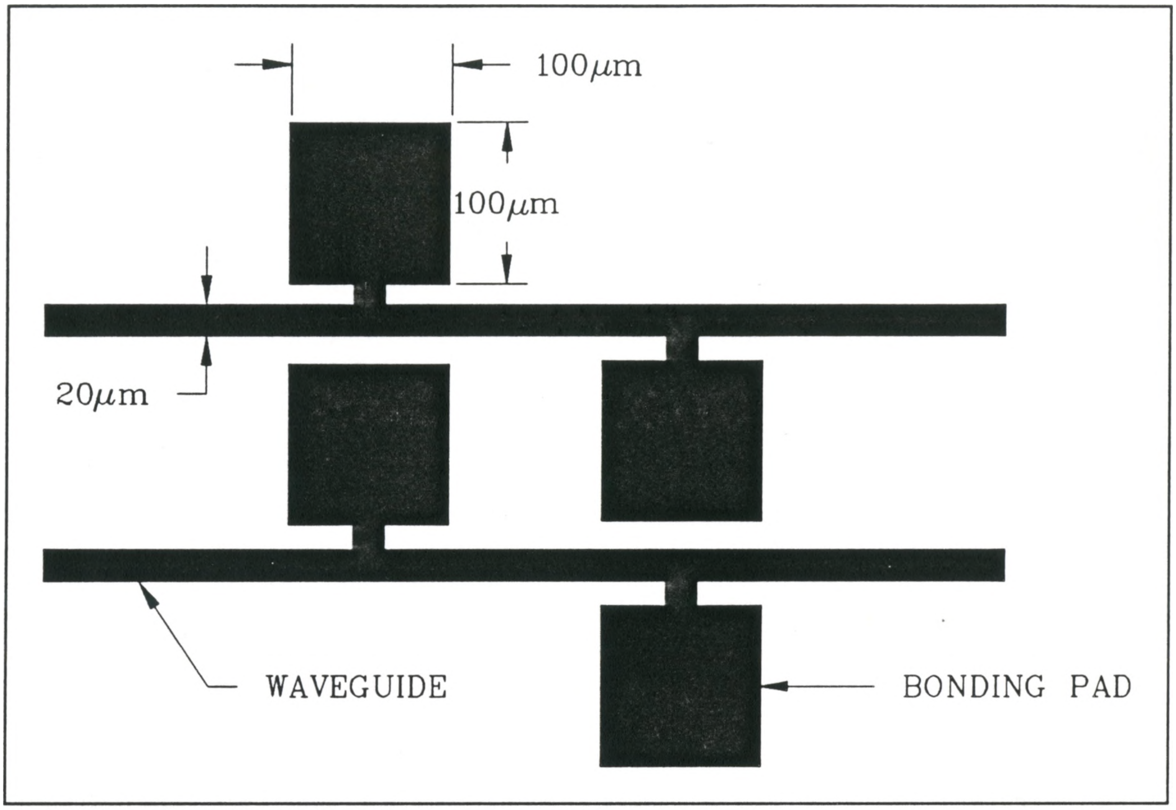

Figure 3.6 Waveguide mask C.

present mask making capabilities at McMaster. This limit is primarily due to the camera resolution. Even at 6 μm a noticeable decrease in the edge quality of the waveguide mask was observed. A wider metallization mask was also made (Figure 3.6) to counter the problem of poor alignment. This wide mask would be a problem in a real application due to a large increase in device capacitance but this modulator was not designed for speed but to demonstrate a concept. The wide mask also helped counter a problem with poor aluminum adhesion due to less than adequate metallization facilities.

Fabrication procedure A was repeated using the new 6 μm mask with little success. The spin-on glass would not stand up to the etch and in some instances the glass strips were broken during cooling in the oven. This problem was presumably due to large thermal stresses caused by the different thermal expansion coefficients of GaAs and glass. The procedure was modified to omit the high temperature (400 °C) glass bake with better but still unsatisfactory results.

3.7 Fabrication Procedure B: General Methods

With the masking problems of the previous procedure and no available substitutes it was decided that a new etch system must be used. The etch system chosen was the sulphuric acid/hydrogen peroxide/water system[19]. It has the advantage of being a popular etch with well documented etching characteristics. This system also has the advantage that hard-baked photoresist is a suitable mask material. The main disadvantage of this system is the highly anisotropic etching characteristics.

One note of caution about this system is the sensitivity in etchant performance to the concentration of hydrogen peroxide. This is important to note since hydrogen peroxide will normally degrade in concentration with time. A new supply is therefore recommended. One further caution is needed since the ratios of components in making up the etch refer to a 30% solution of hydrogen peroxide. This is in general not a problem since this is the usual solution which one obtains when ordering hydrogen peroxide even though this is not always clearly specified.

This new etching system along with the two new masks required a change in the fabrication steps which are updated below.

3.8 Fabrication Procedure B: Steps

The following list details the steps used in fabrication procedure B.

1. Thin wafer to less than 200μm (facilitates cleaving).
2. Clean wafer in: a) Trichloroethylene
   b) Acetone
   c) Methanol
   d) De-ionized water.
3. Dry with nitrogen.
4. Place in the UV-ozone cleaner for 30s.
5. Clean wafer in: a) Buffered HF for 30s
   b) De-ionized water.
6. Dry with nitrogen.

7. Spin on Photo-resist (Shipley Microposit® Photo Resist 1400-27) at 4000 rpm for 30s.
8. Softbake in air at 110°C for 30min.
9. Expose for 6s (Mask B).
10. Develop in (Shipley Microposit® Developer 351) 6 H_2O : 1 developer.
11. Dry.
12. Hardbake in air at 175°C for 2 hours.
13. Etch in 1 H_2SO_4 : 8 H_2O_2 (30%): 80 H_2O (etch rate 0.54μm/min) (etch approximately 1 μm).
14. Remove photo-resist (Shipley Microposit® Remover 1165).
15. Deposit 800 - 1000Å of Aluminum.
16. Spin-on photo-resist at 4000 rpm for 30s.
17. Soft bake in air at 110°C for 30min.
18. Expose for 6s (Mask C).
19. Develop in 6 H_2O : 1 developer.
20. Hard bake in air at 175°C for 2 hours.
21. Etch Aluminum in 1 HCl : 4 H_2O at 80 °C.
22. Remove Photo-resist.
23. Deposit on the backside: 250Å Nickel
    500Å Germanium
    1000Å Gold.

24. Rapid thermal anneal in a carbon boat at 450°C for 30s.

25. Cleave devices to the required length.

3.9 Fabrication Procedure B: Evaluation

The devices made using Procedure B exhibited much improved coupling characteristics. The waveguide edge definition as observed by optical microscopy was much worse than the wider waveguides of Procedure A. This was primarily due to the poor quality of the mask which was caused by working at the limits of the camera resolution in making the masks. A secondary effect was the roughness caused by the non smoothing nature of the sulphuric acid etch. This roughness exhibits itself in bubble-like intrusions into the waveguide wall.

The waveguides fabricated by Procedure B were deemed to be the best attainable with the present fabrication facilities. Suggestions for improvements to these facilities will be discussed later.

CHAPTER FOUR

EXPERIMENTAL OBSERVATION OF THE ELECTROOPTIC EFFECT

4.1 Chapter Introduction

This chapter will detail the experimental method used to measure the modulation. Following this the data will be presented and discussed.

4.2 Experimental Details

The measurement of phase modulation must be done with a coherent detection system. The simplest way to accomplish this optically is to split a laser beam and recombine the phase shifted beam with the reference beam. The resulting interference allows a quantification of the phase shift. The method chosen for this splitting was to place the sample in one arm of a Mach-Zehnder interferometer.

The interferometer consists of two beam splitters and two mirrors. This type of interferometer is more difficult to align than some other types such as a Michelson interferometer but has the advantage of two single pass arms. In one of these arms the modulator was inserted while the other was used as a reference beam.

Figure 4.1 shows the experimental setup. A 1.15 μm helium-neon laser was used as the source. Visible spontaneous emission was a problem in aligning the beam with the guide so it was removed with a filter before entering the interferometer. The beam was split with one arm (reference) having neutral density filters inserted to equalize the output beam powers.

The other beam was coupled into the waveguide with a 20x microscope objective and output coupled with the same. The waveguide was mounted on a dual inline pin package which allowed the selection of up to eight devices without rebonding the electrical connections. This package was then mounted on a micropositioner with three axes of movement and sensitive piezo positioners to ease the fine adjustment of optimizing the coupling.

The coupling was achieved with the help of an infrared camera which was used in a microscope configuration above the sample. This configuration allowed relatively easy input coupling of the waveguides. The camera was also used to image the end of the waveguide and observe the mode pattern.

The spatial filter was added since the waveguide did not exhibit a well behaved mode shape. It was thought that the stress of the aluminum contact was enough to change the index such that the mode shape was effected. The spatial filter cleaned up the beam shape to allow recombination with the reference. Unfortunately the filtered beam was of much less power than the

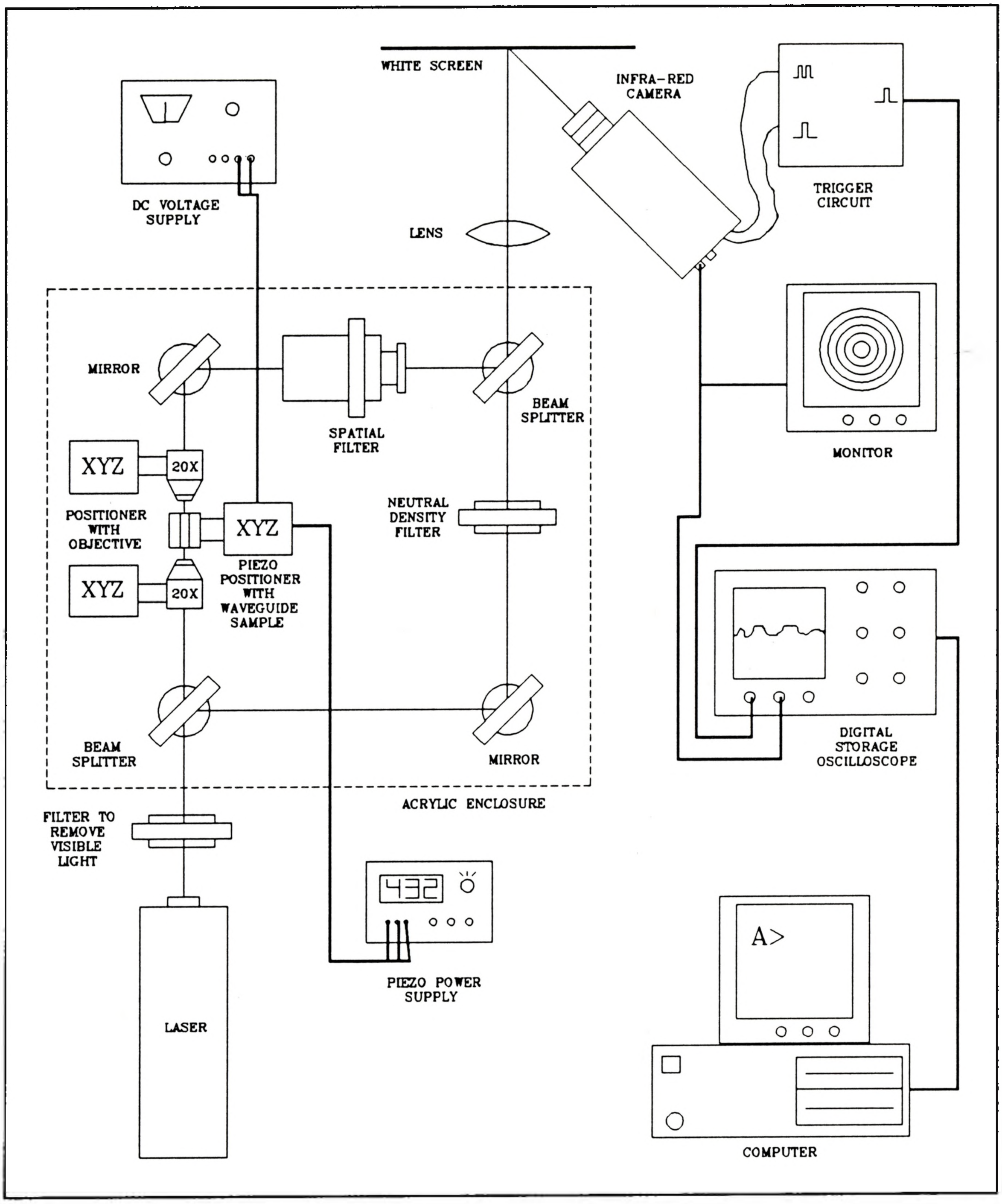

Figure 4.1 The experimental apparatus for the measurement of phase modulation by the electrooptic effect.

before filtering.

The recombined beams were expanded onto a white card which was imaged by the infrared camera. The camera image appeared as concentric circles. To measure the shift, since a 180 degree phase shift was not possible, a detector could not be used. A single scan line from the infrared camera was used. Due to the camera having an interlaced output, the oscilloscope delayed trigger was not sufficient to record multiple images of the single scan line. A line from the camera's horizontal sync. as well as one from the vertical sync. was fed to a circuit which triggered from every second vertical sync. pulse (negating the interlace problem). The trigger for the oscilloscope was then obtained by holding off a specific amount of time to feed the scope the correct horizontal sync. The digital oscilloscope then averaged many of these traces together and the result was transferred to a computer.

Initially the setup did not contain an enclosure for the interferometer. Without such an enclosure air currents had a drastic effect even with doors closed, ventilation off, and controlled movement in the room. The enclosure slowed down changes so that two traces could be taken with a reasonable surety that the environment would remain constant. The original plan of taking a trace every 5 volts of applied voltage had to be abandoned due to inconsistent results.

4.3 Experimental Results

A trace at 0 volts as well as a trace at 30 volts (breakdown occurred at 37 V) were taken. Only two measurements could be taken within a length of time short enough to insure that drift was at a tolerable level. Figure 4.2 shows the results of this measurement. The phase shift is very inconsistent from peak to peak with a shift of $(0.65 \pm 0.05)\pi$ indicated close to the centre of the fringe pattern for a 30 V voltage difference. This translates to a V_π of (46 ± 4) V. The modulator had a length of 2400 μm and should have had a V_π of 47.5 V using the known value of the electrooptic coefficient of $r_{41} = 1.2 \times 10^{-12}$ m/V[20]. The value of the electrooptic coefficient also has some uncertainty and this has not been accounted for in the error estimate.

The inconsistent peak shift is probably due to the poor mode shape of the light output from the waveguide. The mode shape appeared to have two intensity peaks laterally. Even these two spots were not uniform. The likely cause for this poor mode shape is an irregular refractive index profile caused by the stress of the aluminum overlayer[18].

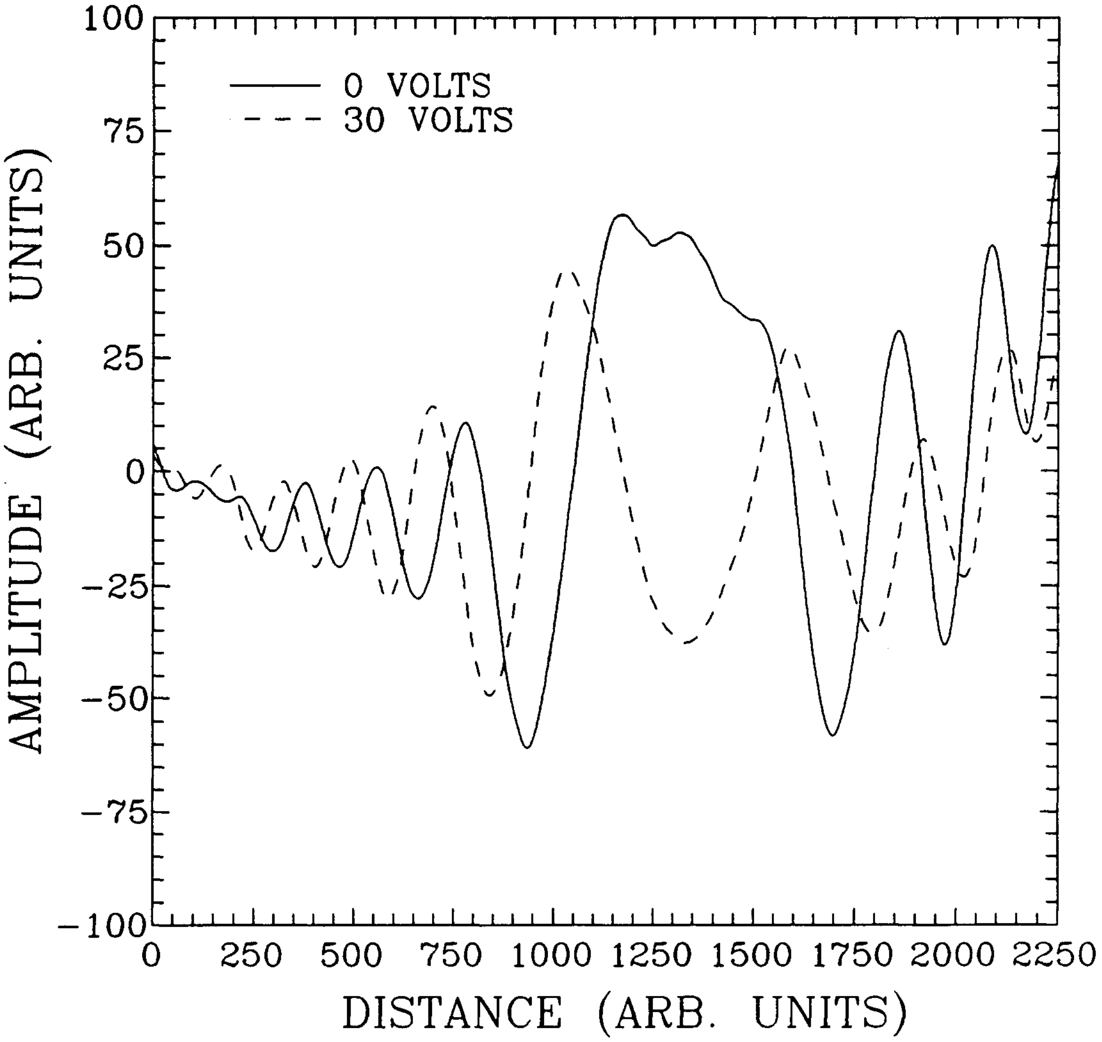

Figure 4.2 The interference fringes for 0 volts and 30 volts applied reverse bias. The centre of the interference pattern occurs at approximately 1350 on the distance scale.

CHAPTER FIVE

SUMMARY OF PHASE MODULATOR RESULTS

5.1 Conclusions

This project succeeded in both fabricating an electrooptic waveguide modulator and measuring the electrooptic effect in GaAs. Each of these two areas was not without its problems.

In the fabrication side of the project many of the problems of wet etching waveguides in III-V materials were encountered. The first of these was the difficulty in working with the bromine-methanol etch. It would seem to be an ideal etch for waveguides due to its smoothing character. Its usefulness is limited until the availability of facilities for dielectric masking. The spin-on glass material used for Fabrication Procedure A seems a reasonable candidate for waveguides of widths 9 μm and greater. The sulphuric acid etch is a reasonable choice for thinner waveguides due to the usefulness of photoresist as a masking material but the poor edge quality and highly anisotropic etching nature are drawbacks.

A further problem encountered was in the area of mask making. The camera that was available is limited to approximately 6 μm features with the edge quality of the features being poor at this size. Narrower waveguides are generally required for single mode integrated optics and many masks will have to be obtained elsewhere. A minor additional problem is the fixed linewidths available with the pen-camera reduction combinations available. To counter this problem some initial pen drawn mask patterns were photographically reduced by McMaster Audio-Visual Services to 2/3 of their original size before being photographed onto a mask plate. This allowed the 6 μm lines to be made with a 0.18 mm pen and a 20x reduction camera. Line quality was good but some large scale distortion occurred. This makes alignment of small features located far apart on the mask difficult.

The most interesting and perhaps most serious problem is the poor waveguiding properties which probably were caused by stress induced by the metallic aluminum contact. This is potentially a serious problem since many devices require the presence of a metal contact layer over a waveguide. This effect will presumably be less in materials which have a cladding layer between the waveguide and the contact but could still be very important. It was not practical to examine this problem more closely due to poor and unpredictable metallization facilities.

The major problem encountered in the measurement of the phase shift was the relatively short term drift of the phase. This was traced to poor environmental room conditions. The small room and poor climate control in the building caused large phase shifts to occur. Superior environmental control should be sought before large interferometric experiments are attempted in the future.

CHAPTER SIX

INTRODUCTION TO QUANTUM WELLS AND DEVICES

6.1 Historical Background

Interest in quantum wells (QW) and superlattices began in 1969 with the proposal by Esaki and Tsu of an "engineered" quantum structure[21]. They proposed two types of band structure engineering utilizing developing techniques in semiconductor epitaxy which is the growing of thin semiconductor layers. The first of these types is a doping superlattice in which periodic changes in the doping of a semiconductor would cause periodic bending of the conduction and valence bands as the Fermi level equalizes throughout the structure. The second type is a compositional superlattice. Such a structure may be formed by depositing layers of different types of semiconductors on top of one another. The band structure is determined by the differing band gaps and electron affinities of the two (or more) materials as well as stress effects due to differing lattice constants.

The compositional superlattice has received the most attention since it tends to create sharper discontinuities at the hetero-interfaces. However, interest in doping superlattices is increasing especially when combining both compositional and doping techniques which promise better carrier mobilities due to carrier separation from the dopant impurities.

Along with the distinction between how the artificial band structure is created there is a distinction between quantum wells and superlattices. Although a superlattice may be said to be made up of a periodic arrangement of quantum wells, a superlattice is not correctly called a multiple quantum well material (MQW). The distinction between a superlattice and a MQW material lies in the coupling of carriers between the wells. When any interaction of carriers between different wells may be ignored the material is referred to as a MQW material. If tunnelling between wells is important the material is a superlattice.

6.2 Properties of Quantum Wells

The confining nature of the well barriers gives rise to the interesting characteristics of quantum wells. The barriers serve to confine carriers to the well region. If the well region has a width of the order of the deBroglie wavelength of the particle, the carriers must exist in a number of discrete allowed energy states. In a planar structure, the carriers are free to move within the plane but are confined in one direction giving rise to a quasi two dimensional system. One dimensional and zero dimensional systems have also been realized[22].

The initial interest in quantum wells was spurred by interest in devices which exhibit negative differential conductivity (NDC). Gunn diodes[23] as well as tunnel diodes[24] exhibit NDC but the quest for faster response and better NDC characteristics pointed to the use of resonant tunnelling through a double barrier structure[25]. Sharp resonances in the tunnelling current had been predicted on the basis of the quantized energy states allowed between the barriers. Such resonances have been observed and very fast device responses have been measured[26].

Interest in optical properties followed soon after. It had long been known that bound hydrogen like states could exist between electrons and holes in semiconductors. These states appeared as sharp resonances in the optical absorption spectrum at low temperatures and were referred to as excitons[27]. Sharp features in any physical property offer hope to device scientists who see such features as offering potential for new devices. Unfortunately excitons are weakly bound systems with binding energies in the 5-10 meV range. Longitudinal optical (LO) phonons in GaAs, for example, have energies of 36 meV at room temperature[28]. At room temperatures these phonons ionize excitons at such a rapid rate that the resonances are not observable.

A further problem complicates the use of excitons for devices even at low temperature. In order to make a useful device one must be able to affect the property to create a useful change. One way of accomplishing this is to apply an electric field. Unfortunately the application of even a small electric field rips apart an exciton due, again, to its low binding energy.

Quantum wells provide a solution to both the above problems. The confinement of the carriers to the well layers effectively increases the exciton binding energy and allows exciton resonances to be observed at room temperature[29]. Further, the confinement also inhibits electric field ionization of the excitons for fields perpendicular to the layers. Excitonic resonances have been observed for fields on the order of 200 kV/cm[30].

The application of electric fields perpendicular to the MQW layers causes a shift in the energy of the primary exciton resonance. This shift is called the quantum-confined Stark effect (QCSE) after the analogous Stark shift in the hydrogen atom. It shows great promise in the areas of electroabsorption modulators[31] and tuneable detectors[32].

Although the exciton resonances near the band edge is the focus of this work, MQW materials also show promise in phase modulation at longer wavelengths. They exhibit a larger figure of merit than bulk materials[33].

CHAPTER SEVEN

EXCITON THEORY

7.1. Chapter Introduction

Excitons are bound electron - hole pairs which form an analog to a hydrogenic system. The creation of excitons produces very sharp resonance peaks in the optical absorption spectrum. For absorption modulators or tuneable detectors excitons are a promising feature due to their sharpness.

In bulk semiconductors excitons are present but are only directly observable at low temperatures due to the ionization at room temperature by longitudinal optical (LO) phonons. At low temperatures ionization occurs on a much longer time scale and observation is practical but the effect is of less interest since room temperature effects are more desirable from a device point of view and electric field ionization is a problem for most foreseeable devices.

With the ability to grow thin semiconductor materials has come the answer to the room temperature exciton problem. If a material with a smaller band gap is sandwiched between a material with a larger bandgap it is possible to have a band diagram as in Figure 5.1. In such a structure electrons and holes will preferentially reside in the smaller band gap material. (Such a band diagram occurs in the AlGaAs-GaAs system and also in other systems. These

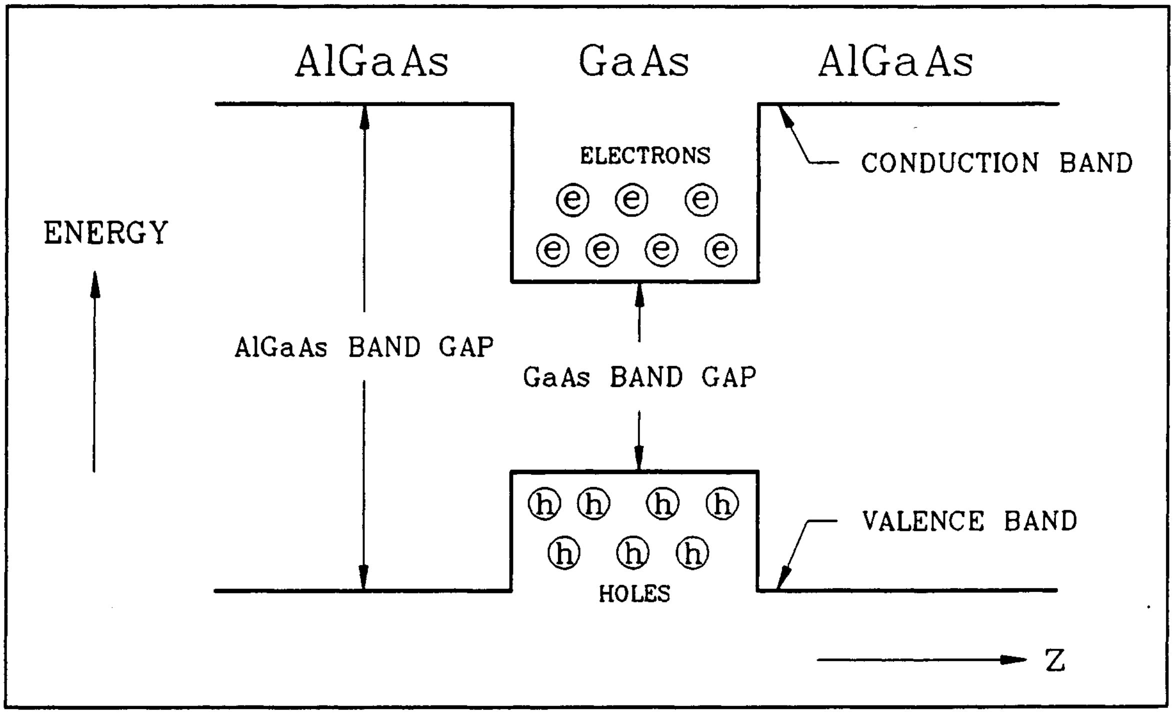

Figure 7.1. A schematic band diagram of a AlGaAs-GaAs quantum well which illustrates the confinement of electrons and holes to the narrow gap material.

will not be discussed although most of this material is directly applicable to other such systems in which the bands form as in figure 5.1.) Although electrons and holes are free to travel in the plane of the layers they are confined perpendicular to the plane. The confinement can prevent phonon ionization of the excitons for a long enough period of time that excitonic resonances are observable at room temperature. The confinement also inhibits electric field ionization for fields perpendicular to the well layers.

This chapter will provide a simple mathematical description of quantum wells and excitons in the GaAs/AlGaAs system. The description will focus on material necessary for the prediction of the position of the primary exciton resonance which, in this system, corresponds to an exciton formed between a ground state conduction band electron and a ground state valence band heavy-hole.

The method used to calculate the electric-field-modified ground state particle wavefunctions was similar to that used by Lengyel et al[34]. Readers of their paper should be cautioned that although they showed good agreement between their measured and calculated exciton shifts this was primarily due to the neglect of the exciton binding energy in their calculations of the excitonic energy. The binding energy that was neglected is of the order of 7meV and is significant to the calculation. Other errors were also present in their calculations but were smaller in magnitude. These stemmed from an improper treatment of the conservation of probability at the hetero-interfaces and resulted in improper square well energy states. A comparison of results from the method which conserves probability and their results are given in appendix A.

7.2. Square Well Theory

The confinement in the z direction has a purely quantum mechanical effect due to the very narrow region to which the particles are confined (≈100Å). It produces distinct allowed energy levels, in each band, within the well layer (Figure 7.2). For a square well potential, within the effective mass approximation, the allowable wavefunctions are sinusoids within the well and decaying exponentials outside the well. The energies of the allowed eigenstates may be found by solving the time independent Schrodinger equation[35].

$$-\frac{\hbar^2}{2m^*(z)}\frac{d^2\psi_n^0(z)}{dz^2} + V^0(z)\,\psi_n^0(z) = E_n^0\,\psi_n^0(z) \tag{7.1}$$

The energies may be found equivalently by solving two transcendental equations[36]

$$\begin{aligned} k_w \tan\left(\frac{k_w L_z}{2}\right) &= \frac{m_w^*}{m_b^*}k_b \\ k_w \cot\left(\frac{k_w L_z}{2}\right) &= -\frac{m_w^*}{m_b^*}k_b \end{aligned} \tag{7.2}$$

where

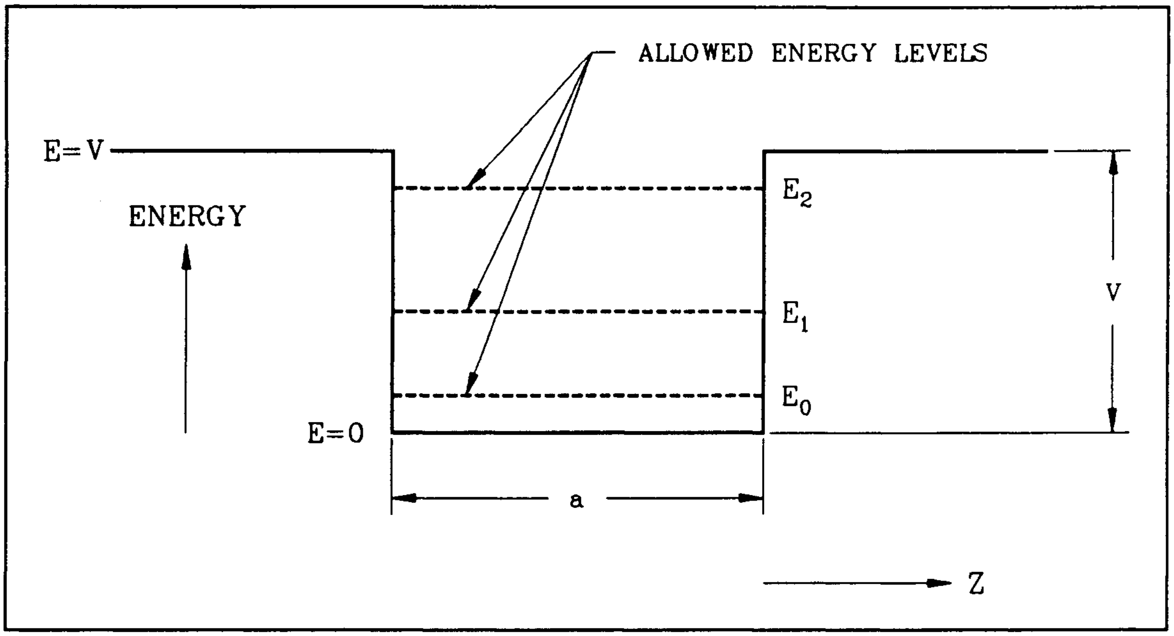

Figure 7.2. A diagram of a square quantum well which illustrates the distinct allowed energy states.

$$k_w = \frac{\sqrt{2m_w^* E}}{\hbar}$$

$$k_b = \frac{\sqrt{2m_b^*(V-E)}}{\hbar} \; . \tag{7.3}$$

which results from imposing the boundary conditions of the continuity of the wavefunction ψ at the boundary as well as continuity of $\frac{1}{m^*}\psi'$ at the boundary. The second boundary condition differs from the usual condition (continuity of the derivative at the boundary) in order to conserve probability current at the boundary between two materials where the particle has differing effective masses. This can be argued on the grounds that no net particle transfer should take place in the time independent approximation.

The solution of Equations 7.2 for both the conduction band well and the valence band well defines a finite number of allowed energy states in each well. The energy of the lowest allowed electron eigenstate (ground state) is greater than that of the conduction band minimum and the energy of the ground state hole level is less than the top of the valence band. Therefore the effective optical band gap of the quantum well material will be greater than the bulk bandgap of the well material itself. In other words, neglecting any other interactions, the energy required to create the ground state exciton is the difference in energy between the ground state electron level and the ground state hole level (Figure 5.3).

It should be noted that due to the valence band structure of GaAs, there exists two important sets of valence band energy states, each set given by a separate solution of Equations 7.2. This results from the existence of heavy hole and light hole subbands[37] which have different hole effective masses. Since the ground state heavy hole is the closest to the top of the valence band it is generally the most important and will be primary effect considered here. A further important effect is the coulomb interaction between the two particles which binds the electron and hole into an exciton. This shifts the energy required to create an exciton to lower energies from that discussed above. This will be discussed later.

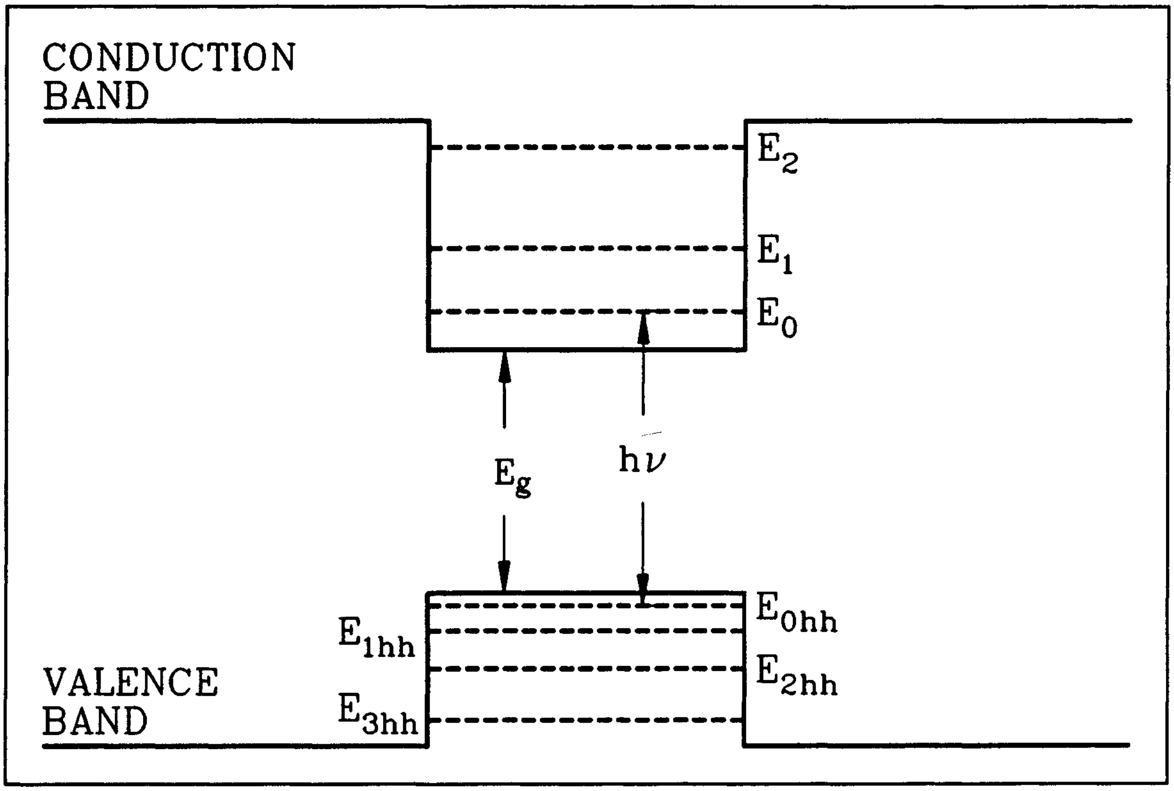

Figure 7.3 The band diagram of a quantum well which illustrates that the effective band gap is larger than the band gap of the well material due to the absence of allowed states at the band edge.

7.3 Electric Field Effects on the Energy Levels

In bulk semiconductors the application of an electric field results in a slight red shift of the band edge as well as a moderation in the slope of the band edge. This effect is known as the Franz-Keldysh effect[38] and is related to band bending but not to excitons since they are not detectable at room temperature in bulk materials. Devices using this effect have been demonstrated[39,40] but the weakness of the effect tends to make them larger than is ideal for large scale integration. The sharp exciton resonances in MQW materials can exhibit a larger shift while retaining most of the edge sharpness of the resonance due to the confinement. These factors make the excitonic shift a better prospect for devices than the Franz-Keldysh effect. The excitonic shift is known as the quantum confined stark effect (QCSE) or occasionally the quantum-confined Franz-Keldysh effect[41].

The QCSE can be qualitatively as well as quantitatively be understood by examining the behaviour of quantum well energy levels in the presence of an electric field. When an electric field is applied perpendicular to the layers in a MQW structure the band diagram approximates that of Figure 7.4. The energy eigenvalues of the quantum wells shift towards a lower energy (higher in the valence band). Since, in a real material, this translates into both the conduction band and valence band states moving closer together a red shift in the band gap is the effect.

7.4 A Mathematical Model of the Energy Level Shift

To understand the exciton energy shift in the presence of an electric field one can solve the Schrodinger equation for the energy levels as before except that the Hamiltonian must be modified to account for the electric field as well as for both bands. The coulomb interaction between the electrons and

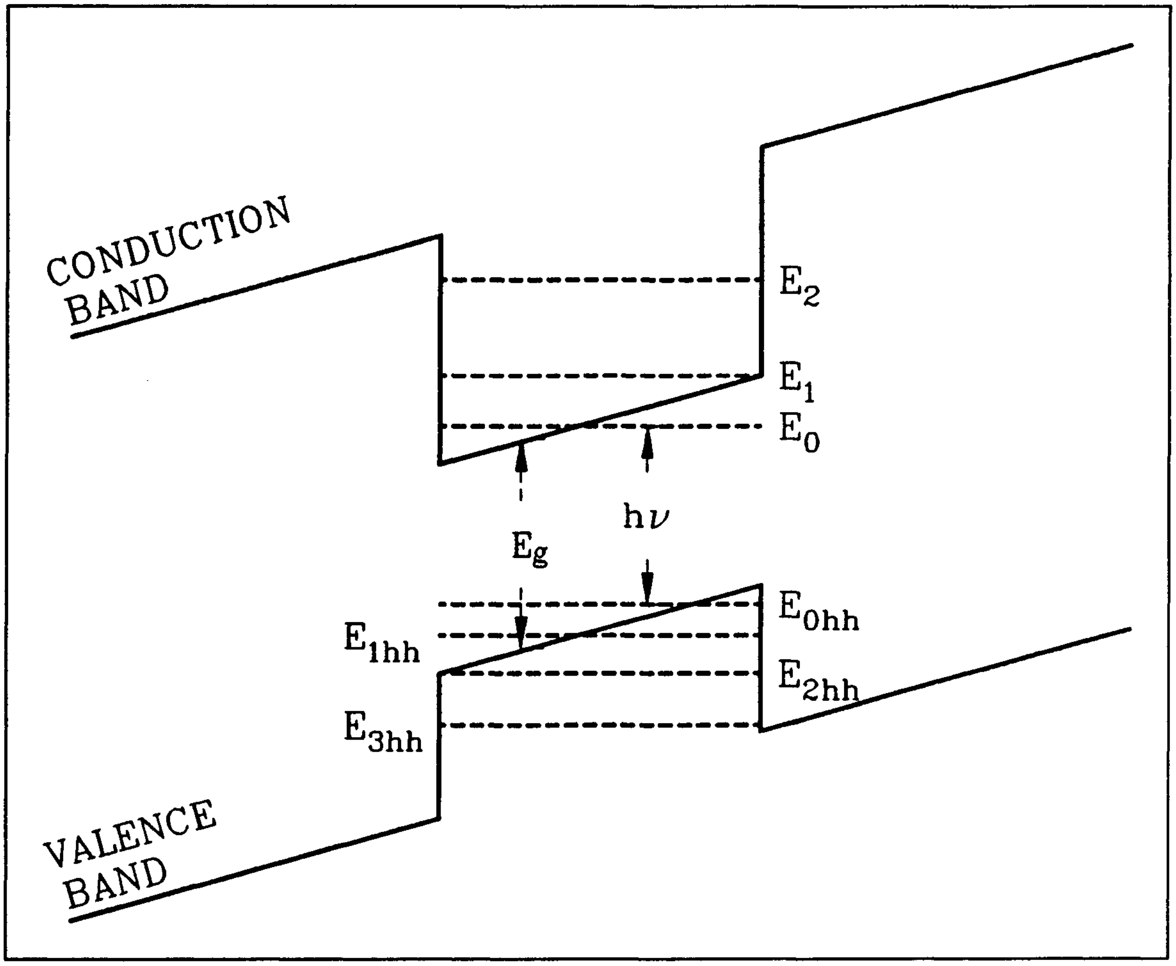

Figure 7.4. In the presence of an electric field, perpendicular to the semiconductor layers, the allowed energy levels shift towards the gap which makes the effective band gap smaller.

holes is also important and will now be considered. The modified Hamiltonian has the form

$$\begin{aligned} H = &-\frac{\hbar^2}{2m^*(z)}\frac{d^2}{dz_e^2} + V_e(z_e) \\ &-\frac{\hbar^2}{2m^*(z)}\frac{d^2}{dz_h^2} + V_h(z_h) \\ &-\frac{\hbar^2}{2\mu}\frac{1}{r}\frac{d}{dr}\left(r\frac{d}{dr}\right) - \frac{e^2}{4\pi\varepsilon\sqrt{r^2+(z_e-z_h)^2}} \end{aligned} \qquad (7.4)$$

where the electric field dependence is incorporated into the well potentials. μ is the effective mass of the hydrogenic system given by

$$\mu = \frac{m^*_{e\parallel}\, m^*_{h\parallel}}{m^*_{e\parallel} + m^*_{h\parallel}} \qquad (7.5)$$

where the parallel signifies parallel to the plane of the layers, e signifies electrons and h signifies holes.

The wavefunction can be seen to originate from three parts - the confinement of electrons, the confinement of holes and the coulomb interaction. The problem would be easy to solve if the solution was a separable wavefunction. This will clearly not be the case due to the coulomb potential term - it depends on all three space variables. One can, however, realize that the confinement of electrons and holes to distances (z component) of 100Å means that the coulomb term will be dominated by the in-plane contribution. This leads to an approximation of the radial (x,y) part of the wavefunction by a wavefunction of the same form as the ground state wavefunction for a particle in a two dimensional coulomb potential with a fitting parameter ρ . The full trial wavefunction is then of the form

$$\psi(r,z_e,z_h) = \psi_e(z_e)\,\psi_h(z_h)\,N\exp\left(-\frac{r}{\rho}\right) \tag{7.6}$$

where

$$r = \sqrt{x^2 + y^2} \quad . \tag{7.7}$$

With the above form assumed the problem can be separated to allow the independent solution of the z dependent electron and hole wavefunctions. For clarity the hamiltonian is separated below

$$H_1 = -\frac{\hbar^2}{2m^*(z)}\frac{d^2}{dz_e^2} + V_e(z_e)$$

$$H_2 = -\frac{\hbar^2}{2m^*(z)}\frac{d^2}{dz_h^2} + V_h(z_h) \qquad (7.8)$$

$$H_3 = -\frac{\hbar^2}{2\mu}\frac{1}{r}\frac{d}{dr}\left(r\frac{d}{dr}\right) - \frac{e^2}{4\pi\varepsilon\sqrt{r^2+(z_e-z_h)^2}}$$

7.5 Solution of the Electron and Hole Confinement

The problems specified by the Hamiltonians H_1 and H_2 are similar problems, therefore only the solution of the conduction band states will be described in detail.

When the electric field is non-zero the potential term in the Hamiltonian H_1 becomes

$$V_e(z_e) = V_e^0(z_e) - eFz \qquad (7.9)$$

The solution to such a problem is found in terms of Airy functions[42]. The use of Airy function solutions has generally been attempted by using infinite well approximations to finite wells. The reason for this is the difficulty in calculating Airy functions and the large amount of computer time such solutions require. Further difficulties occur due to normalization problems. These problems as well as the average person's non-familiarity with these functions present a difficulty when simple and intuitive models are required.

Alternatively one can use an approximate technique to get solutions in terms of the zero field eigenstates[43]. This approximation is only valid when the well has two or more bound states at zero field. The more bound states it has the more accurate the solution will be. Similarly as the field increases more of the higher energy solutions will be mixed in and the method will become less accurate due to the absence of higher energy states.

The procedure has the advantage of requiring less computational power than a full Airy function solution. It is also more intuitive due to the fact that non-zero field solutions can easily be compared to zero field solutions and the solutions are expressed in terms of linear combinations of trigonometric and exponential functions which are generally more familiar than Airy functions.

The procedure first requires the solution of the quantum well problem in the absence of an electric field. This calculation has already been described and it is assumed that these solutions are now known.

Given solutions ψ_n^0 for the zero field square well problem in the conduction band

$$H^0\psi_n^0 = \left[\frac{p_z^2}{2m^*(z_e)} + V_e^0(z_e)\right]\psi_n^0 = E_n^0\psi_n^0 \tag{7.11}$$

one wishes to find solutions to a new problem given by

$$H'\psi_n' = \left[\frac{p_z^2}{2m^*(z_e)} + V'(z)\right]\psi_n' = E_n'\psi_n' \tag{7.12}$$

where

$$V'(z_e) = V^0(z_e) + v(z_e) \qquad v(z_e) = eFz_e \tag{7.13}$$

The solutions are expressed in terms of a linear combination of zero field solutions given by

$$\psi_n'(z) = \sum_l a_{nl}\psi_l^0(z) \tag{7.14}$$

which when substituted back into the Schrodinger equation gives

$$\sum_l a_{nl}(E_n' - E_l^0)\psi_l^0(z) = \sum_l a_{nl} v(z)\, \psi_l^0(z) \ . \tag{7.15}$$

Using the approximate orthonormal relation

$$\int_{-\infty}^{\infty} \psi_m^*(z)\psi_l(z)dz = 0 \qquad m \neq l \tag{7.16}$$

and the notation

$$v_{ml} = \int_{-\infty}^{\infty} \psi_m^*(z)\, v(z)\, \psi_l(z)dz \tag{7.17}$$

the following is obtained

$$a_{nm}(E_n' - E_m^0) = \sum_l a_{nl} v_{ml} \ . \tag{7.18}$$

The orthonormal relation is only approximate since the wavefunction exists in two materials with different effective masses. In effect one is solving the wave equation for two non-identical particles and joining the wavefunction at the interface. Due to the small change in effective mass and the fact that most of the wavefunction exists within the well, this approximation is good.

The above equation is an eigenvalue equation which may be expressed in matrix form as

$$\begin{bmatrix} v_{11}+E_1^0 & v_{12} & v_{13} & \cdots \\ v_{21} & v_{22}+E_2^0 & v_{23} & \cdots \\ v_{31} & v_{32} & v_{33}+E_3^0 & \cdots \\ \cdot & \cdot & \cdot & \\ \cdot & \cdot & \cdot & \\ \cdot & \cdot & \cdot & \end{bmatrix} \begin{bmatrix} a_{l1} \\ a_{l2} \\ a_{l3} \\ \cdot \\ \cdot \\ \cdot \end{bmatrix} = E_l' \begin{bmatrix} a_{l1} \\ a_{l2} \\ a_{l3} \\ \cdot \\ \cdot \\ \cdot \end{bmatrix} . \tag{7.19}$$

The solution of which gives the energy eigenvalues E_l' and the eigenvectors a_{ln} which are the coefficients which determine the mixing of the unperturbed, zero field states into the perturbed non-zero field states. In this case one is only interested in the ground state wavefunction so the lowest energy eigenvalue and corresponding eigenvector are the required quantities. The higher order energies will be less accurate due to the absence of a full spanning set of mixing eigenfunctions.

If the zero field wavefunctions are normalized, then the non-zero field wavefunctions are normalized by insuring the following

$$\sum_m a_{nm}^2 = 1 \tag{7.19}$$

With the above normalization carried out the ground state wavefunction and its energy are completely specified. Repeating the above procedure for the analogous valence band will result in the ground state heavy hole wavefunction and energy being found for arbitrary electric field.

The solution to the problems specified by the H_1 and H_2 Hamiltonians has been outlined but for the total exciton energy to be known the radial problem must be solved as well.

7.6 The Radial Solution

The H_3 term in the complete Hamiltonian describes the interaction of the two particles by the coulomb force. It is this coulomb force which actually creates the hydrogen-like system which is called an exciton.

The assumed form of the trial wavefunction given by

$$\psi_r(r) = \sqrt{\frac{2}{\pi}\frac{1}{\rho}}\exp\left[\frac{-r}{\rho}\right] \tag{7.20}$$

which has a fitting parameter ρ . This form is identical to the ground state wavefunction for a particle in a two dimensional coulomb potential and may be found by using a series solution.

It remains to determine a value for the variable parameter. The easiest method is to calculate the expectation value of the Hamiltonian H_3 and to vary the parameter until this expectation value is at a minimum. The expectation value so obtained will be a good approximation of the binding energy.

$$BINDING\ ENERGY = -\iiint \psi\, H_3\, \psi\, d\phi\, dr\, dz_e\, dz_h \tag{7.21}$$

The calculation of the binding energy requires the evaluation of a triple integral which requires a large amount of computer time. Fortunately due to the form of the radial wave function which we have chosen, the radial part may be done analytically by using the following tabulated integral.

$$G(\gamma) \equiv \frac{2}{\rho}\int_{r=0}^{\infty} \frac{r\exp(-2r/\rho)dr}{\sqrt{\gamma^2+r^2}}$$

$$G(\gamma) = \frac{2|\gamma|}{\rho}\left\{\frac{\pi}{2}\left[H_1\left(\frac{2|\gamma|}{\rho}\right) - N_1\left(\frac{2|\gamma|}{\rho}\right)\right] - 1\right\} \tag{7.22}$$

In the above integral H_1 is the first order Struve function and N_1 is the first order Neumann function.

The total energy required to create the ground state heavy hole exciton may now be calculated as the sum of the expectation values of H_1, H_2, and the binding energy. In the calculation of the z dependence of the electron and hole the energy eigenvalues were referenced from the band edges at the middle of the well for both the conduction and valence bands. To reference the energies from the same point it is also necessary to add in the energy of the band gap of the well material. The photon energy needed to excite the exciton resonance is then given by

$$h\nu = E_e + E_{hh} - E_{binding} + E_{gap} \tag{7.23}$$

where the binding energy is defined as a positive value.

CHAPTER EIGHT

CALCULATION OF THE EXCITON RESONANCE SHIFT

8.1. Chapter Introduction

In order to design modulators and detectors which operate near the band gap it must be possible to predict the position and character of the excitonic resonance as a function of electric field. With such predictions it would be possible to design a semiconductor structure on paper and minimize the amount of trial and error in the material parameters. Such a method was described in the previous chapter and in this chapter it will be implemented on the structure shown in Figure 8.1 which has been designated MBE 852.

8.2. Model Assumptions

The mathematics of the model was described in the previous chapter. Some of the model's underlying assumptions will be discussed for clarity.

The first assumption is that of square wells both in the conduction and valence bands. This model neglects band bending at the interfaces and assumes perfect crystal interfaces. Despite these two simplifications, the square well model has been shown to be a very good model in most

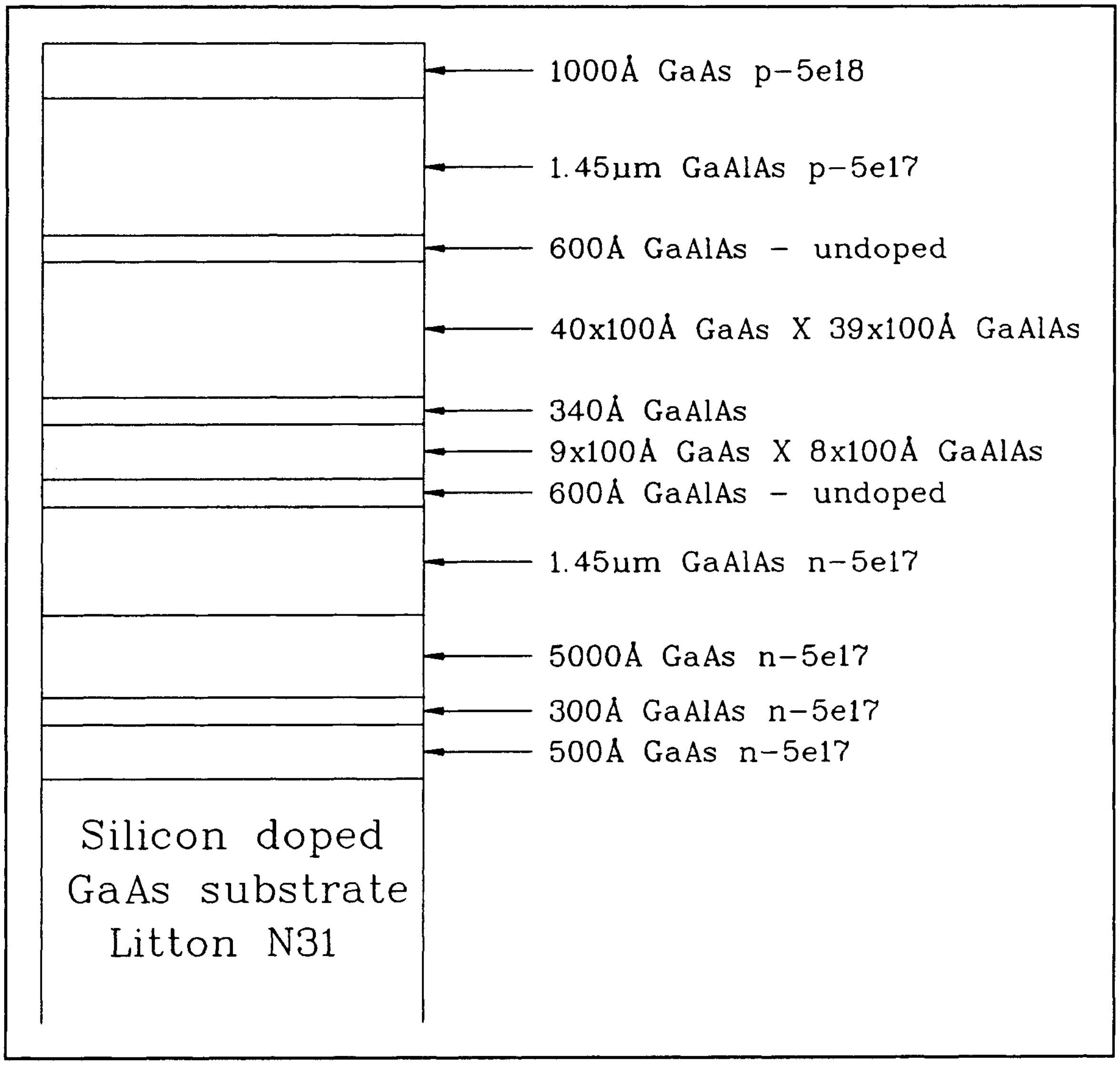

Figure 8.1 The structure of sample MBE 852.

circumstances dealing with quantum wells.

The materials parameters for both GaAs and AlGaAs were obtained from data compiled by Adachi[28] and are given in table 8.1. The effective mass model is used.

TABLE 8.1

MATERIALS PARAMETERS

PARAMETER	*GaAs*	$Al_xGa_{1-x}As$
E_{gap} (eV)	1.424	$1.424 + 1.247x$
ε_r	13.18	$13.18 - 3.12x$
m_e^*	0.067	$0.067 + 0.083x$
m_{lh}^*	0.087	$0.087 + 0.063x$
m_{hh}^*	0.62	$0.62 + 0.14x$

8.3. Calculations and Results

A computer program was written to calculate the exciton position as a function of electric field. A listing appears in Appendix B as well as a sample output in Appendix C. It requires the user to input the well width, the concentration of aluminum in the barriers and the fraction of the band discontinuity which appears in the conduction band. With these parameters and the parameters of Table 8.1 the square well problems for both the conduction and valence bands are completely specified and are solved as described in the previous chapter. The field is then accounted for as described in Chapter seven and the exciton binding energy calculated.

The calculations were carried out using the input parameters of Table 8.2. The square well energy values are given in Table 8.3. Once the energies of all the square well states are found, they give all necessary information to allow the construction of the zero field wavefunctions. These wavefunctions are pictured in Figures 8.2, 8.3 and 8.4. There are two conduction band energy states and five heavy-hole valence band energy states. The wavefunctions clearly show the discontinuity in slope at the interface which is necessary to conserve probability current across an interface between two materials with different effective masses.

TABLE 8.2

PROGRAM INPUT PARAMETERS FOR MBE 852

PARAMETER	VALUE
WELL WIDTH	100 Å
ALUMINUM CONCENTRATION	0.30
CONDUCTION BAND DISC.	0.60

TABLE 8.3

CALCULATED SQUARE WELL ENERGY VALUES FOR MBE 852

CONDUCTION BAND	
E_0	29.7 meV
E_1	116 meV
VALENCE BAND	
E_0	-5.83 meV
E_1	-23.2 meV
E_2	-51.9 meV
E_3	-90.9 meV
E_4	-137 meV

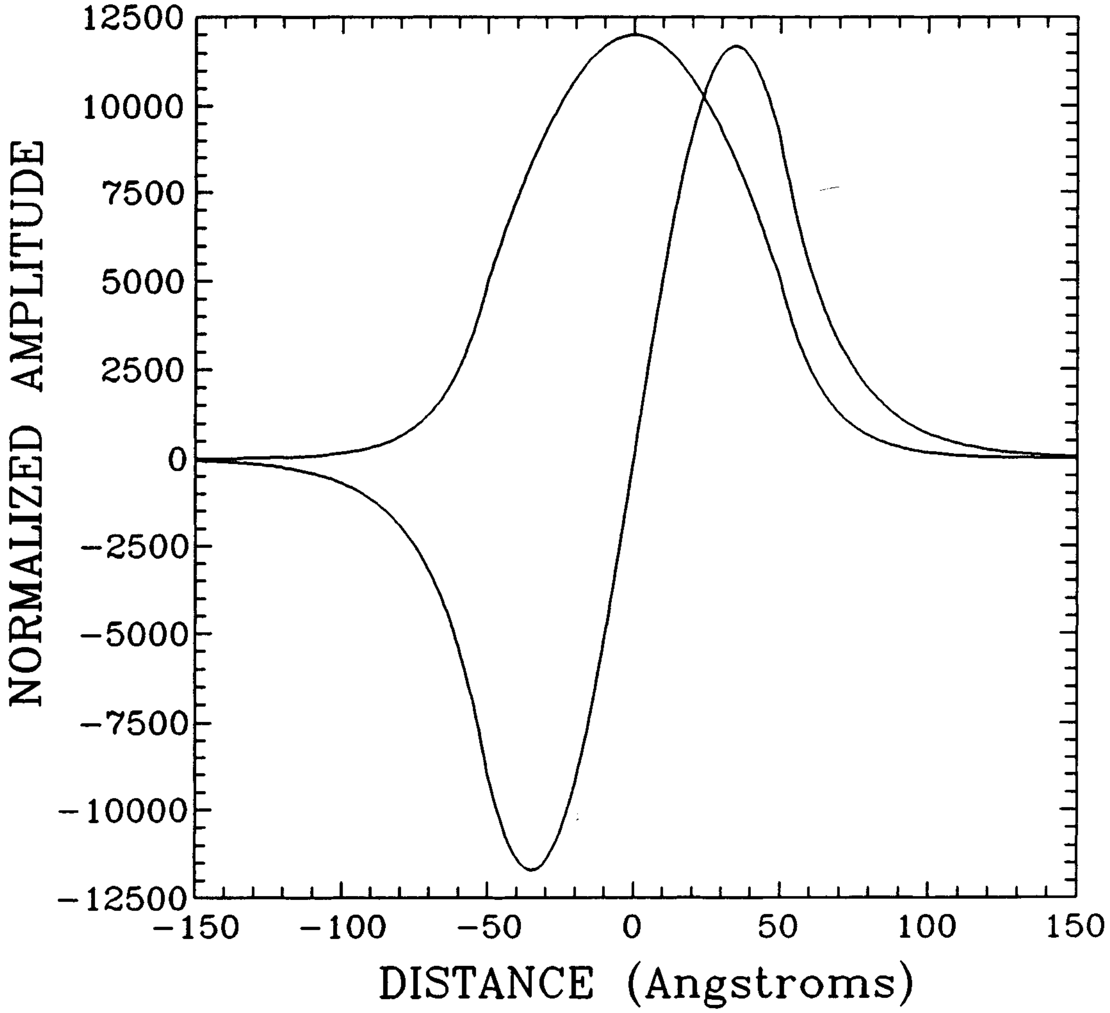

Figure 8.2 The two allowed conduction band wavefunctions at zero field.

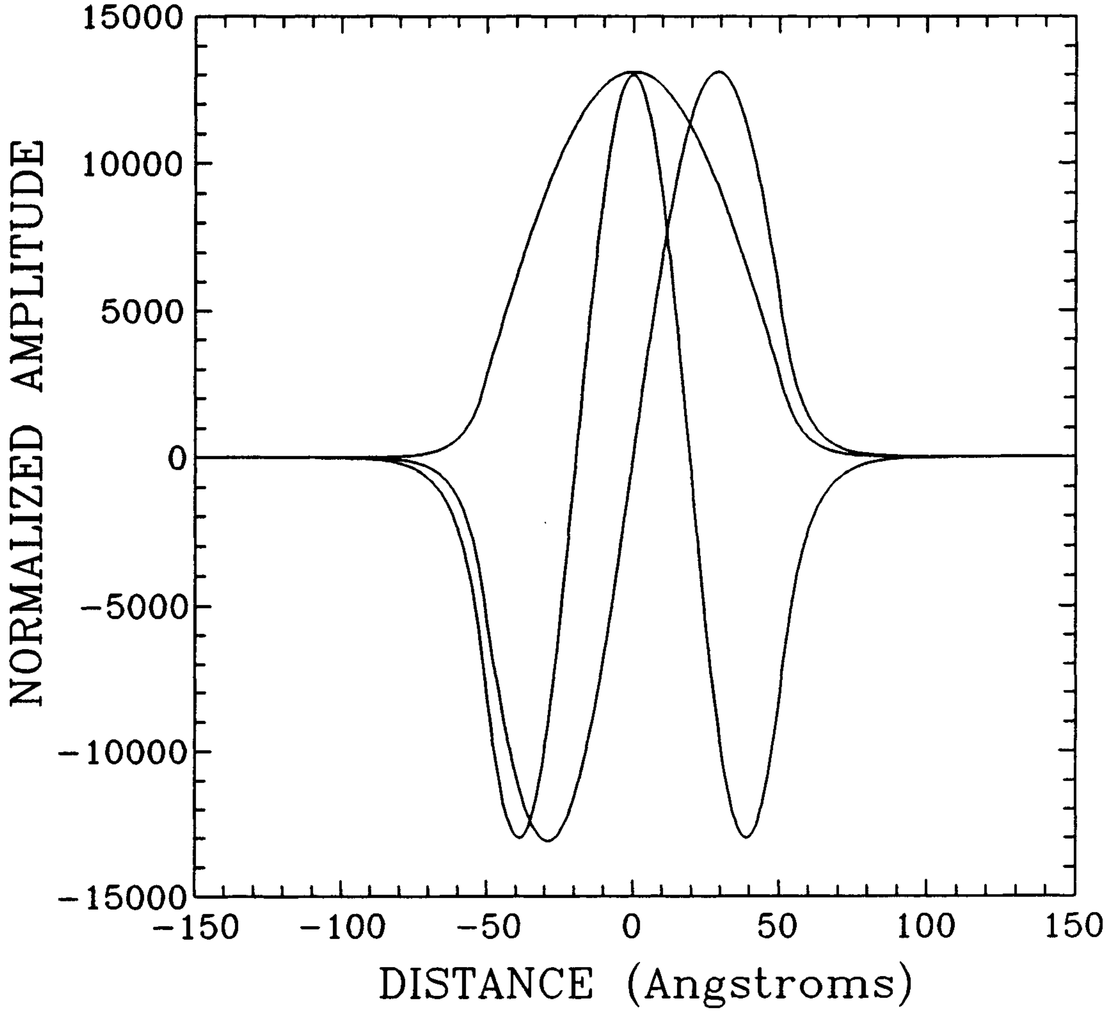

Figure 8.3 The three highest energy (closest to the gap) valence band states at zero field.

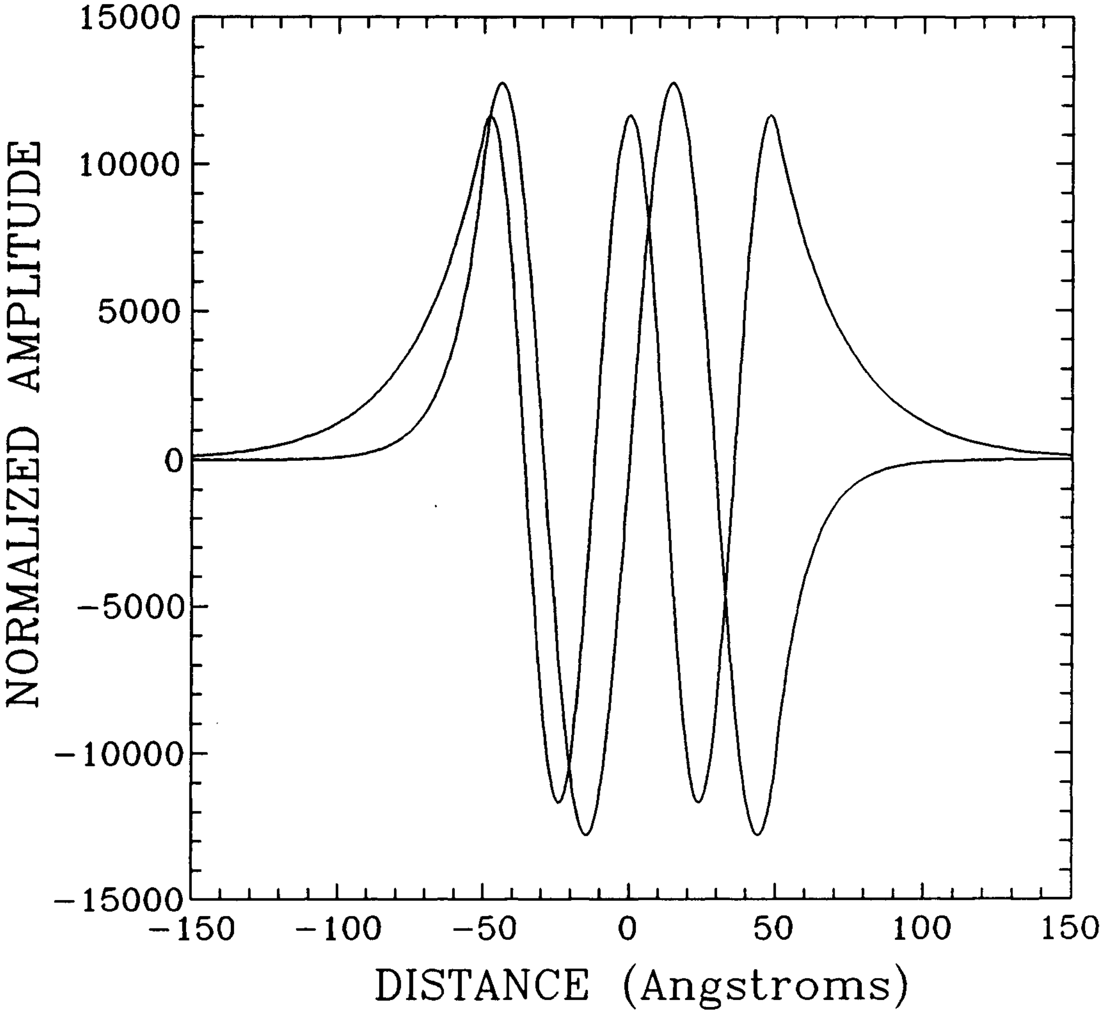

Figure 8.4 The two lowest energy wave functions (furthest from the gap) in the valence band at zero field.

TABLE 8.4

RESULTS OF FIELD ON GROUND STATE ELECTRON

FIELD (kV/cm)	a_0	a_1	E_e
0	1.000	0.000	29.7
20	0.998	-0.581	29.4
40	0.993	-0.114	28.5
60	0.986	-0.168	27.1
80	0.976	-0.217	25.2
100	0.965	-0.261	22.9
120	0.954	-0.301	20.1
140	0.942	-0.336	17.1
160	0.930	-0.367	13.8
180	0.919	-0.394	10.2
200	0.908	-0.418	6.44

TABLE 8.5

RESULTS OF FIELD ON GROUND STATE HEAVY HOLE

FIELD (kV/cm)	a_0	a_1	a_2	a_3	a_4	E_{hh}
0	1.00	0.00	0.00	0.00	0.00	-5.83
20	0.973	0.228	-0.0227	-0.00515	0.000935	-4.85
40	0.914	0.397	-0.0761	-0.0156	0.00369	-2.17
60	0.851	0.506	-0.138	-0.0320	0.00819	1.69
80	0.794	0.573	-0.197	-0.0527	0.0143	6.37
100	0.745	0.613	-0.249	-0.0756	0.0217	11.6
120	0.704	0.638	-0.294	-0.0995	0.0302	17.3
140	0.668	0.653	-0.333	-0.123	0.0394	23.3
160	0.637	0.661	-0.365	-0.146	0.0491	29.6
180	0.610	0.664	-0.393	-0.168	0.0590	36.1
200	0.586	0.665	-0.416	-0.189	0.0690	42.8

The field is assumed to be constant over the MQW region and the new energy eigenstates are assumed to be linear combinations of the zero field eigenstates. The two wavefunctions of Figure 8.2 are mixed to give the perturbed conduction band wavefunction and the five wavefunctions of Figures 8.3 and 8.4 are mixed to give the perturbed valence band wavefunction. Tables 8.4 and 8.5 give the coefficients of the linear combinations as well as the new energy eigenvalues for the ground state electron level and ground state heavy hole level. The energies for the electron state are referenced from the bottom-centre of the conduction band well and for the heavy hole state from the top-centre of the valence band (middle of the well in both cases).

Using the coefficients of the linear combination and the zero field wavefunctions, the ground state electron and ground state heavy hole wavefunction can be calculated for the fields of Tables 8.4 and 8.5. These wavefunctions are shown for a range of fields in Figures 8.5 and 8.6. The confining nature of the well is very evident in the thinning and peaking of the wavefunctions at high field.

If it were not for the coulomb interaction in the form of the exciton the calculation would now be complete. However, the coulomb potential produces a red shift in the excitonic resonance peak. A method of calculating this binding energy was outlined in the previous chapter. It consists of using the calculated single ground state wavefunctions, a simplified form of the complete

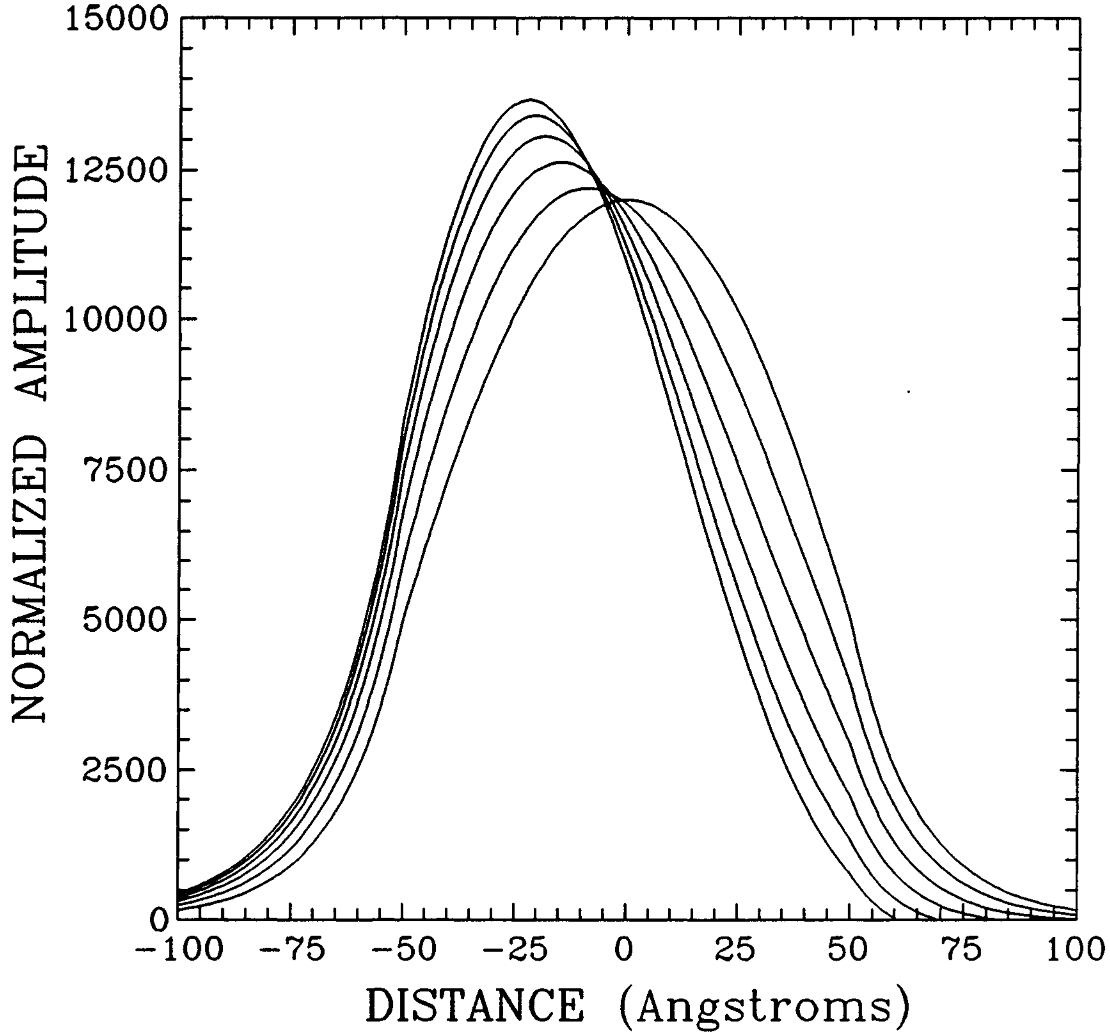

Figure 8.5 The ground state conduction band wavefunctions for 0 to 200 kV/cm applied fields in 40 kV/cm increments (well ±50Å).

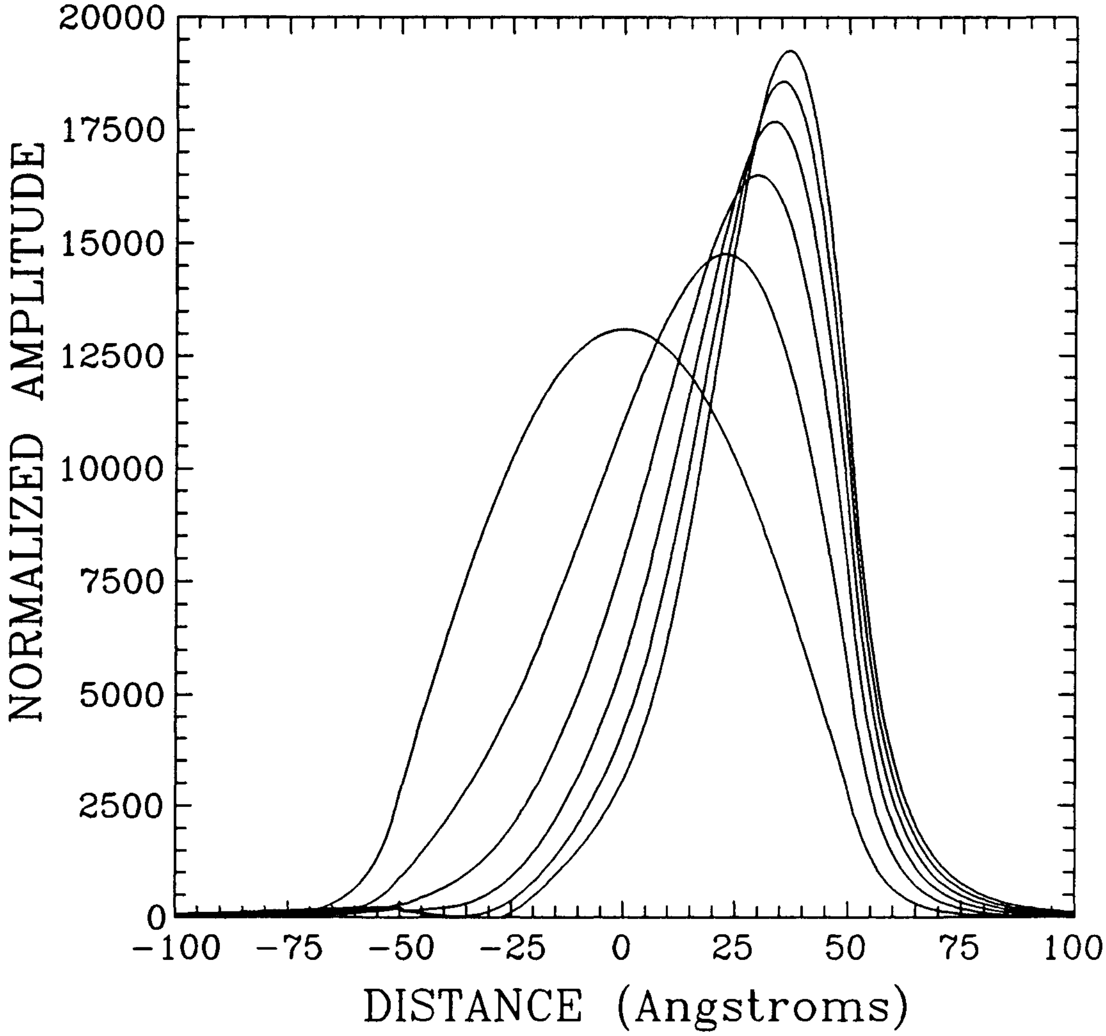

Figure 8.6 Ground state valence band wave functions from 0 to 200 kV/cm of applied field in 40 kV/cm increments (well ±50Å).

excitonic wavefunction and a fitting parameter. The parameter was changed to minimize the expectation value of the simplified radial Hamiltonian which was given in the previous chapter. The results of just such a calculation are presented in Figure 8.7.

The binding energy is a maximum at zero field since the expectation value of the distance between the particles (the excitonic radius) is a minimum. As the field is increased the particles are forced to opposite sides of the well and the average coulomb force is smaller. Note that the binding energy tends to saturate out at high fields. This saturation may be partially an artifact of the model. It is due to the model not being able to predict the extent of the wavefunction which exists outside the well at high fields (tunnelling neglected). This failure occurs due to the finite number of states over which the linear combinations are taken.

Figure 8.8 gives the expectation value of the in-plane excitonic radius as a function of electric field. It is easy to see the reason for the lesser binding energy at high fields since the electrons and holes clearly have a greater separation both radially and perpendicular to the layers.

Finally the position of the heavy hole exciton resonance peak may be found. The photon energy required to excite the resonance is the difference

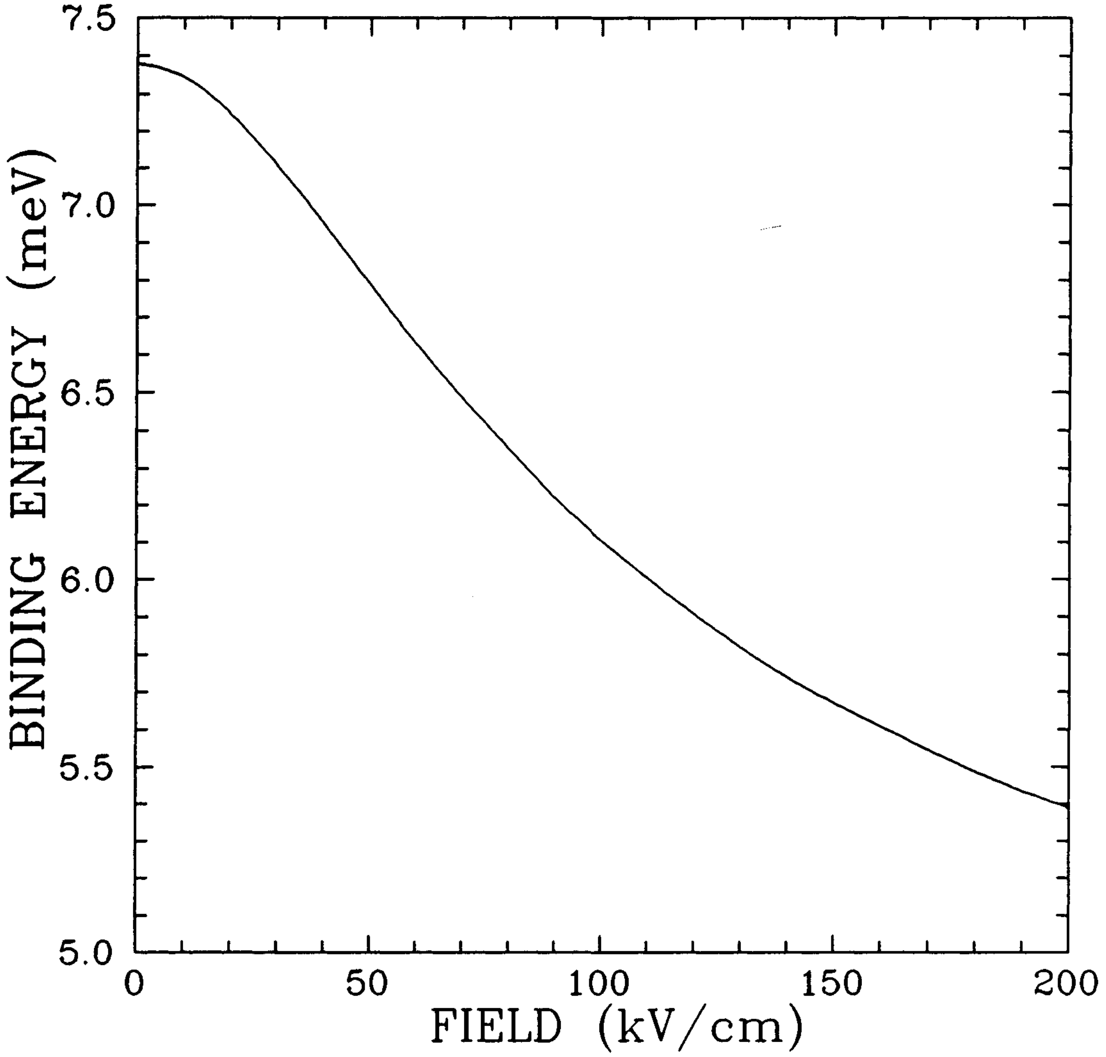

Figure 8.7 The exciton binding energy as a function of the applied electric field for material MBE 852.

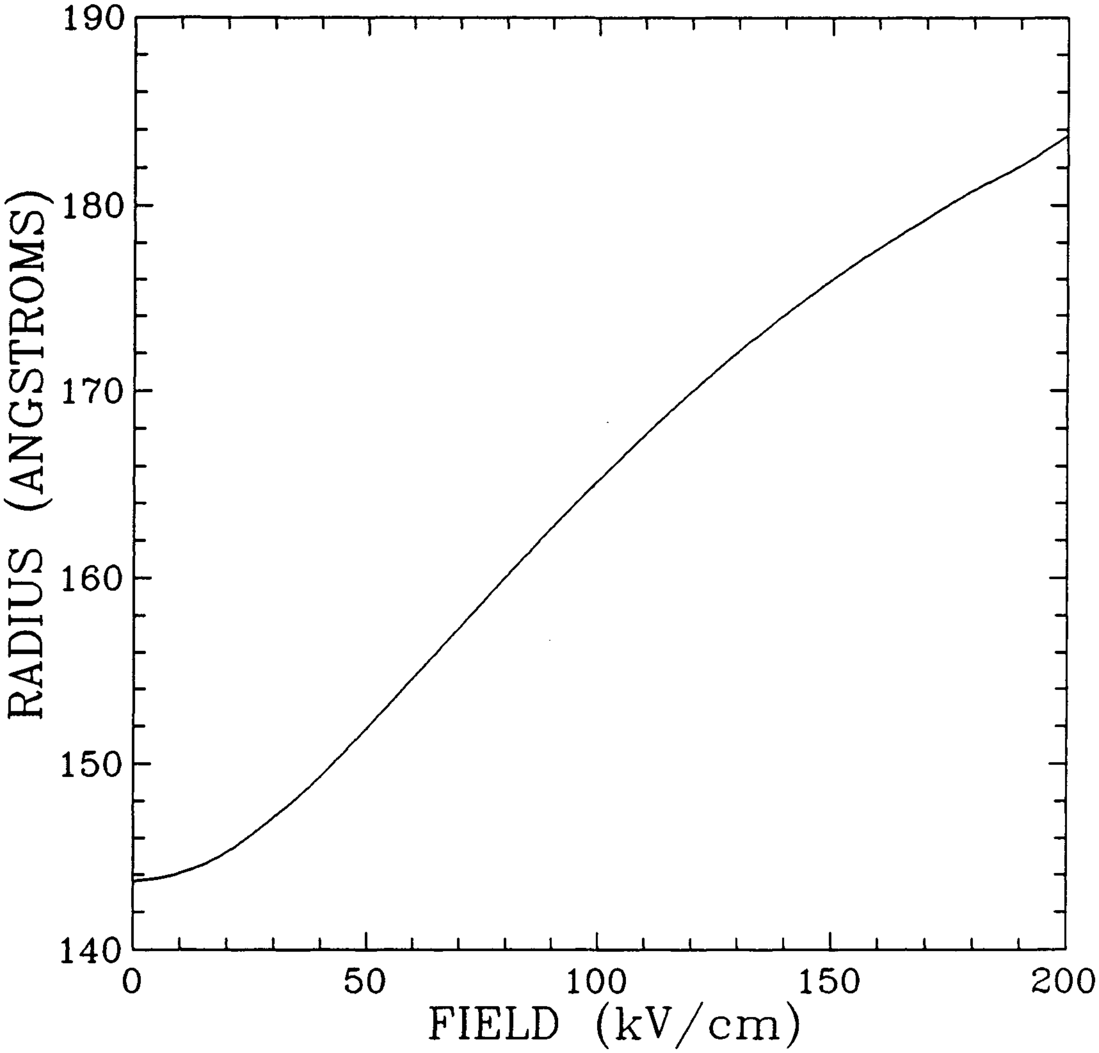

Figure 8.8 The expectation value of the in-plane component of the excitons radius.

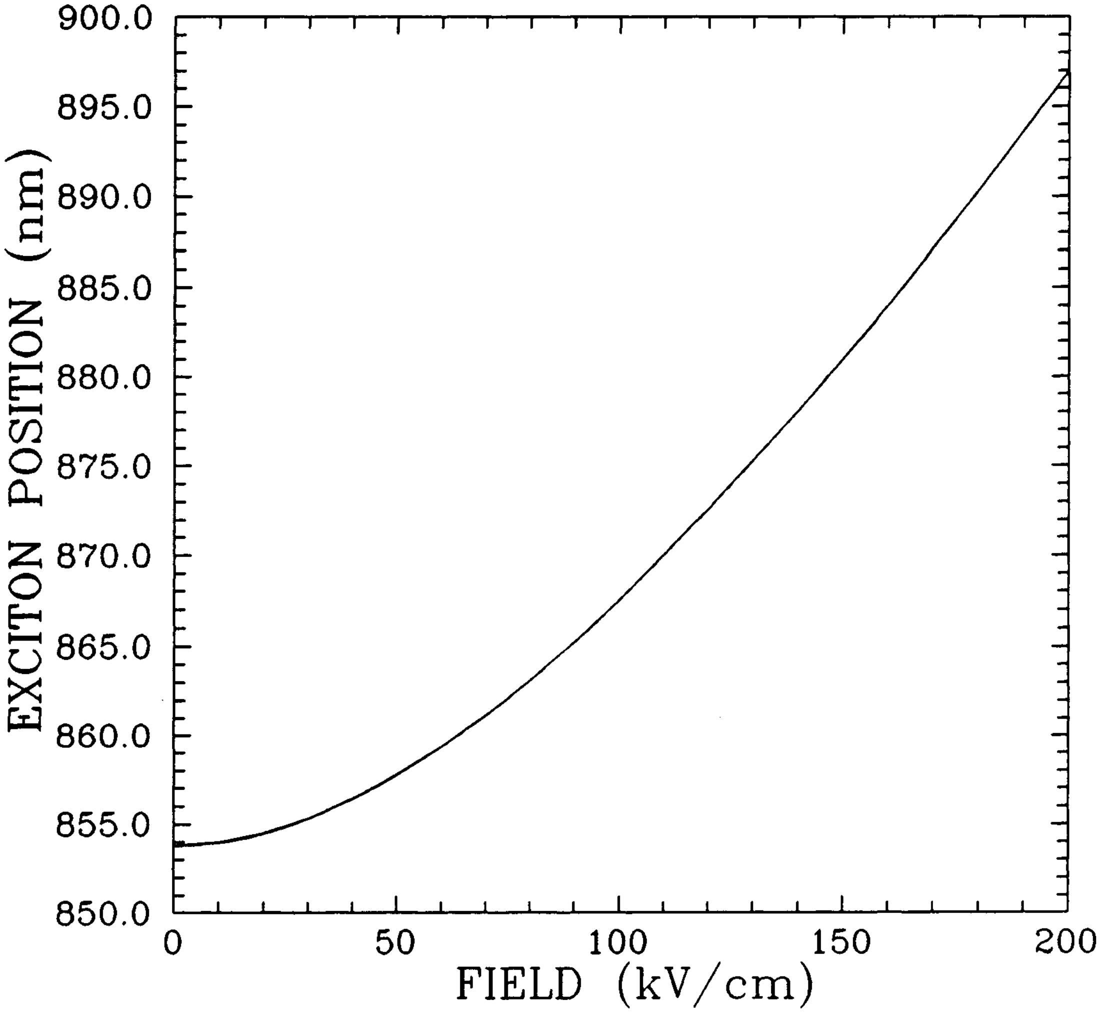

Figure 8.9 The excitonic transition wavelength as a function of electric field.

in energy between the ground heavy hole state and the ground electron state less the binding energy. The expected position of the resonance peak for the MBE 852 material is shown in Figure 8.9.

CHAPTER NINE

MEASUREMENT OF THE FIELD INDUCED EXCITON SHIFT

9.1 Chapter Introduction

In order to observe the shift of the effective optical band edge as a function of field (due to the QCSE), two types of experiments were performed. The first of these was the measurement of the optical transmission spectrum as a function of applied reverse bias voltage in a waveguide geometry. The sample MBE 852 will waveguide light in the plane of its layers with the intrinsic MQW region being the waveguide.

The optical transmission characteristics are the quantity of interest in the design of optical modulators. The transmission characteristics were examined for a range of between zero and ten volts reverse bias. The light output measured was the TE polarization which is the polarization of interest for integration due to the output of semiconductor lasers being predominately TE polarized.

The second type of experiment consisted of examining the photocurrent produced by optical excitation of specific wavelengths. Again this was performed for TE polarized light in a waveguide geometry as well as for light perpendicularly incident on the active MQW layers. This type of experiment is useful for the examination of these materials as detectors.

9.2 Transmission Measurement Technique

The experimental apparatus for examining the transmission characteristics of the multiple quantum well material MBE 852 are pictured in Figure 9.1. A tungsten-halogen lamp was monochromated (20 Å spectral width) and used as the light source. The difficulty with this source is the low spectral power density which translates into a low optical power available for this experiment.

The output of the monochromator was coupled into a single mode fibre splitter with two inputs and two outputs. One of these outputs was butt coupled to a cleaved edge of the sample material. A 1.15μm helium-neon laser was coupled into the other fibre input. The helium-neon laser was required for alignment purposes to couple light from the fibre into the samples waveguide region. The very low power available from the monochromated white light source (~3 pW) was inadequate for observation of the waveguide output with an infra-red viewer. The laser output could be observed quite easily and once coupling into the waveguide region was observed the laser was turned off and not used for any other purpose.

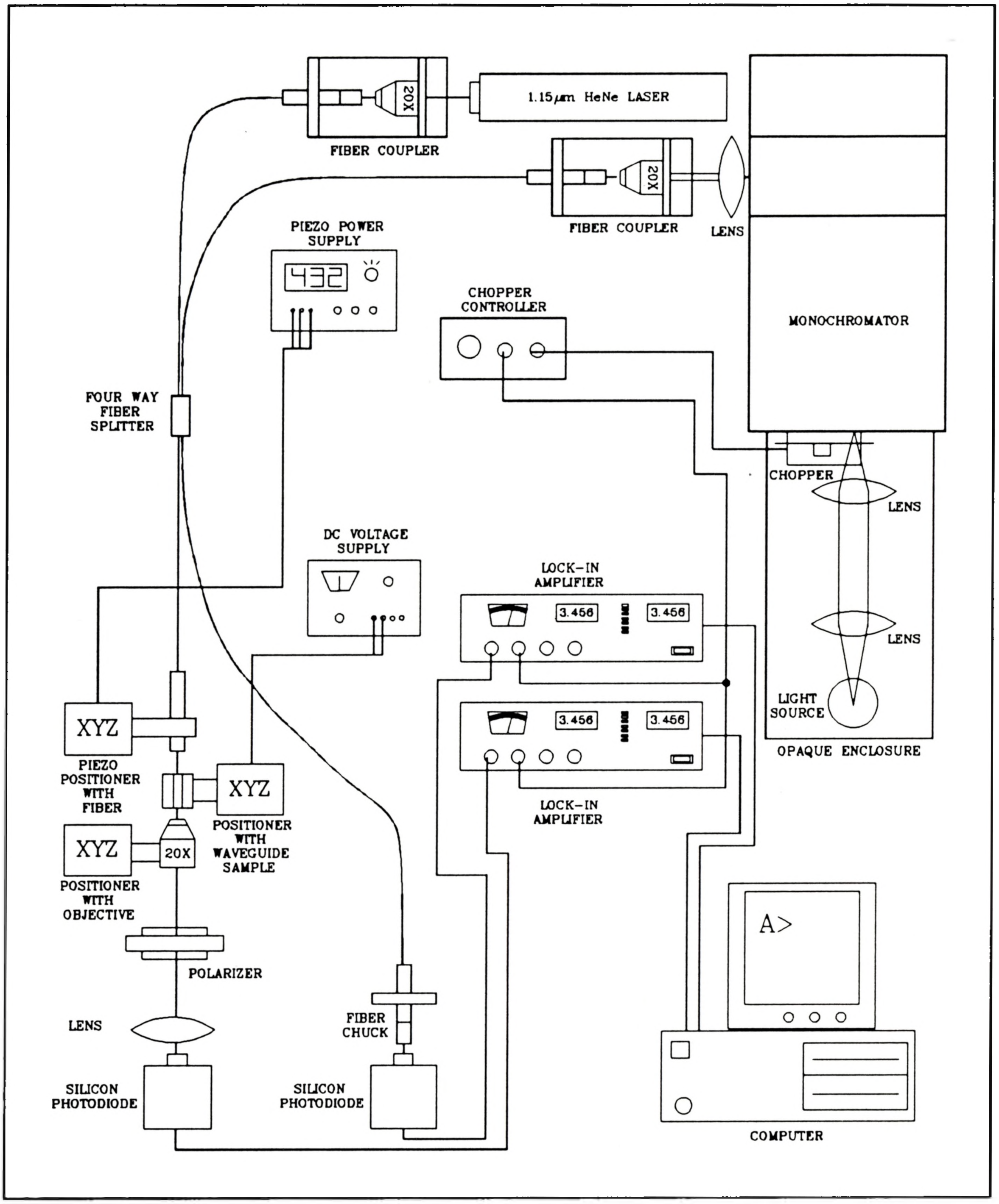

Figure 9.1 The experimental apparatus for the optical transmission measurements.

The second fibre output was used to monitor the real-time power output of the light source. This provided a way of correcting for changes in the actual power in the fibre due to source or coupling changes. The power was monitored with a silicon photodiode. The wavelength dependency of the fibre coupler was accounted for.

The light transmitted through the sample was collected and collimated with a 20x microscope objective. A polarizer was used to select the polarization component of interest and the resulting beam was focused onto a second silicon photodiode. The entire experiment was computer controlled and lock-in detection was used. The optical chopper provided the reference signal for the lock-in amplifiers. Data collection consisted of scanning the monochromator over the interesting wavelength range and measuring the transmitted power every 2Å. The applied voltage was then changed and the scan repeated.

9.3 Transmission Measurement Results

The optical transmission spectrum for TE polarized light is shown in Figure 9.2. The shift in the band edge is approximately 12 nm over the 10 volts applied bias range. The sample length used in these experiments was 1.4mm long. Shorter sample lengths would have been preferred for reasons

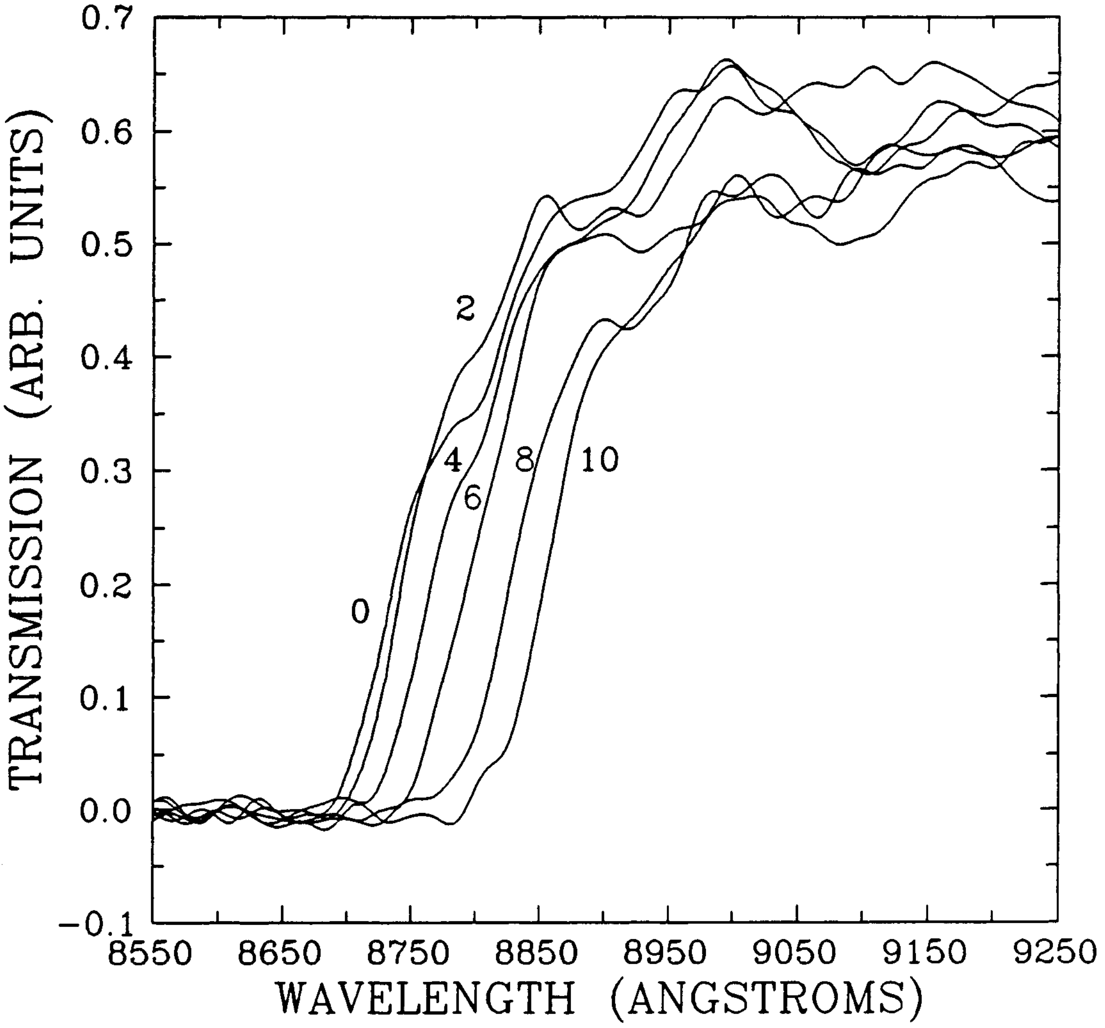

Figure 9.2 The transmission spectra for TE polarized light waveguiding through the intrinsic MQW region. Applied voltages of 0,2,4,6,8 and 10 V.

outlined below. Unfortunately, shorter samples were not practical in this material due to difficulties in cleaving good end faces in short samples. There is no observable exciton peak in these results due to the long samples. Since the waveguiding light traverses such a long length of material, it has a large total absorption (due to the interaction length) even when there is only a small amount of excitonic absorption present. The result of this is that the edge feature which is being observed is the long wavelength tail of the heavy hole exciton peak. The point at which the exciton peak occurs the sample is essentially non-transmitting.

Due to the low power at which the experiment was carried out and the unknown effects of coupling changes it is difficult to get a measure of the actual switching ratios which may be attained although the data indicate that approximately 20 to 1 switching ratio is present. This estimate was corroborated by photocurrent data which will be discussed in the next two sections.

9.4 Photocurrent Measurement Technique

The experimental apparatus used to measure the photocurrent spectrum of the MBE 852 material is pictured in figure 9.4. It uses an argon laser pumped titanium-sapphire laser as a tuneable pump source. This laser can be

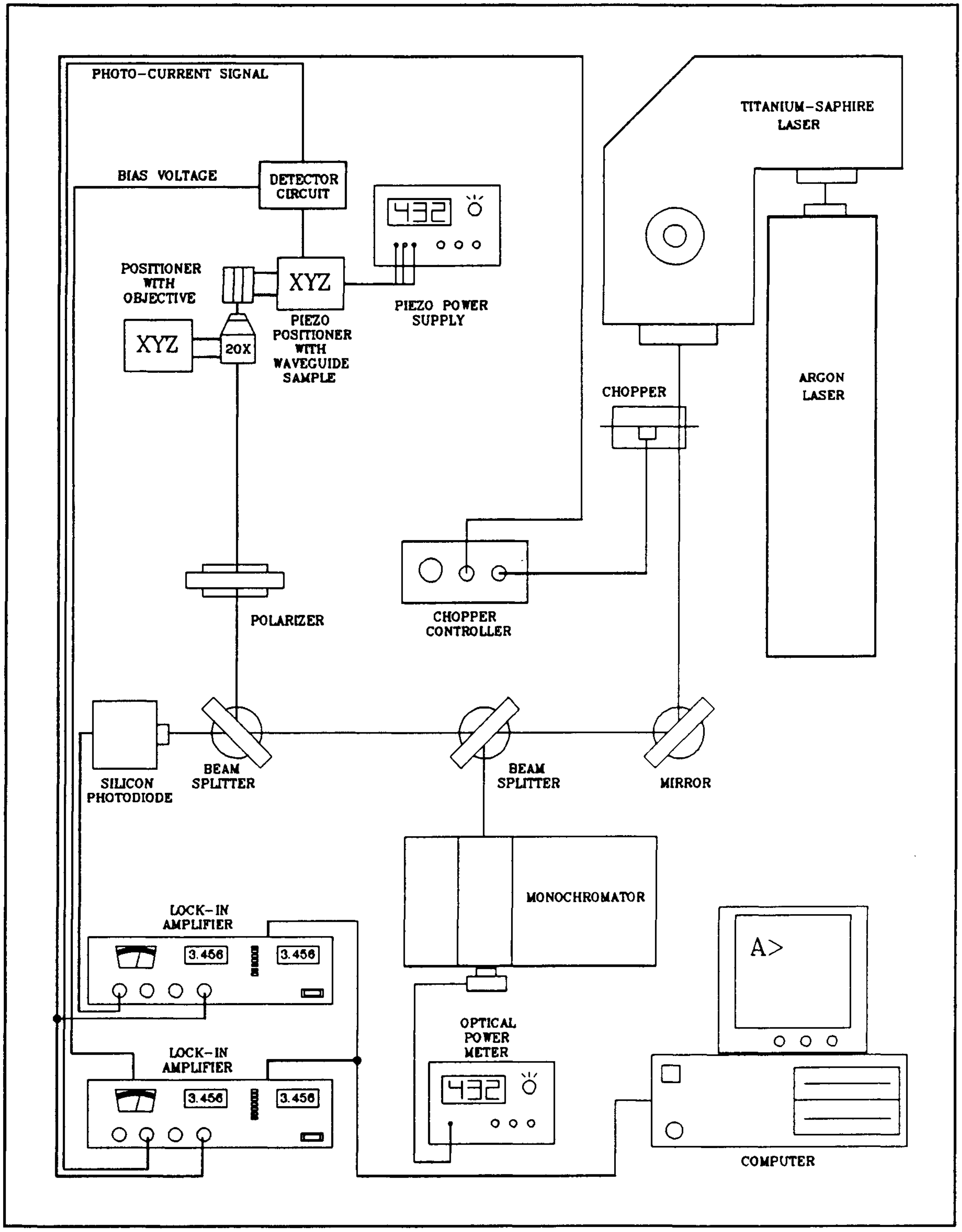

Figure 9.3. The experimental apparatus for the photocurrent measurements.

tuned from 700 to 1000 nm with a spectral width of less than 2 GHz. The argon pump was in the three to six Watt range and the titanium sapphire laser produced output powers in the one Watt range at the wavelengths of interest.

Due to the excess of power that was available from the laser much of it had to be bled off to assure measurements which did not saturate the detector response. Two beams which constituted the great majority of the power of the laser were split off. One of these was used to monitor the output power of the laser by directing it to a silicon photodiode. The other beam was used, along with a monochromator, to tune the laser to the desired wavelength.

The remaining beam had an optical power of approximately 300 μW. It was coupled into the waveguide region with a 20x microscope objective. Both the photocurrent and the output of the photodiode were measured with lock-in amplifiers. The bias voltage was controlled from an analog output which was incorporated in one of the lock-in amplifiers.

The entire experiment was controlled by a computer via an IEEE 488 bus. The exception to this was the laser wavelength which had no provision for remote scanning.

Data were taken for the TE polarization which was selected by a Glan-Thompson polarizing prism. A single measurement set consisted of applying bias voltages between zero and ten volts at 0.025 V intervals at a specific wavelength. Scans were taken at wavelength intervals of 2Å.

Data were also taken for a beam which was incident perpendicular to the layers. The advantage of this geometry is the interaction length becomes the approximate thickness of the multiple quantum well region which in this case is just over a micron. This short interaction length allows features at the high absorption end of the spectrum to be visible. The sample had a window etched through the gold contact and through the absorbing GaAs cap layer.

9.5 Photocurrent Measurement Results

The photocurrent response to TE polarized light in the waveguide geometry is shown in three formats in Figures 9.4, 9.5 and 9.6. Figure 9.4 is a three dimensional surface plot where the photocurrent is shown as a function of both the wavelength of incident light and the applied bias voltage. Figure 9.5 shows the same data but is presented in a topographical format which gives a view of the surface which is not affected by the perspective chosen. Finally Figure 9.6 shows photocurrent response as a function of wavelength for the two extremes of applied bias voltage. Similar curves for the transverse geometry is presented in Figures 9.7, 9.8 and 9.9.

In a multiple quantum well structure one expects a quantum efficiency of close to one. The photocurrent spectra should then be the equivalent of the absorption spectra. With this in mind a comparison of the edge position in

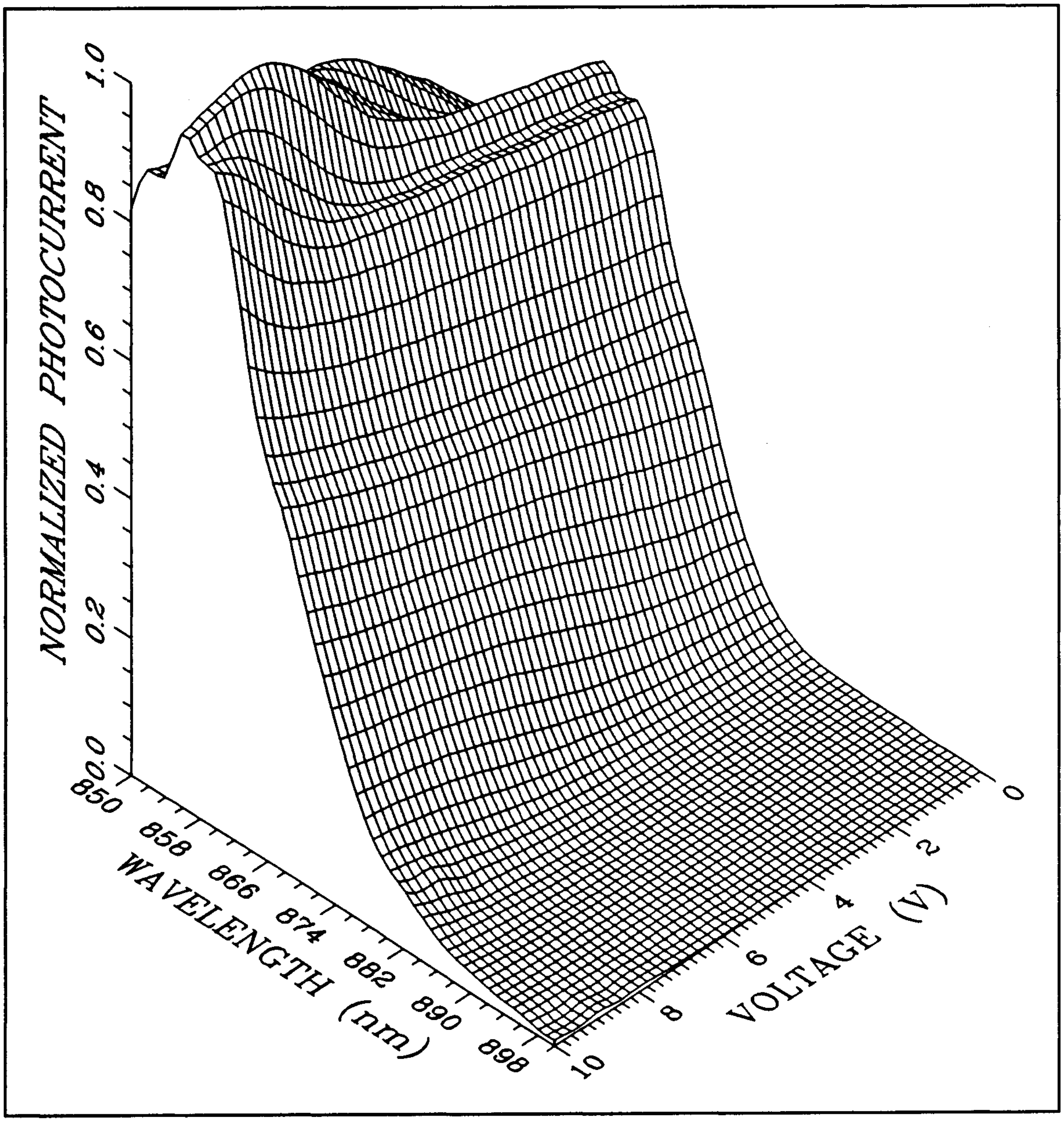

Figure 9.4 A surface plot of the photocurrent response of sample MBE 852 to TE polarized light.

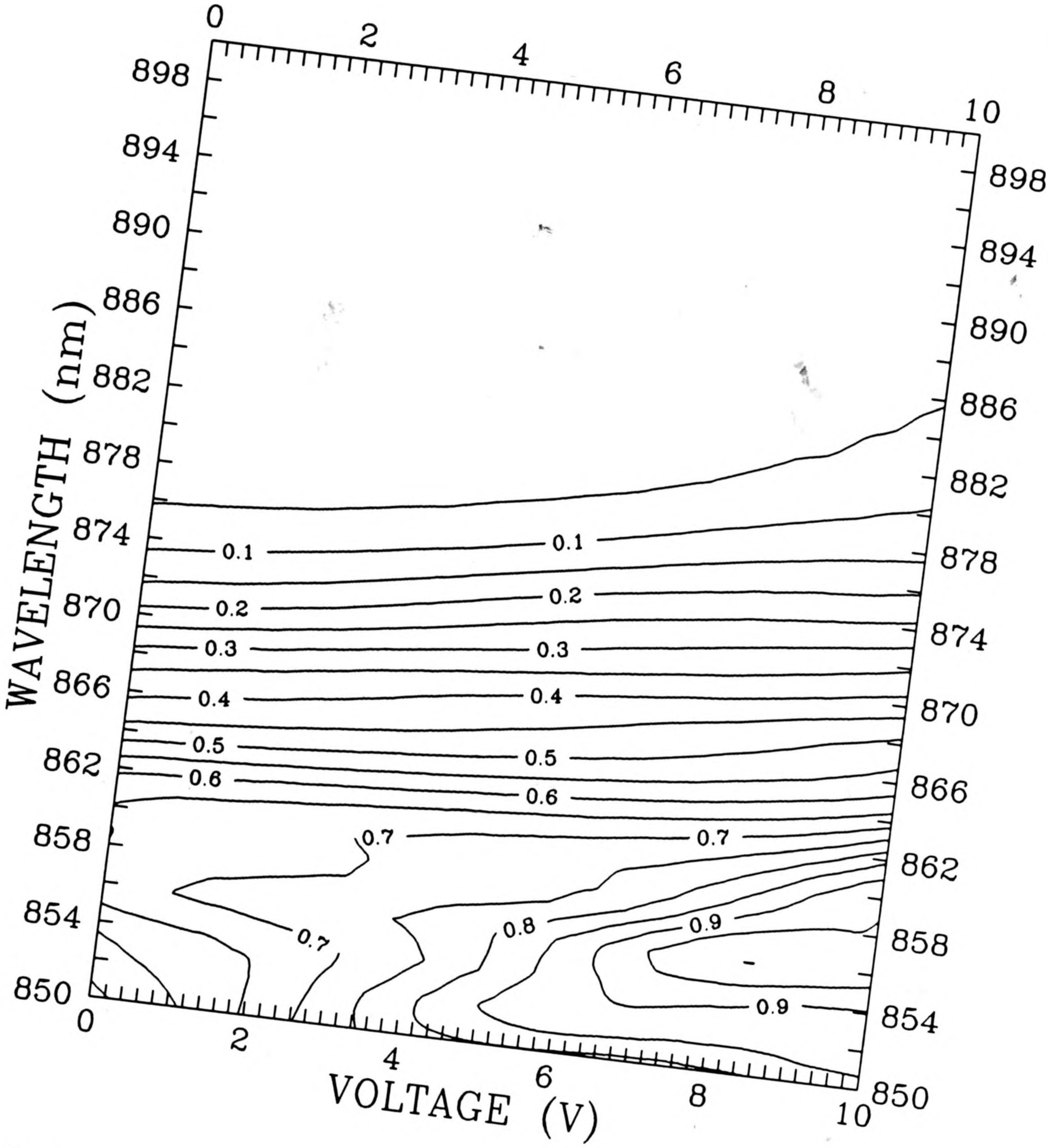

Figure 9.5 A topographical plot of the photocurrent response to TE polarized light waveguiding in the intrinsic MQW region.

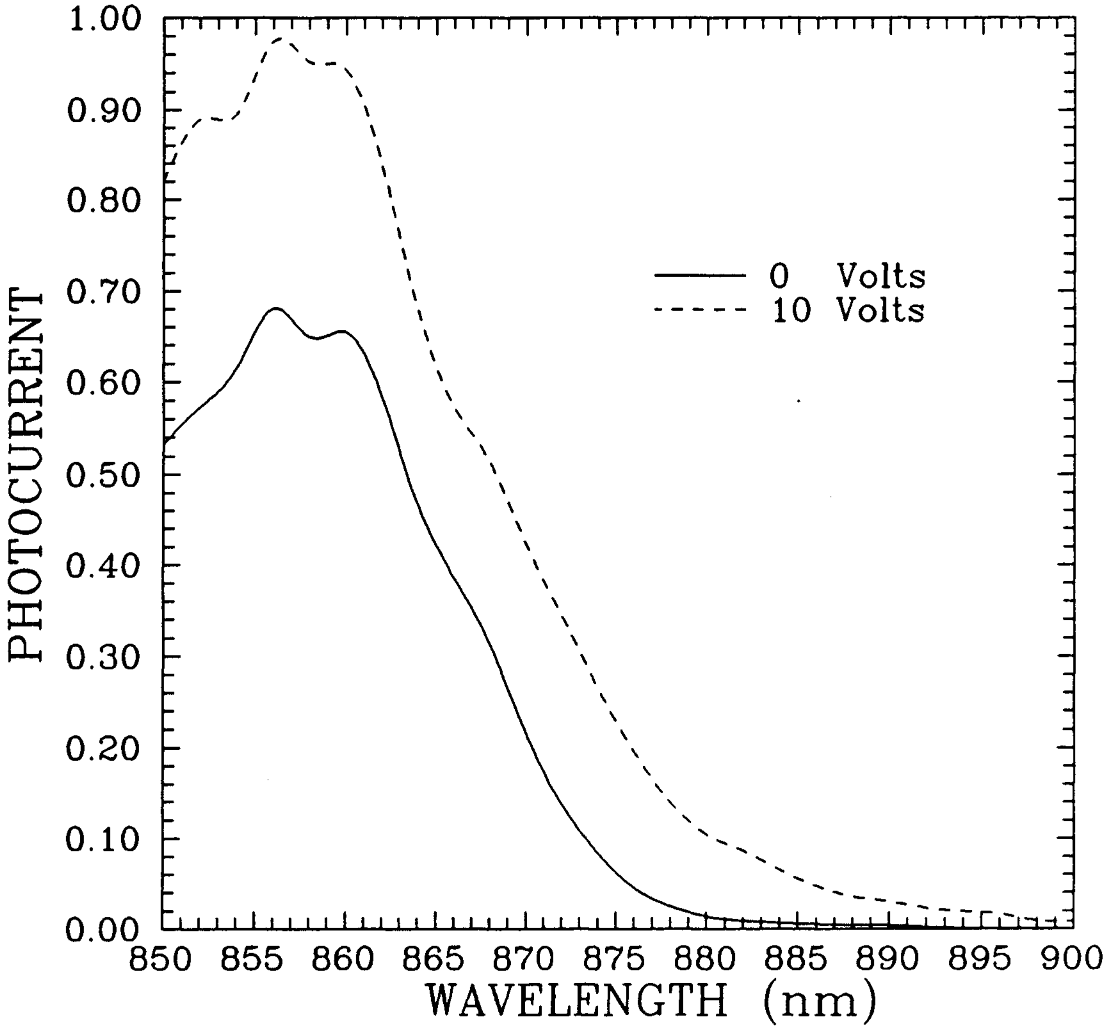

Figure 9.6 The photocurrent as a function of wavelength for TE incident light in sample MBE 852 for the two extremes of applied bias voltages of this experiment - zero and ten volts.

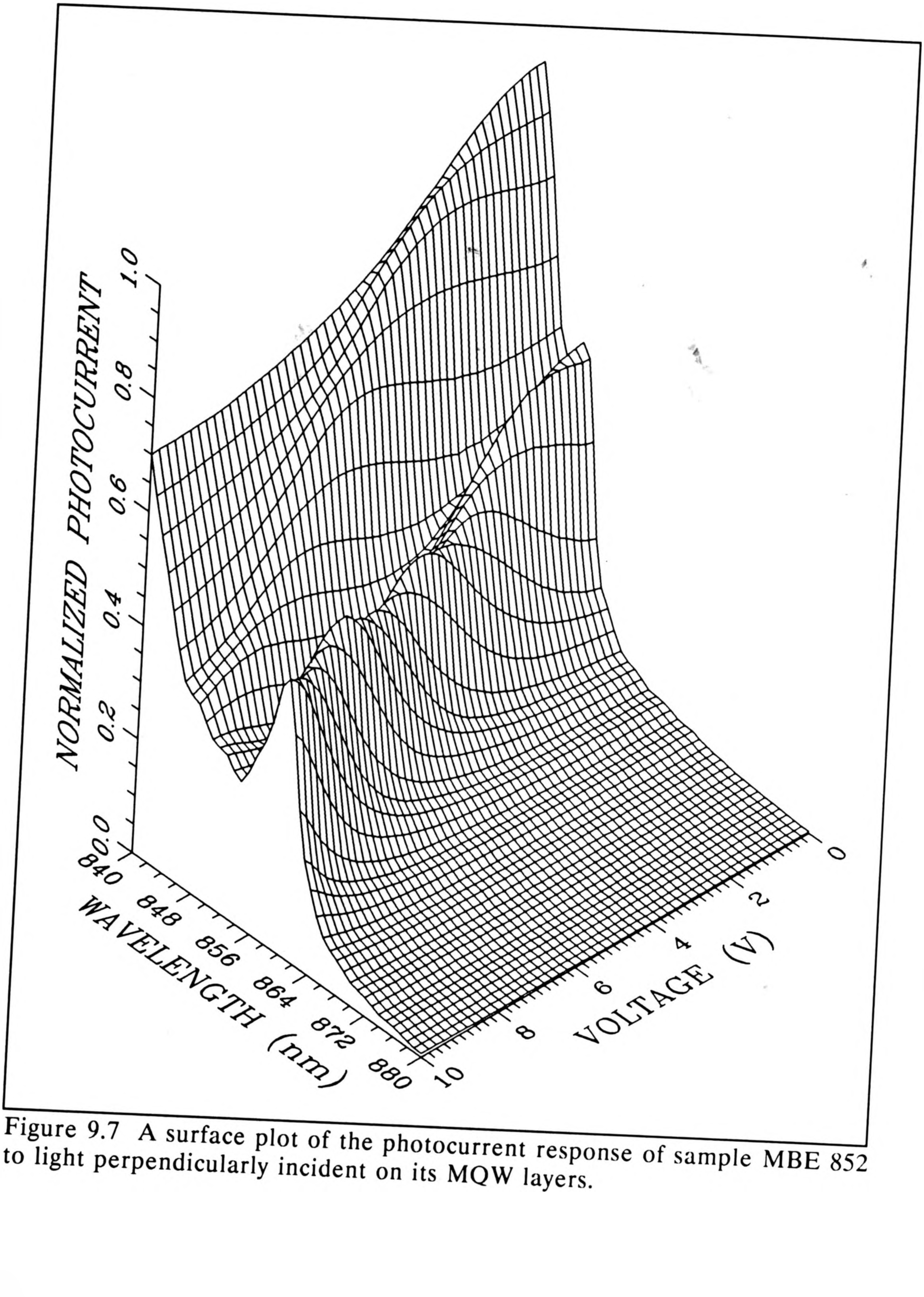

Figure 9.7 A surface plot of the photocurrent response of sample MBE 852 to light perpendicularly incident on its MQW layers.

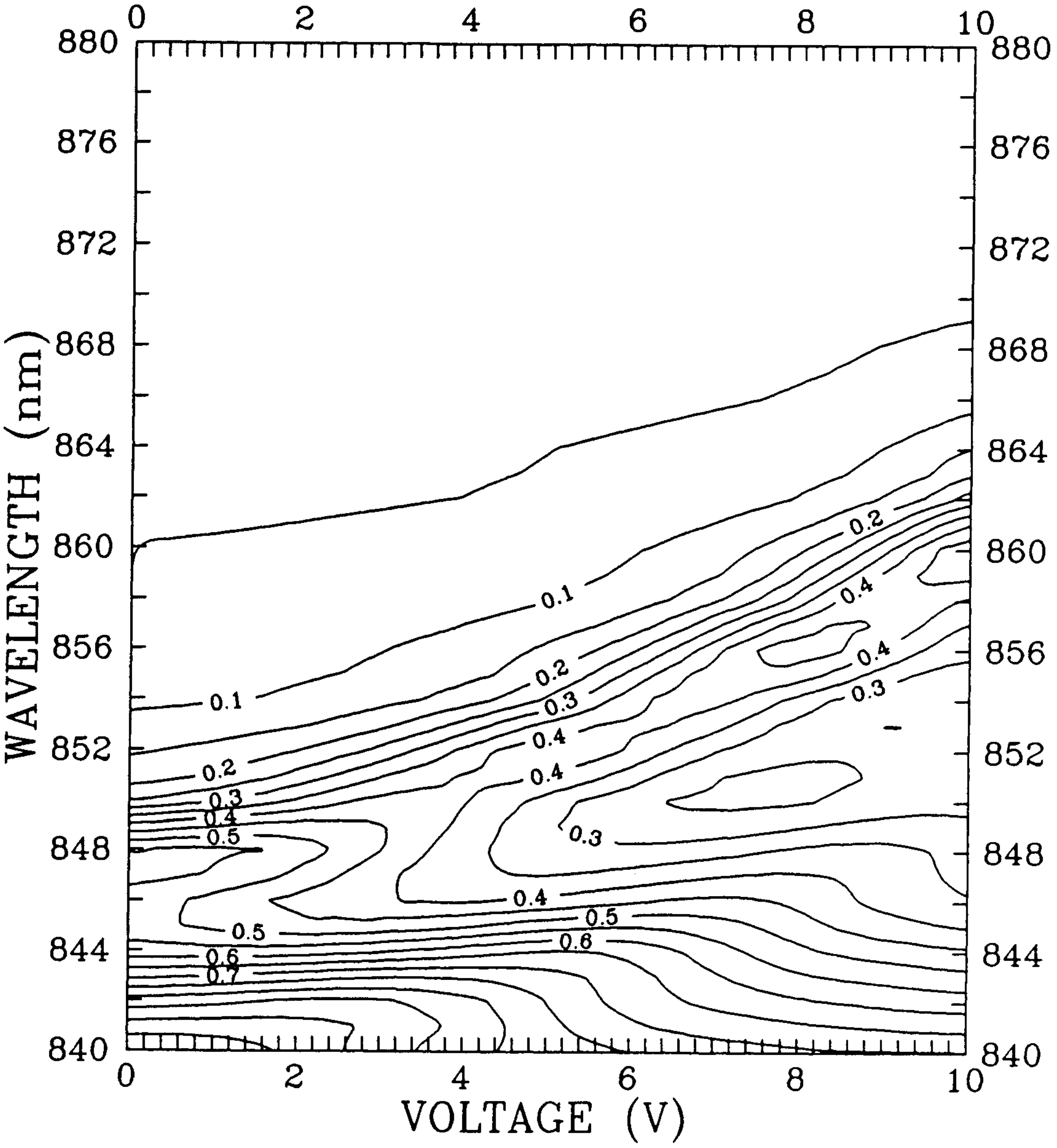

Figure 9.8 A topographical plot of the photocurrent response of sample MBE 852 to light perpendicularly incident on its MQW layers.

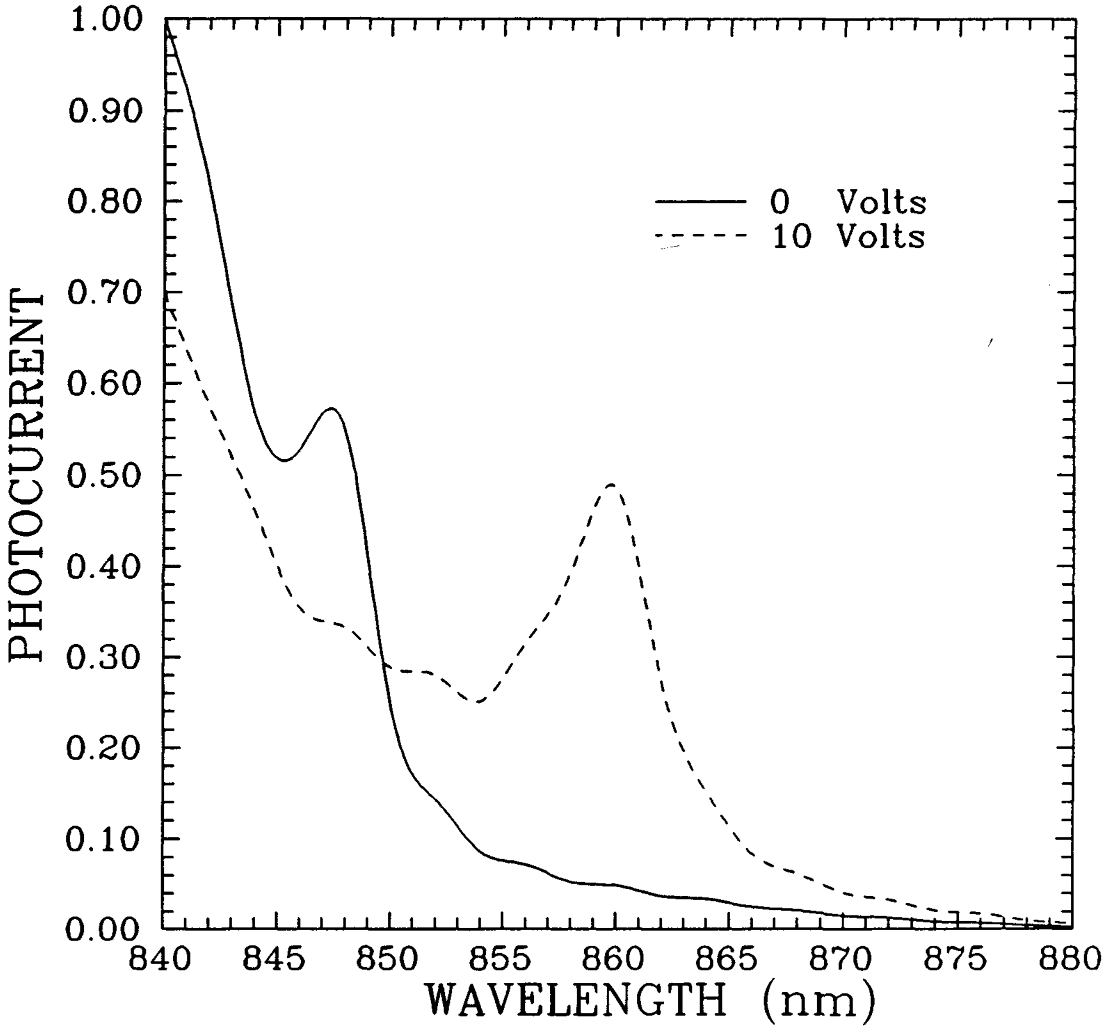

Figure 9.9 The photocurrent as a function of wavelength for light perpendicularly incident on the MQW layers for two applied bias voltages used in this experiment - zero and ten volts.

Figure 9.2 with the surface plot in Figure 9.4 illustrates that the transmission curve features are in fact just the tail end of the exciton feature.

In the TE waveguide plots there are some interesting and unexpected features. It was expected that as the absorption increased that somewhere on the short wavelength side of the exciton peak essentially all of the light would be absorbed. This would result in a near flat top surface. Figure 9.4 clearly show that a peaking occurs. This is most likely due to light that is not coupled into the waveguide mode but still passes through the active layer. Otherwise the waveguide photocurrent results are just as expected.

Figure 9.7 is very interesting due to the visibility of the heavy-hole excitonic resonance peak. Its shift to longer wavelengths with increasing field is very evident in all three figures (9.7, 9.8 and 9.9). Also noticeable is the peak height lowers with increasing height as would be expected from overlap integral arguments (transition probability) although this lowering is less than would be expected from such calculations. Broadening of the peak with field is also visible although difficult to measure due to the background and the sparseness of data. Such broadening is expected because as fields increase the tunnelling probability increases and lifetime broadening occurs.

The shift induced with a ten volt applied bias is ~ 12 nm. The maximum ratio of photocurrents measured was approximately 20 to 1 range and occurred far down in the exciton tail but approximately the same ratio was observable in both geometries. This is interesting since the longer interaction length of the waveguide sample would predict a higher switching ratio. The reasons why this is not the case are difficult to ascertain due to the absence of absolute measurements. Of particular importance would be a measurement of the optical transmission spectrum perpendicular to the layers. This was not possible since the sample used here was not grown with AlAs stop-etch layers which are required if one is to use wet chemical etching to remove the absorbing substrate.

The usefulness of an absolute transmission measurement over a small interaction length lies in its ability to closely approximate the absorption coefficient spectrum. Information on absolute values of the absorption coefficients could be obtained, including the bulk absorption. These numbers are important for both the photocurrent experiments as well as for the waveguide transmission spectrum.

The importance of these absolute numbers for interpreting the transverse photocurrent data stems from possible differences in the two spectra from changes in the quantum efficiency of the device with field. This information is especially important when magnified by the interaction length of a waveguide experiment.

Absolute absorption values are also important for the design of a waveguide modulator. It is apparent from a comparison of the waveguide data and the transverse photocurrent data that as the interaction length is increased, the useful wavelength of the device shifts to longer wavelengths. At these longer wavelengths, the bulk absorption effects as well as the waveguide losses will become more comparable to the losses due to the exciton. These other losses will adversely affect the switching ratio in longer devices.

Perhaps the most practical waveguide devices will be of very short interaction length or have small waveguide mode overlap with the high absorption well layers as compared to the waveguide device examined here. These devices would make use of the high 10:1 absorption coefficient change at the exciton's 10 volt position. Due to the lack of information, as discussed previously, numerical predictions of the characteristics of such a device are not practical based on the data presented here.

CHAPTER TEN

SUMMARY OF QCSE RESULTS

10.1 Chapter Introduction

This chapter will first compare the results of the calculated exciton position with the observed exciton position. Areas for future additions to the model will be discussed.

Areas of experimental difficulties and suggested improvements for future similar experiments will be considered.

Finally the future thrust of this research will be discussed.

10.2 Evaluation of the Model

Figure 10.1 shows the experimentally determined exciton positions as a function of applied field as well as the calculated positions using the model (These calculated values are different from those of Figure 8.9 due to a temperature correction of the GaAs bandgap.). The solid line is a result of the method of calculation described in this thesis. The dashed line which closely follows the solid line is a calculation using an Airy function solution[44]. The Airy function solution is exact for linear potential variations and shows

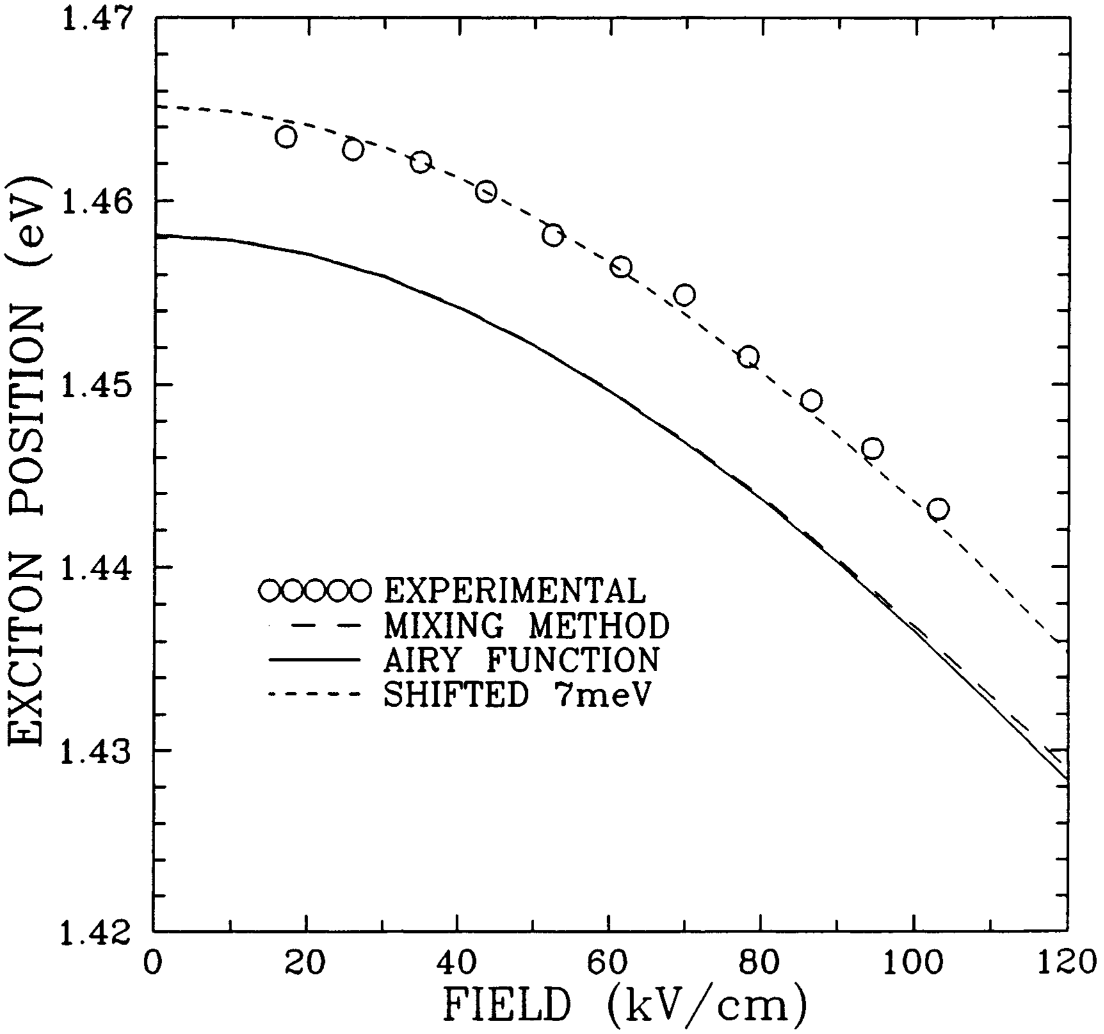

Figure 10.1. A comparison of the calculated and experimental shifts. The dashed line is the actual calculated result. The solid line is blue shifted by 7 meV to allow comparison of the shifts with experimental data (circles).

the validity of this model. The other dashed curve is blue shifted by 7 meV to allow comparison of the shifts assuming the discrepancy is due to a wider well gap.

Comparison with the experimental results of Lengyel et al[34]. show a similar shift. However Miller et al[29]. present experimental results which would agree with this type of calculation. The reason for these large discrepancies of absolute exciton position in such nominally similar materials is unknown but, in general, the wells need to be more confining than predicted or there must be some mechanism for increasing the bandgap in the wells. Aluminum contamination of the wells is one possible explanation. Such a contamination of less than one percent Al in the well regions is all that is required to account for the shift. The important thing to note about this discrepancy is that it is not an artifact of this method. Any model which begins with the square well approximation at zero field will predict a similar shift. This shift is too large to be strictly from uncertainties in the materials parameters.

10.3 Failures of the Model

Although the shifts can be well modelled, if good predictions of actual device characteristics are required, additional parameters must be added to the model. In Chapter Nine, the importance of the exciton spectral width was seen. In the waveguide transmission curves it was pointed out that the difference between significant transmission and absorption can, depending on interaction length, lead to device operation on the long wavelength tail of the exciton. Not only must the zero field broadening be included but field dependent broadening mechanisms must be included. The broadening mechanisms include phonon ionization, tunnelling, and field non-uniformity. These broadening mechanisms will probably not be able to be treated well using the approximate wavefunctions of this method. However, if some general rules and expectations of the broadening can be developed, this method of modelling the shifts would present a quick and easy tool for designing electroabsorption modulators and detectors.

10.4 Conclusions

This project has produced the grounding for future work in optical waveguide modulators and wavelength selective detectors. Good qualitative understanding of the mechanisms which affect the absorption of MQW materials at the bandgap has been found. This qualitative understanding provides the grounding for the design of better and more complex experiments in the future which will allow for more quantitative measurements.

Quantitatively the approximate maximum field-induced change in the absorption coefficient of this material was found to be approximately 20:1 with the ratio being 10:1 at the exciton's 10 volt position. It is believed that proper modelling of the exciton broadening will give insight which will allow better ratios to be obtained in the future. The quantum-confined Stark shift was shown to be fairly well modelled by examining the shift in the single particle conduction and valence band energies along with the shift in the Coulombic binding energy. The absolute exciton position was not well predicted and the reason for this is unknown, although this is not an isolated observation.

Work in the future should focus on single mode waveguide measurements and modelling. The waveguide experiments in this work were accomplished in a multi-mode slab geometry which is difficult to model. Single mode waveguides will allow more consistent measurements to be made and better comparisons with theoretical predictions. Single mode waveguide fabrication was not attempted due to the present lack of dry etching facilities and the difficulty in wet etching the narrow, deep ribs required.

A further benefit to fabrication improvements would be the ability to fabricate small waveguide devices which would show the exciton feature in the waveguide geometry. This would also allow the non-waveguiding light to be removed from the experiment which would give a more accurate and consistent picture of the effective band edge.

Future experiments in this area need to concentrate on both optical absorption spectroscopy and photocurrent spectroscopy. The availability of both sets of information will allow the separation of any field induced change in the quantum efficiency of the device. Furthermore work should be done in both transverse and waveguide geometries. The advantage of the transverse geometry is the simplicity of the experiment and the ability to determine absolute absorption measurements with very few external problems. Unfortunately, the present background doping in nominally intrinsic material causes a significant deviation in field across the MQW layers. This is a significant broadening mechanism. If the intrinsic layer is grown with only one well this mechanism will be eliminated. However, the interaction length will be so small that the absorption feature will be more difficult to detect.

Similar experiments in a waveguide geometry hold promise to negate this effect. The waveguide could increase the interaction length of the light with a single quantum well enough that absorption features will be observed. Unfortunately the difficulty of coupling into the waveguide and the proper modelling of the coupling and possible leaky modes add to the complexity of interpreting this type of experiment as well.

APPENDIX A

COMPARISON OF CALCULATIONS FROM PROGRAM EXCITON AND THOSE OF LENGYEL et al.[34]

A.1 Material Parameters

TABLE A.1	
MATERIAL PARAMETERS USED BY LENGYEL et al.[34]	
WELL WIDTH	10.5 nm
BARRIER Al CONC.	0.32
ELECTRON EFFECTIVE MASS	$m_e^* = 0.067 + 0.083 x_{Al}$
HOLE EFFECTIVE MASS	$m_{hh}^* = 0.48 + 0.31 x_{Al}$
COND. BAND DISC. FRACTION	0.60

A.2 Comparison of Results

TABLE A.2		
CONDUCTION BAND SQUARE WELL ENERGY LEVELS		
ELECTRON LEVEL	ENERGY (meV) (Lengyel *et al*[34].)	ENERGY (meV) (This Work)
0	34.21	28.01
1	127.90	110.38
2	233.49	228.39

TABLE A.3

VALENCE BAND SQUARE WELL ENERGY LEVELS

HEAVY HOLE LEVEL	ENERGY (meV) (Lengyel *et al*[34].)	ENERGY (meV) (This Work)
0	-5.75	-5.40
1	-22.86	-21.52
2	-50.83	-48.15
3	-88.47	-84.70
4	-132.69	-129.33

TABLE A.4

GROUND STATE ELECTRON LEVEL vs ELECTRIC FIELD
(Values from the Work of Lengyel *et al*[34].)

FIELD (kV/cm)	ΔE_0 (meV)	a_0	a_1	a_2
0	0	1	0	0
20	-0.216	0.999	-0.048	-0.00092
40	-0.862	0.995	-0.095	-0.0036
60	-1.924	0.990	-0.141	-0.0081
80	-3.387	0.983	-0.185	-0.014
100	-5.226	0.974	-0.226	-0.021

TABLE A.5

GROUND STATE ELECTRON LEVEL vs ELECTRIC FIELD
(Values Calculated with Program EXCITON)

FIELD (kV/cm)	ΔE_0 (meV)	a_0	a_1	a_2
0	0	1	0	0
20	-0.325	0.998	-0.063	-0.00177
40	-1.291	0.992	-0.124	-0.0070
60	-2.876	0.983	-0.182	-0.0153
80	-5.048	0.971	-0.237	-0.026
100	-7.764	0.957	-0.287	-0.039

TABLE A.6

GROUND STATE HEAVY HOLE LEVEL vs ELECTRIC FIELD
(Values from the Work of Lengyel *et al*[34].)

FIELD kV/cm	ΔE_0 (meV)	a_0	a_1	a_2	a_3	a_4
0	0	1	0	0	0	0
20	0.996	0.973	0.231	-0.023	-0.0038	0.00025
40	3.689	0.913	0.401	-0.076	-0.013	0.0012
60	7.547	0.850	0.508	-0.137	-0.027	0.0034
80	12.176	0.794	0.574	-0.195	-0.046	0.0068
100	17.338	0.747	0.614	-0.245	-0.066	0.011

TABLE A.7

GROUND STATE HEAVY HOLE LEVEL vs ELECTRIC FIELD
(Values Calculated with Program EXCITON)

FIELD kV/cm	ΔE_0 (meV)	a_0	a_1	a_2	a_3	a_4
0	0	1	0	0	0	0
20	1.136	0.967	0.252	-0.028	-0.0060	0.00115
40	4.166	0.899	0.428	-0.090	-0.019	0.0045
60	8.455	0.830	0.534	-0.159	-0.038	0.0099
80	13.565	0.770	0.595	-0.222	-0.062	0.0171
100	19.249	0.721	0.630	-0.275	-0.088	0.026

APPENDIX B

B.1 Notes on program EXCITON

The following program calculates shifts in the ground state energy eigenvalues and exciton binding energy as a function of electric field. This information allows the calculation of the exciton peak by adding the energy difference between the ground state heavy hole and the ground state electron and subtracting the positive binding energy.

The program closely follows the method of Chapter Seven. Many of the routines in this program are from or have been modified from *Numerical Recipes*[45].

B.2 Structure of the program EXCITON

The program structure is complex due to its length and will be presented in a diagram of procedure and function hierarchies. General program flow is in a downward direction and program level is shown by indentations.

```
EXCITON
  WAVEFUNCTION
```

```
    ENERGY
        ROOT
            FEVEN
            FODD
    NORMODD
    NORMEVEN
GAMMA
    QROMB
        TRAPZD
            EXPECTVAL
                EVENWAVE
                ODDWAVE
        POLINT
JACOBI
EIGSRT
MNBRAK
    SIGN
    HAMIL
        COULOMB
            QROMB2
                TRAPZD3
                    COULELECS
                        QROMB1
                            TRAPZD2
                                COULHOLES
                                    PSIV
                                    G
                                        STMINNEU
                                        NEUMAN1
                                            BESSJ1
                                              SIGN
                                        STRUVE
                            POLINT
                        PSIE
                POLINT
BRENT
    SIGN
    HAMIL
        COULOMB
            QROMB2
                TRAPZD
                    COULELECS
```

```
      QROMB1
         TRAPZD
            COULHOLES
               PSIV
               G
                  STMINNEU
                  NEUMAN1
                     BESSJ1
                       SIGN
                  STRUVE
         POLINT
      PSIE
POLINT
```

B.3 Listing of the program EXCITON

```
{------------------------------------------------------------------------}
{------------------------------------------------------------------------}
PROGRAM EXCITON(INPUT,OUTPUT);
{------------------------------------------------------------------------}
{   This program calculates the position of the heavy hole exciton peak in a
AlGaAs GaAs multiple quantum well material. It does this by calculating the
square well energy eigenvalues for both the conduction and valence bands. It
then calculates the shift in these states for applied electric field values.
The binding energy is calculated , once these energies and wavefunctions are
known, by using an approximate form of the exciton wavefunction with a fitting
parameter and minimizing the binding energy as a function of this parameter.
The exciton position can be obtained by adding the bulk GaAs band gap to the
ground state conduction band energy, subtracting the negative ground state
heavy hole valence band energy and adding the negative binding energy.
    The program requires as input parameters the concentration of aluminum
in the barriers, the width of the well, and the fraction of the band
discontinuity which appears in the conduction band.
    The program first provides the square well energy eigenvalues and
normalization constants for the conduction and valence bands. Next it gives
the energies of the ground states and the wavefunctions in terms of mixing the
square well eigenstates. The mixing coefficients are provided to allow
construction of the electric field perturbed wavefunctions. The value of the
```

```
exciton binding energy is then provided for the same values of field as
before.}
{----------------------------------------------------------------------}

USES
  PRINTER;

CONST
  M0 = 9.109E-31; {electron rest mass}
  PI=3.14159265358979323844; {value of the constant pi}
  HBAR = 1.055E-34; {Planck's constant/2pi}
  EPS0 = 8.854E-12; {permittivity of free space}
  ECHARGE = 1.602E-19; {electronic charge}


TYPE
  FT = FUNCTION(X1,X2,X3,X4:EXTENDED):EXTENDED;
  FT2= FUNCTION(X1,X2,X3,X4,X5:EXTENDED):EXTENDED;
  FT3 = FUNCTION(X1:EXTENDED):EXTENDED;
  NORMARR = ARRAY [0..10] OF EXTENDED;
  SQUARE = ARRAY[0..10,0..10] OF EXTENDED;

VAR
  NUM,NUMC,NUMV,I,J,FIELD :INTEGER;
  XAL, LZ,
DELTAE,DELEEL,DELEHOL,ME,MH,PARAM,LIMIT,EFIELD:EXTENDED;
  MBELEC,MBHOLE,MWELEC,MWHOLE:EXTENDED;
  ECEVEN,ECODD,EVEVEN,EVODD,K1C,K2C,K1V,K2V: NORMARR;
  GLIT,NROTC,NROTV:INTEGER;
  NORMCEV,NORMCOD,NORMVEV,NORMVOD,A1C,A2C,A1V,A2V:NORM
ARR;
  EC,EV,DC,DV,ALPHA:NORMARR;
  K11,K22,K12,K21,A11,A12,A21,A22,STEP:EXTENDED;
  BAND:BOOLEAN;
  FUNC1,FUNC2:FT2;
  FUNC3:FT3;
  VARRAYC,VARRAYV,VC,VV,VVC,VVV:SQUARE;

TERM,TERM1,TERM2,TERM2A,TERM2B,TERM3,TERM4,TERM5,DELTA:E
XTENDED;

TERM1A,TERM1B,TERM3A,TERM3B,TERM4A,TERM4B,AX,BX,CX,XMIN:
```

```
EXTENDED;
 BDC,K,KW,KB,ANS,FA,FB,FC,MU:EXTENDED;
 OUTFILE: TEXT;
 SP: STRING;



{-----------------------------------------------------------------------}
{-----------------------------------------------------------------------}
FUNCTION
FEVEN(EPS,MSTARW,MSTARB,DELTA:EXTENDED):EXTENDED;
{-----------------------------------------------------------------------}
{ This function is the eigenvalue equation used for the even parity        }
{ solutions.  EPS is an energy related value and FEVEN should be zeroed.     }
{-----------------------------------------------------------------------}

VAR
 T,TERM1,TERM2:EXTENDED;

BEGIN {FEVEN}
 { Check that sqrt argument is positive }
 T:=MSTARW*M0*DELTA*LZ*LZ/(2*HBAR*HBAR);

 IF (T<SQR(EPS)) THEN
  TERM1:=0
 ELSE
  TERM1 := SQRT(MSTARW/MSTARB)*SQRT(T - EPS*EPS);

 TERM2 := EPS*SIN(EPS)/COS(EPS);
 FEVEN := TERM1 - TERM2;
END; {FEVEN}



{-----------------------------------------------------------------------}
{-----------------------------------------------------------------------}
FUNCTION
FODD(EPS,MSTARW,MSTARB,DELTA:EXTENDED):EXTENDED;
{-----------------------------------------------------------------------}
{ This function is the eigenvalue equation used for the odd parity solutions.}  {
EPS is an energy related variable and FODD should be zeroed.              }
{-----------------------------------------------------------------------}
```

```
VAR
 T,TERM1,TERM2:EXTENDED;

BEGIN {FODD}
 { Check that sqrt argument is positive}
 T:=MSTARW*M0*DELTA*LZ*LZ/(2*HBAR*HBAR);

 IF (T<SQR(EPS)) THEN
  TERM1:=0
 ELSE
  TERM1 := SQRT(MSTARW/MSTARB)*SQRT(T - EPS*EPS);

 TERM2 := EPS*COS(EPS)/SIN(EPS);
 FODD := TERM1 + TERM2;
END;   {FODD}



{-----------------------------------------------------------------------}
{-----------------------------------------------------------------------}
PROCEDURE NORMEVEN(K1,K2:EXTENDED;VAR A1,A2:EXTENDED);
{-----------------------------------------------------------------------}
{ This procedure calculates the normalization constants A1 and A2 of the even}
{ parity wavefunctions given the values of the wave number K1 and K2.       }
{-----------------------------------------------------------------------}

VAR
  A,TERM1,TERM2: EXTENDED;

BEGIN { NORMEVEN }
 A := COS(K1*LZ/2)*EXP(K2*LZ/2);
 { integrate cos^2 inside well }
 TERM1 := 0.5*(LZ+(1/K1)*SIN(K1*LZ));
 { integrate the exponential outside the well }
 TERM2 := 2*SQR(A)*(1/(2*K2))*EXP(-K2*LZ);

 { the coefficients are }
 A1 := 1/SQRT(TERM1+TERM2);
 A2 := A1*A;
END; { NORMEVEN }
```

```
{----------------------------------------------------------------------}
{----------------------------------------------------------------------}
PROCEDURE NORMODD(K1,K2:EXTENDED;VAR A1,A2:EXTENDED);
{----------------------------------------------------------------------}
{ This procedure calculates the normalization constants A1 and A2 of the even}
{ parity wavefunctions given the values of the wave number K1 and K2.        }
{----------------------------------------------------------------------}

VAR
  A,TERM1,TERM2:EXTENDED;

BEGIN { NORMODD }
 A:= SIN(K1*LZ/2)*EXP(K2*LZ/2);
 { integrate the sin^2 inside the well }
 TERM1:= 0.5*(LZ-(1/K1)*SIN(K1*LZ));
 { integrate the exponential outside the well}
 TERM2 := 2*SQR(A)*(1/(2*K2))*EXP(-K2*LZ);

 { the coefficients are }
 A1 := 1/SQRT(TERM1+TERM2);
 A2 := A1*A;
END;  { NORMODD }



{----------------------------------------------------------------------}
{----------------------------------------------------------------------}
FUNCTION ROOT(X1,X2,XACC: EXTENDED; OEFLAG:
BOOLEAN;MSTARW,MSTARB,DELTA:
          EXTENDED): EXTENDED;
{----------------------------------------------------------------------}
{ This function uses the bisection method to calculate the root of          }
{ the function FX.  FX is chosen depending on the value of OEFLAG.  OEFLAG
}
{ is true for symmetric wavefunctions.  X1 and X2 must bracket the root.    }
{ XACC is the required accuracy in real units                               }
{----------------------------------------------------------------------}

LABEL 99;

CONST
 JMAX=40;
```

```
VAR
  DX,F,FMID,XMID,RTB: EXTENDED;
  J: INTEGER;
  FX: FT;

BEGIN {ROOT}
  { set function for even or odd parity wavefunction }
  IF OEFLAG THEN
    FX := FEVEN
  ELSE
    FX := FODD;

  FMID:=FX(X2,MSTARW,MSTARB,DELTA);  { DELTA is the well depth }
  F:=FX(X1,MSTARW,MSTARB,DELTA);

  IF((F*FMID) >= 0.0) THEN
    BEGIN
      WRITELN('pause in RTBIS');
      WRITELN('bracketed roots needed for bisection.');
      READLN;
    END;

  IF (F < 0.0) THEN
    BEGIN
      RTB:=X1;
      DX:=X2-X1;
    END
  ELSE
    BEGIN
      RTB:=X2;
      DX:=X1-X2;
    END;

  FOR J:=1 TO JMAX DO
    BEGIN
      DX:=DX*0.5;
      XMID:=RTB+DX;
      FMID:=FX(XMID,MSTARW,MSTARB,DELTA);
      IF(FMID <= 0.0) THEN RTB:=XMID;
      { check for accuracy }
      IF((ABS(DX) < XACC) OR (FMID = 0.0)) THEN GOTO 99
    END;
```

```
  WRITELN('pause in RTBIS - too many bisections');
  READLN;
  99: ROOT := RTB;
END;  {ROOT}



{---------------------------------------------------------------------------}
{---------------------------------------------------------------------------}
PROCEDURE
ENERGY(OEFLAG:BOOLEAN;DELTA,MSTARW,MSTARB,PARAM:EXTEN
DED;                              NUM:INTEGER; VAR E:NORMARR);
{---------------------------------------------------------------------------}
{ This procedure calculates the energy eigenvalues of the unperturbed      }
{  square well and outputs them in the array E. OEFLAG is even for symmetric }
{  wavefunctions. E is actually an energy related value not actual energy.  }
{---------------------------------------------------------------------------}

VAR
  COUNT,I:INTEGER;

BEGIN { WAVEFUNCTION }

  IF OEFLAG THEN    { if symmetric are to be calculated }
    BEGIN
      FOR COUNT := 1 TO NUM DO
        BEGIN
          { the first root is between 0 and pi}
          E[COUNT] :=
ROOT(PI*(COUNT-1),PI*(COUNT-1)+ARCTAN(PARAM),
                      1.0E-6,OEFLAG,MSTARW,MSTARB,DELTA);
        END;
    END
  ELSE    { if antisymmetric }
    BEGIN
      FOR COUNT := 1 TO NUM DO
        BEGIN
          { the odd roots occur between pi/2 - 3pi/2 etc }
          E[COUNT] :=
ROOT(PI/2+(COUNT-1)*PI,PI/2+(COUNT-1)*PI+ARCTAN(PARAM),
                      1.0E-6,OEFLAG,MSTARW,MSTARB,DELTA);
        END;
```

```
  END
END; {ENERGY}



{-----------------------------------------------------------------------}
{-----------------------------------------------------------------------}
FUNCTION EVENWAVE(K1,K2,A1,A2,Z:EXTENDED):EXTENDED;
{-----------------------------------------------------------------------}
{ this function returns the value of the even parity wavefunction at Z given }
{  the K values and the normalization constants A1 and A2                    }
{-----------------------------------------------------------------------}

VAR
 TEMP1:EXTENDED;

BEGIN
 IF ((Z<=LZ/2) AND (Z>=-LZ/2)) THEN     { if inside well }
  TEMP1 := A1*COS(K1*Z)
 ELSE
  IF (Z>LZ/2) THEN              { if outside, + Z }
   TEMP1 := A2*EXP(-K2*Z)
  ELSE
   TEMP1 := A2*EXP(K2*Z);        { if outside, - Z }
 EVENWAVE := TEMP1;
END; { EVENWAVE }



{-----------------------------------------------------------------------}
{-----------------------------------------------------------------------}
FUNCTION ODDWAVE(K1,K2,A1,A2,Z:EXTENDED):EXTENDED;
{-----------------------------------------------------------------------}
{ This function returns the value of the odd parity wavefunction at Z given  }
{  the K values and the normalization constants A1 and A2                    }
{-----------------------------------------------------------------------}

VAR
 TEMP1:EXTENDED;

BEGIN
 IF ((Z<=LZ/2) AND (Z>=-LZ/2)) THEN  { if inside well }
```

```
  TEMP1 := A1*SIN(K1*Z)
 ELSE
  IF (Z>LZ/2) THEN                { if outside, + Z }
   TEMP1 := A2*EXP(-K2*Z)
  ELSE
   TEMP1 := -A2*EXP(K2*Z);        { if outside, - Z }
 ODDWAVE:=TEMP1;
END; { ODDWAVE }



{--------------------------------------------------------------------}
{--------------------------------------------------------------------}
FUNCTION EXPECTVAL(Z:EXTENDED):EXTENDED;
{--------------------------------------------------------------------}
{ This function returns the value of the function being integrated for the   }
{  expectation value of the potential perturbation.  BAND is true for cond.  }
{--------------------------------------------------------------------}

VAR
TEMP1,TEMP2,TEMP3:EXTENDED;

BEGIN
 IF BAND THEN
  BEGIN
   TEMP1 := FUNC1(K11,K12,A11,A12,Z);
   TEMP2 := FUNC2(K21,K22,A21,A22,Z);
   TEMP3 := TEMP1*TEMP2*EFIELD*Z;
  END
 ELSE
  BEGIN
   TEMP1 := FUNC1(K11,K12,A11,A12,Z);
   TEMP2:=FUNC2(K21,K22,A21,A22,Z);
   TEMP3:=TEMP1*TEMP2*(-EFIELD*Z);
  END;
 EXPECTVAL := TEMP3;
END; { EXPECTVAL }



{--------------------------------------------------------------------}
{--------------------------------------------------------------------}
```

```
PROCEDURE POLINT(XA,YA: NORMARR; N: INTEGER; X: EXTENDED;
VAR Y,DY: EXTENDED);
{-----------------------------------------------------------------------}
{ This procedure interpolates a polynomial from a finite set of points.   }
{  It is used in the integration routines.  XA and YA are arrays of length N.}
{  X is the point to return a value Y for and DY is an error estimate.     }
{-----------------------------------------------------------------------}

VAR
  NS,M,I: INTEGER;
  W,HP,HO,DIFT,DIF,DEN: EXTENDED;
  C,D: NORMARR;

BEGIN  { POLINT }
  NS := 1;
  DIF := ABS(X-XA[1]);
  FOR I:=1 TO N DO          { find closest array value }
    BEGIN
      DIFT := ABS(X-XA[I]);
      IF (DIFT<DIF) THEN
        BEGIN
          NS := I;
          DIF := DIFT;
        END;
      C[I] := YA[I];         { correction terms }
      D[I] := YA[I];
    END;
  Y := YA[NS];              { initial approximation }
  NS := NS-1;
  FOR M:=1 TO N-1 DO         { update correction terms }
    BEGIN
      FOR I:=1 TO N-M DO
        BEGIN
          HO := XA[I]-X;
          HP := XA[I+M]-X;
          W := C[I+1]-D[I];
          DEN := HO-HP;
          IF (DEN=0.0) THEN    { if two XA values are identical }
            BEGIN
              WRITELN('PAUSE IN ROUTINE POLINT');
              READLN;
            END;
```

```
        DEN := W/DEN;
        D[I] := HP*DEN;
        C[I] := HO*DEN;
      END;
    IF ((2*NS)<(N-M)) THEN        { use C or D as a correction to Y }
      BEGIN
        DY := C[NS+1]
      END
    ELSE
      BEGIN
        DY := D[NS];
        NS := NS-1
      END;
    Y := Y+DY
  END
END; { POLINT }


{-----------------------------------------------------------------------}
{-----------------------------------------------------------------------}
PROCEDURE QROMB(A,B:EXTENDED;FUNC3:FT3;VAR SS:EXTENDED);
{-----------------------------------------------------------------------}
{ This procedure integrates FUNC3 from A to B by the technique of romberg    }
{   integration. It uses TRAPZD and POLINT.                             }
{-----------------------------------------------------------------------}

LABEL 99;

CONST
  EPS=1.0E-7;     { fractional accuracy }
  JMAX = 20;       { maximum steps }
  JMAXP=21;  { JMAX+1}
  K=5;       { number of points used to extrapolate the integral }

VAR
  I,J,GLIT: INTEGER;
  DSS: EXTENDED;
  H,S: ARRAY [1..JMAXP] OF EXTENDED;
  C,D: NORMARR;
```

```
{----------------------------------------------------------------------}
{----------------------------------------------------------------------}
PROCEDURE TRAPZD(A,B:EXTENDED;VAR S:EXTENDED;N:INTEGER);
{----------------------------------------------------------------------}
{ This procedure employs the trapezoidal rule for integrating the function   }
{   FUNC3.                                                   }
{----------------------------------------------------------------------}

VAR
 J: INTEGER;
 X,TNM,SUM,DEL: EXTENDED;

BEGIN  { TRAPZD }
 IF (N=1) THEN
   BEGIN
    S := 0.5*(B-A)*(FUNC3(A)+FUNC3(B)); { initial estimate, one trap }
    GLIT := 1;
   END
 ELSE
   BEGIN
    TNM := GLIT;       { number of steps }
    DEL := (B-A)/TNM;
    X := A+0.5*DEL;
    SUM := 0.0;
    FOR J:=1 TO GLIT DO
      BEGIN
        SUM := SUM + FUNC3(X);
        X := X + DEL;
      END;
    S := 0.5*(S+(B-A)*SUM/TNM); { estimate of answer }
    GLIT := 2*GLIT; { next time twice the number of steps }
   END;
END; { TRAPZD }



{----------------------------------------------------------------------}

BEGIN   { QROMB }
 H[1] := 1.0;
 FOR J := 1 TO JMAX DO
   BEGIN
```

```
    TRAPZD(A,B,S[J],J);  { do trapezoidal integration }
    IF (J> =K) THEN
      BEGIN
        FOR I:=1 TO K DO
          BEGIN
            C[I] := H[J-K+I];
            D[I] := S[J-K+I];
          END;
        POLINT(C,D,K,0.0,SS,DSS);    { extrapolate for error and answer }
        IF (ABS(DSS)<EPS*ABS(SS)) THEN GOTO 99
      END;
    S[J+1] := S[J];
    H[J+1] := 0.25*H[J]
  END;
 WRITELN('PAUSE IN QROMB - TOO MANY STEPS');
 READLN;
99: END; { QROMB }



{------------------------------------------------------------------------}
{------------------------------------------------------------------------}
PROCEDURE WAVEFUNCTION(VAR
K1C,K2C,A1C,A2C,EC,K1V,K2V,A1V,A2V,EV:NORMARR;
                    VAR NUMC,NUMV:INTEGER);
{------------------------------------------------------------------------}
{ This procedure takes the square well energy related eigenvalues and        } {
calculates the enrgy values and the rest of the wavefunction parameters  } {    for
the unperturbed functions                                                 }
{------------------------------------------------------------------------}

VAR
 J,NUMEVENC,NUMODDC,NUMEVENV,NUMODDV:INTEGER;
 PARAM:EXTENDED;
 ECEVEN,ECODD:NORMARR;

BEGIN

 { calculate the number of bound conduction band states }
 PARAM := SQRT(M0*MWELEC*DELEEL*SQR(LZ)/(2*HBAR*HBAR));
 NUMEVENC := TRUNC(PARAM/PI)+1;
 NUMODDC := TRUNC((PARAM+(PI/2))/PI);
```

```
  { calculate the symmetric cond. band energy eigenvalues }

ENERGY(TRUE,DELEEL,MWELEC,MBELEC,PARAM,NUMEVENC,ECEVE
N);
  { calculate the antisymmetric cond. band eigenvalues }
  ENERGY(FALSE,DELEEL,MWELEC,MBELEC,PARAM,NUMODDC,ECOD
D);

  { calculate the number of bound valence band states }
  PARAM :=
SQRT(M0*MWHOLE*DELEHOL*SQR(LZ)/(2*HBAR*HBAR));
  NUMEVENV := TRUNC(PARAM/PI)+1;
  NUMODDV := TRUNC((PARAM+(PI/2))/PI);

  { calculate the symmetric val. band energy eigenvalues }

ENERGY(TRUE,DELEHOL,MWHOLE,MBHOLE,PARAM,NUMEVENV,EVE
VEN);
  { calculate the antisymmetric val. band eigenvalues }

ENERGY(FALSE,DELEHOL,MWHOLE,MBHOLE,PARAM,NUMODDV,EVO
DD);

  { now set energy values in one array from 0.. For each band }
  J := 1;
  WHILE (J<=NUMEVENC) DO
    BEGIN
      EC[(2*J)-2] := ECEVEN[J];
      EC[(2*J)-1] := ECODD[J];
      J := J+1;
    END;
  J := 1;
  WHILE (J<=NUMEVENV) DO
    BEGIN
      EV[(2*J)-2] := EVEVEN[J];
      EV[(2*J)-1] := EVODD[J];
      J := J+1;
    END;

  { now set the number of states in each band }
  NUMC := NUMEVENC + NUMODDC;
  NUMV := NUMEVENV + NUMODDV;
```

```
  { now calculate the real energy values from EPS and the k values }

  { conduction band }
  FOR I:=0 TO NUMC-1 DO
    BEGIN
      EC[I] := SQR(EC[I])*2*SQR(HBAR)/(MWELEC*M0*SQR(LZ));
      K1C[I] := SQRT(2*M0*MWELEC*EC[I])/HBAR;
      K2C[I] := SQRT(2*M0*MBELEC*(DELEEL-EC[I]))/HBAR;
      { calculate the normalization constants }
      IF (ODD(I)) THEN
        NORMODD(K1C[I],K2C[I],A1C[I],A2C[I])
      ELSE
        NORMEVEN(K1C[I],K2C[I],A1C[I],A2C[I]);
    END;

  { valence band }
  FOR I:=0 TO NUMV-1 DO
    BEGIN
      EV[I] := SQR(EV[I])*2*SQR(HBAR)/(MWHOLE*M0*SQR(LZ));
      K1V[I] := SQRT(2*M0*MWHOLE*EV[I])/HBAR;
      K2V[I] := SQRT(2*M0*MBHOLE*(DELEHOL-EV[I]))/HBAR;
      { calculate the normalization constants }
      IF (ODD(I)) THEN
        NORMODD(K1V[I],K2V[I],A1V[I],A2V[I])
      ELSE
        NORMEVEN(K1V[I],K2V[I],A1V[I],A2V[I]);
    END;

END; {WAVEFUNCTION}



{----------------------------------------------------------------------}
{----------------------------------------------------------------------}
PROCEDURE
GAMMA(NUMC,NUMV:INTEGER;K1C,K2C,K1V,K2V,A1C,A2C,A1V,A2V:
              NORMARR;VAR VARRAYC,VARRAYV:SQUARE);
{----------------------------------------------------------------------}
{ This procedure calculates the potential expectation value for each         }
{  combination of wavefunctions and stores them in matrix form.  Note that  }
{  sym-antisym or antisym-sym integrals will be zero.                      }
{----------------------------------------------------------------------}
```

```
VAR
J:INTEGER;

BEGIN
 { do conduction band }
 BAND := TRUE;
 FOR I:=0 TO NUMC-1 DO
  BEGIN
   FOR J:=I TO NUMC-1 DO
    BEGIN
     { if I and J are not of the same parity then assign the
      proper functions}
     IF (ODD(I) XOR ODD(J)) THEN
      BEGIN
       IF NOT ODD(I) THEN
        FUNC1 := EVENWAVE
       ELSE
        FUNC1 := ODDWAVE;
       IF NOT ODD(J) THEN
        FUNC2 := EVENWAVE
       ELSE
        FUNC2 := ODDWAVE;

       K11:=K1C[I];K12:=K2C[I];K21:=K1C[J];K22:=K2C[J];
       A11:=A1C[I];A12:=A2C[I];A21:=A1C[J];A22:=A2C[J];

       { decide which K is larger for int limits )
       IF (K2C[I]>K2C[J]) THEN
        { calculate the I+1,J+1 matrix element}
        QROMB(0.0,6*1/K2C[J]+LZ/2,FUNC3,VARRAYC[I+1,J+1]);
       IF (K2C[I]<=k2C[J]) THEN
        QROMB(0.0,6*1/K2C[I]+LZ/2,FUNC3,VARRAYC[I+1,J+1]);
       VARRAYC[I+1,J+1]:=2*VARRAYC[I+1,J+1];
        { if they are of the same parity integral will be zero }
      END
     ELSE
      BEGIN
       VARRAYC[I+1,J+1] := 0.0;
      END;
      VARRAYC[J+1,I+1] := VARRAYC[I+1,J+1];
    END;
  END;
```

```
  { do valence band }
  BAND := FALSE;
  FOR I:=0 TO NUMV-1 DO
    BEGIN
      FOR J:=I TO NUMV-1 DO
        BEGIN
          { if I and J are not of the same parity then assign the
            proper functions}
          IF (ODD(I) XOR ODD(J)) THEN
            BEGIN
              IF NOT ODD(I) THEN
                FUNC1 := EVENWAVE
              ELSE
                FUNC1 := ODDWAVE;
              IF NOT ODD(J) THEN
                FUNC2 := EVENWAVE
              ELSE
                FUNC2 := ODDWAVE;

              K11:=K1V[I];K12:=K2V[I];K21:=K1V[J];K22:=K2V[J];
              A11:=A1V[I];A12:=A2V[I];A21:=A1V[J];A22:=A2V[J];

              { decide which K is larger for int limits )
              IF (K2V[I]>K2V[J]) THEN
                { calculate the I+1,J+1 matrix element}
                QROMB(0.0,6*1/K2V[J]+LZ/2,FUNC3,VARRAYV[I+1,J+1]);
              IF (K2V[I]<=K2V[J]) THEN
                QROMB(0.0,6*1/K2V[I]+LZ/2,FUNC3,VARRAYV[I+1,J+1]);
              VARRAYV[I+1,J+1]:=2*VARRAYV[I+1,J+1];
                { if they are of the same parity integral will be zero }
            END
          ELSE
            VARRAYV[I+1,J+1] := 0.0;
        VARRAYV[J+1,I+1] := VARRAYV[I+1,J+1];
        END;
    END;
END;  { GAMMA }


{-----------------------------------------------------------------------}
{-----------------------------------------------------------------------}
```

```
PROCEDURE JACOBI(VAR A:SQUARE; N:INTEGER; VAR D:NORMARR;
             VAR V:SQUARE; VAR NROT:INTEGER);
{-----------------------------------------------------------------------}
{ This procedure uses the cyclic jacobi method to calculate the energy      }
{  eigenvalues and mixing coefficient eigenvectors for the perturbed        }
{  solutions.  The problem is defined by the input NxN matrix A.            }
{  The eigenvalues are returned in the first N elements of D and V contains }
{  the eigenvectors in its N columns.                                }
{-----------------------------------------------------------------------}

LABEL 99;

CONST
    NMAX=100;

VAR
   J,IQ,IP,I:INTEGER;
   TRESH,THETA,TAU,T,SM,S,H,G,C:EXTENDED;
   B,Z: ARRAY [1..10] OF EXTENDED;

BEGIN
  FOR IP:=1 TO N DO               { make an identity matrix }
    BEGIN
      FOR IQ:=1 TO N DO
        BEGIN
          V[IP,IQ]:=0.0
        END;
      V[IP,IP]:=1.0
    END;
    FOR IP:=1 TO N DO
      BEGIN                   { initialize arrays B and D as diag A }
        B[IP]:=A[IP,IP];
        D[IP]:=B[IP];
        Z[IP]:=0.0
      END;
    NROT:=0;
    FOR I:=1 TO 50 DO
      BEGIN
        SM:=0.0;
        FOR IP:=1 TO N-1 DO       { sum off diagonal elements }
          BEGIN
            FOR IQ:= IP+1 TO N DO
```

```
      BEGIN
        SM:=SM+ABS(A[IP,IQ])
      END
  END;
IF (SM=0.0) THEN GOTO 99;   { convergence }
IF (I<4) THEN TRESH :=0.2*SM/SQR(N)  { first three sweeps }
ELSE TRESH:=0.0;  { after three sweeps }
FOR IP:=1 TO N-1 DO
  BEGIN
    FOR IQ:=IP+1 TO N DO
      BEGIN
        G:=100.0*ABS(A[IP,IQ]);
        { skip rotation if element is small }
        IF ((I>4) AND ((ABS(D[IP])+G)=ABS(D[IP])) AND
          ((ABS(D[IQ])+G)=ABS(D[IQ]))) THEN A[IP,IQ]:=0.0
        ELSE IF (ABS(A[IP,IQ])>TRESH) THEN
          BEGIN
            H:=D[IQ]-D[IP];
            IF ((ABS(H)+G) = ABS(H)) THEN
              BEGIN
                T:=A[IP,IQ]/H
              END
            ELSE BEGIN
                THETA := 0.5*H/A[IP,IQ];
            T:= 1.0/(ABS(THETA)+SQRT(1.0+SQR(THETA)));
            IF (THETA<0.0) THEN T:=-T
          END;
        { do rotations }
        C:=1.0/SQRT(1+SQR(T));
        S:=T*C;
        TAU:=S/(1.0+C);
        H:=T*A[IP,IQ];
        Z[IP]:=Z[IP]-H;
        Z[IQ]:=Z[IQ]+H;
        D[IP]:=D[IP]-H;
        D[IQ]:=D[IQ]+H;
        A[IP,IQ]:=0.0;
        FOR J:=1 TO IP-1 DO
          BEGIN
            G:=A[J,IP];
            H:=A[J,IQ];
            A[J,IP]:=G-S*(H+G*TAU);
```

```
              A[J,IQ]:=H+S*(G-H*TAU)
            END;
          FOR J:=IP+1 TO IQ-1 DO
            BEGIN
              G:=A[IP,J];
              H:=A[J,IQ];
              A[IP,J]:=G-S*(H+G*TAU);
              A[J,IQ]:=H+S*(G-H*TAU);
            END;
          FOR J:=IQ+1 TO N DO
            BEGIN
              G:=A[IP,J];
              H:=A[IQ,J];
              A[IP,J]:=G-S*(H+G*TAU);
              A[IQ,J]:=H+S*(G-H*TAU);
            END;
          FOR J:=1 TO N DO
            BEGIN
              G:=V[J,IP];
              H:=V[J,IQ];
              V[J,IP]:=G-S*(H+G*TAU);
              V[J,IQ]:=H+S*(G-H*TAU);
            END;
          NROT:=NROT+1;
        END
      END
    END
  END;
 FOR IP:=1 TO N DO
  BEGIN
    B[IP]:=B[IP]+Z[IP];
   D[IP]:=B[IP];
   Z[IP]:=0.0;
  END;
 WRITELN('PAUSE IN ROUTINE JACOBI');  { too many iterations }
 READLN;
99: END;  { JACOBI }


{----------------------------------------------------------------------}
{----------------------------------------------------------------------}
```

```
PROCEDURE EIGSRT(VAR D:NORMARR; VAR V:SQUARE;
N:INTEGER);
{-----------------------------------------------------------------------}
{ This procedure sorts the eigenvalues and eigenvectors from jacobi into    }
{   ascending order so the lowest one can be picked out.                    }
{-----------------------------------------------------------------------}

VAR
  K,J,I: INTEGER;
  P: EXTENDED;

BEGIN
  FOR I:=1 TO N-1 DO
    BEGIN
      K:=I;
      P:=D[I];
      FOR J:=I+1 TO N DO
        BEGIN
          IF (D[J]<=P) THEN
            BEGIN
              K:=J;
              P:=D[J];
            END;
        END;
      IF (K<>I) THEN
        BEGIN
          D[K]:=D[I];
          D[I]:=P;
          FOR J:=1 TO N DO
            BEGIN
              P:=V[J,I];
              V[J,I]:=V[J,K];
              V[J,K]:=P;
            END
        END
    END
END;  { EIGSRT }


{-----------------------------------------------------------------------}
{-----------------------------------------------------------------------}
```

```
FUNCTION PSIE(Z:EXTENDED):EXTENDED;
{-------------------------------------------------------------------------}
{ This function calculates the value of the z dependent part of the          } {
wavefunction in the conduction band.                                 }
{-------------------------------------------------------------------------}

{ FIELD: INTEGER FROM 0 TO NUMBER OF APPLIED FIELDS
CALCULATED              }
{ K1,K2,A1,A2: EXTENDED ARRAY FROM 0 TO NUMC(V)-1
     }
{  MIX: SQUARE ARRAY WITH THE MIXING COEFFICIENTS IN THE
COLUMNS            }
{      (0..NUMC(V)-1) FOR ROWS (0..5) FOR COLUMNS)
}

{ for each e or h wave function there will be num terms to the wavefunction  } {
summation                                                              }

VAR
 SUM,D: EXTENDED;
I:INTEGER;
BEGIN { PSI }
SUM:=0;
FOR I:=0 TO NUMC-1 DO
BEGIN
  { the mixing coefficients will be in the column field of an array}
  { for I odd then the term of the summation corresponds to an even wf}
  IF (Z<=LZ/2) AND (Z>=-LZ/2) THEN
    BEGIN
      IF ODD(I) THEN
        D:= A1C[I]*SIN(K1C[I]*Z)
      ELSE
        D:= A1C[I]*COS(K1C[I]*Z);
    END
  ELSE
    BEGIN
      IF (Z>LZ/2) THEN
        D:= A2C[I]*EXP(-K2C[I]*Z)
      ELSE
        BEGIN
          IF ODD(I) THEN
            D:=-A2C[I]*EXP(K2C[I]*Z)
```

```
        ELSE
          D:= A2C[I]*EXP(K2C[I]*Z);
       END
    END;
    SUM:= SUM+VVC[I,FIELD]*D; { add on next mixed state }
END;
PSIE:=SUM;
END;      { PSIE }



{-----------------------------------------------------------------------}
{-----------------------------------------------------------------------}
FUNCTION PSIV(Z:EXTENDED):EXTENDED;
{-----------------------------------------------------------------------}
{ This function calculates the value of the z dependent part of the          } {
wavefunction in the conduction band.                                 }
{-----------------------------------------------------------------------}

{ FIELD: INTEGER FROM 0 TO NUMBER OF APPLIED FIELDS
CALCULATED              }
{ K1,K2,A1,A2: EXTENDED ARRAY FROM 0 TO NUMC(V)-1
     }
{  MIX: SQUARE ARRAY WITH THE MIXING COEFFICIENTS IN THE
COLUMNS             }
{      (0..NUMC(V)-1) FOR ROWS (0..5) FOR COLUMNS)
}

{ for each e or h wave function there will be num terms to the wavefunction  } {
summation                                                   }

VAR
 SUM,D: EXTENDED;
I:INTEGER;
BEGIN { PSI }
SUM:=0;
FOR I:=0 TO NUMV-1 DO
BEGIN
  { the mixing coefficients will be in the column field of an array}
  { for I odd then the term of the summation corresponds to an even wf}
  IF (Z<=LZ/2) AND (Z>=-LZ/2) THEN
    BEGIN
```

```
      IF ODD(I) THEN
        D:= A1V[I]*SIN(K1V[I]*Z)
      ELSE
        D:= A1V[I]*COS(K1V[I]*Z);
    END
  ELSE
    BEGIN
      IF (Z>LZ/2) THEN
        D:= A2V[I]*EXP(-K2V[I]*Z)
      ELSE
        BEGIN
          IF ODD(I) THEN
            D:=-A2V[I]*EXP(K2V[I]*Z)
          ELSE
            D:= A2V[I]*EXP(K2V[I]*Z);
        END
    END;
    SUM:= SUM+VVV[I,FIELD]*D;  { add on next mixed state }
END;
PSIV:=SUM;
END;     { PSIV }



{--------------------------------------------------------------------}
{--------------------------------------------------------------------}
FUNCTION COULOMB(LAMBDA:EXTENDED):EXTENDED;
{--------------------------------------------------------------------}
{ This function gives the expectation value of the coulomb term            }
{   in the hamiltonian as a function of the fitting parameter LAMBDA.        }
{--------------------------------------------------------------------}

VAR
  TERM1,TERM2,TERM3:EXTENDED;



{--------------------------------------------------------------------}{------------------------------
-------------------------------------------}
FUNCTION COULELECS(ZE:EXTENDED):EXTENDED;
{--------------------------------------------------------------------}
{ This function gives the product of the ZE dependence times              }
```

```
{  the integral of the ZH dependence times the integral of the           }
{   radial dependence. It rquires global variables LAMBDA, K2V, LZ, and
NUMV}
{----------------------------------------------------------------------}

VAR
  TERM1,TERM2,TERM3,TEMP:EXTENDED;



{----------------------------------------------------------------------}
{----------------------------------------------------------------------}
FUNCTION COULHOLES(ZH:EXTENDED):EXTENDED;
{----------------------------------------------------------------------}
{ This function gives the product of the ZH dependence times               }
{  the integral of the radial part. It requires global variables        }
{   ZH and LAMBDA                                                       }
{----------------------------------------------------------------------}

 VAR
  TEMP:EXTENDED;



{----------------------------------------------------------------------}{------------------------------
-------------------------------------------}
FUNCTION G:EXTENDED;
{----------------------------------------------------------------------}
{ This function calculates the value of the integral g(gamma) which is      }
{  the radial part of the wavefunction. It requires the global         }
{   variables ze,zh and lambda                                       }
{----------------------------------------------------------------------}

 CONST
  PI=3.1415926535897932384;

 VAR
  Z,N,ST:EXTENDED;



{----------------------------------------------------------------------}{------------------------------
```

```
------------------------------------------}
FUNCTION NEUMAN1(X:EXTENDED):EXTENDED;
{-------------------------------------------------------------------}
{ This function provides the value of the first order Neuman function       }
{-------------------------------------------------------------------}

VAR
  XX,Z:EXTENDED;
  Y,ANS,ANS1,ANS2:EXTENDED;



{-------------------------------------------------------------------}{---------------------------
------------------------------------------}
FUNCTION BESSJ1(X:EXTENDED):EXTENDED;
{-------------------------------------------------------------------}
{  This function provides the value of the first order Bessel function      }
{   of the first kind.                                              }
{-------------------------------------------------------------------}

VAR
  AX,XX,Z:EXTENDED;
  Y,ANS,ANS1,ANS2:EXTENDED;



{-------------------------------------------------------------------}{---------------------------
------------------------------------------}
FUNCTION SIGN(X:EXTENDED):EXTENDED;
{-------------------------------------------------------------------}
{ This function provides a value of -1 for X<=0 or +1 for X<0.              }
{-------------------------------------------------------------------}

BEGIN  {SIGN}
   IF X>=0.0 THEN SIGN := 1.0
   ELSE SIGN:=-1.0;
END;  {SIGN}



{-------------------------------------------------------------------}
```

```
BEGIN  {BESSJ1}
  { matches up to forms at X=8 }
  IF (ABS(X)<8.0) THEN BEGIN
    Y:=SQR(X);

ANS1:=X*(72362614232.0+Y*(-7895059235.0+Y*(242396853.1+Y*(-2972611.439
+
          Y*(15704.48260+Y*(-30.16036606))))));
    ANS2:=144725228442.0+Y*(2300535178.0+Y*(18583304.74+
          Y*(99447.43394+Y*(376.9991397+Y*1.0))));
    BESSJ1:=ANS1/ANS2
    END
  ELSE BEGIN
    AX:=ABS(X);
    Z:=8.0/AX;
    Y:=SQR(Z);
    XX:=AX-2.356194491;
    ANS1:=1.0+Y*(0.183105E-2+Y*(-0.3516396496E-4+
          Y*(0.2457520174E-5+Y*(-0.240337019E-6))));
    ANS2:=0.04687499995+Y*(-0.2002690873E-3+Y*(0.8449199096E-5+
          Y*(-0.88228987E-6+Y*0.105787412E-6)));

BESSJ1:=SQRT(0.636619772/AX)*(COS(XX)*ANS1-Z*SIN(XX)*ANS2)*SIGN(
X);
    END
END;  {BESSJ1}



{-----------------------------------------------------------------------}

BEGIN  {NEUMAN1}
 { matches up two forms at X=8 }
  IF(X<8.0) THEN BEGIN
   Y:=SQR(X);
   ANS1:=X*(-0.4900604943E13+Y*(0.1275274390E13+Y*(-0.5153438139E11+
         Y*(0.7349264551E9+Y*(-0.4237922726E7+Y*0.8511937935E4)))));
   ANS2:=0.2499580570E14+Y*(0.4244419664E12+Y*(0.3733650367E10+

Y*(0.2245904002E8+Y*(0.1020426050E6+Y*(0.3549632885E3+Y*1.0)))));
   ans1:=(ans1/ans2);
   ans2:=bessj1(x);
```

```
    ans2:=ans2*ln(x);
    NEUMAN1:=ANS1+0.636619772*(ans2-1.0/X);
    END
  ELSE BEGIN
    Z:=8.0/X;
    Y:=SQR(Z);
    XX:=X-2.356194491;
    ANS1:=1.0+Y*(0.183105E-2+Y*(-0.3516396496E-4+Y*(0.2457520174E-5+
          Y*(-0.240337019E-6))));
    ANS2:=0.04687499995+Y*(-0.2002690873E-3+Y*(0.8449199096E-5+
          Y*(-0.88228987E-6+Y*0.105787412E-6)));
    ANS2:=Z*COS(XX)*ANS2;
    NEUMAN1:=SQRT(0.636619772/X)*(SIN(XX)*ANS1+ANS2);
    END
END; {NEUMAN1}



{-----------------------------------------------------------------------}{------------------------------
------------------------------------------}
 FUNCTION STRUVE(Z:EXTENDED):EXTENDED;
{-----------------------------------------------------------------------}
{ This function provides the first order Struve function.              }
{-----------------------------------------------------------------------}

 CONST
   TOL=1E10;
   PI=3.14159265358979323 84;
   FACT=2/PI;
   ENDPOINT=20;
   NUMPOINT=200;

 VAR
   SUM,STEP,NEWTERM,OLDTERM:EXTENDED;
   I,TERM:INTEGER;

 BEGIN; { STRUVE }

   OLDTERM:=0.0;
   TERM := 1;
   NEWTERM:=SQR(Z)/3;
   SUM:=NEWTERM;
```

```
  WHILE (ABS(SUM)/ABS(NEWTERM)<TOL) DO BEGIN  { check for
accuracy }
    TERM:=TERM+1;
    OLDTERM:=NEWTERM;
    NEWTERM:=OLDTERM*(-SQR(Z))/((2*TERM+1)*(2*TERM-1));
    SUM:=SUM+NEWTERM;
  END;

  STRUVE:=SUM*FACT;

 END;  { STRUVE }



{-----------------------------------------------------------------------}
{-----------------------------------------------------------------------}
 FUNCTION STMINNEU(Z:EXTENDED):EXTENDED;
{-----------------------------------------------------------------------}
{ This function provides the difference between the Struve and Neuman      }
{  functions and must be used for large values of the argument due to     }
{  the limits of machine precision.
{-----------------------------------------------------------------------}

 CONST
  TOL=1E10;
  PI=3.14159265358979323 84;
  FACT=2/PI;
  ENDPOINT=20;
  NUMPOINT=200;

 VAR
  SUM,STEP,NEWTERM,OLDTERM:EXTENDED;
  I,TERM:INTEGER;

 BEGIN; { STMINNEU }

  OLDTERM:=1.0;
  TERM := 1;
  NEWTERM:= 1.0/SQR(Z);
  SUM:=NEWTERM+OLDTERM;

  WHILE (ABS(SUM)/ABS(NEWTERM)<TOL) DO BEGIN
```

```
    TERM:=TERM+1;
    OLDTERM:=NEWTERM;
    NEWTERM:=OLDTERM*(-1/SQR(Z))*((2*TERM-3)*(2*TERM-1));
    SUM:=SUM+NEWTERM;
   END;

   STMINNEU:=SUM*FACT;

  END;  { STMINNEU }



{-----------------------------------------------------------------------}

BEGIN  { G }

 Z := 2*ABS(ZE-ZH)/LAMBDA;
 IF (Z>1.0E-200) THEN BEGIN
  IF(Z>25.0) THEN BEGIN    { for large arguments use STMINNEU }
   N:=STMINNEU(Z);
   G:=Z*(PI/2*N-1);
   END
  ELSE BEGIN
   N:=NEUMAN1(Z);
   ST:=STRUVE(Z);
   G:= Z*(PI/2*(ST-N)-1);
   END;
  END
 ELSE BEGIN
  G:=0.0;
  END;

END; { G }



{-----------------------------------------------------------------------}

BEGIN    { COULHOLES }

 TEMP := PSIV(ZH);
 TEMP := SQR(TEMP);
```

```
  COULHOLES := TEMP*G;

END;  { COULHOLES }



{----------------------------------------------------------------------}{------------------------------
------------------------------------------}
PROCEDURE QROMB1(A,B:EXTENDED;VAR SS:EXTENDED);
{----------------------------------------------------------------------}
{ This procedure integrates func3 from a to b by the technique of romberg
    integration. It uses TRAPZD and POLINT.}
{----------------------------------------------------------------------}

LABEL 99;

CONST
  EPS=1.0E-6;   { required fractional tolerance }
  JMAX = 20;    { maximum number of steps }
  JMAXP=21;  { JMAX+1}
  K=5;          { number of points for extrapolation }

VAR
  I,J,GLIT: INTEGER;
  DSS: EXTENDED;
  H,S: ARRAY [1..JMAXP] OF EXTENDED;
  C,D: NORMARR;



{----------------------------------------------------------------------}{------------------------------
------------------------------------------}
PROCEDURE TRAPZD2(A,B:EXTENDED;VAR
S:EXTENDED;N:INTEGER);
{----------------------------------------------------------------------}
{ This procedure employs the trapezoidal rule for integrating the function   }
{  COULHOLES                                                    }
{----------------------------------------------------------------------}

VAR
  J: INTEGER;
  X,TNM,SUM,DEL: EXTENDED;
```

```
BEGIN  { TRAPZD2 }
  IF (N=1) THEN
    BEGIN
     S := 0.5*(B-A)*(COULHOLES(A)+COULHOLES(B));
     GLIT := 1;
    END
  ELSE
    BEGIN
     TNM := GLIT;
     DEL := (B-A)/TNM;
     X := A+0.5*DEL;
     SUM := 0.0;
     FOR J:=1 TO GLIT DO
       BEGIN
         SUM := SUM + COULHOLES(X);
         X := X + DEL;
       END;
     S := 0.5*(S+(B-A)*SUM/TNM);
     GLIT := 2*GLIT;
    END;
END; { TRAPZD2 }



{-----------------------------------------------------------------------}

BEGIN   { QROMB1 }
  H[1] := 1.0;
  FOR J := 1 TO JMAX DO
    BEGIN
      TRAPZD2(A,B,S[J],J);
      IF (J>=K) THEN
        BEGIN
          FOR I:=1 TO K DO
            BEGIN
              C[I] := H[J-K+I];
              D[I] := S[J-K+I];
            END;
          POLINT(C,D,K,0.0,SS,DSS);
          IF (ABS(DSS)<EPS*ABS(SS)) THEN GOTO 99
        END;
      S[J+1] := S[J];
```

```
    H[J+1] := 0.25*H[J]
   END;
  WRITELN('PAUSE IN QROMB1 - TOO MANY STEPS');
  READLN;
99: END; { QROMB1 }



{----------------------------------------------------------------------}

BEGIN   { COULELECS }

  QROMB1(6*-1/K2V[NUMV-1]-LZ/2,6*1/K2V[NUMV-1]+LZ/2,TERM1);

  TEMP := SQR(PSIE(ZE));
  COULELECS := TEMP*TERM1;

END;    { COULELECS }



{----------------------------------------------------------------------}{-----------------------------
-------------------------------------------}
PROCEDURE QROMB2(A,B:EXTENDED;VAR SS:EXTENDED);
{----------------------------------------------------------------------}
{ This procedure integrates func3 from a to b by the technique of romberg
   integration. It uses TRAPZD and POLINT. }
{----------------------------------------------------------------------}

LABEL 99;

CONST
  EPS=1.0E-5;
  JMAX = 20;
  JMAXP=21;  { JMAX+1}
  K=5;

VAR
  I,J,GLIT: INTEGER;
  DSS: EXTENDED;
  H,S: ARRAY [1..JMAXP] OF EXTENDED;
  C,D: NORMARR;
```

```
{----------------------------------------------------------------------}{-----------------------------
-------------------------------------------}
PROCEDURE TRAPZD3(A,B:EXTENDED;VAR
S:EXTENDED;N:INTEGER);
{----------------------------------------------------------------------}
{ This procedure employs the trapezoidal rule for integrating the function   }
{  COULELECS.                                                           }
{----------------------------------------------------------------------}

VAR
  J: INTEGER;
  X,TNM,SUM,DEL: EXTENDED;

BEGIN  { TRAPZD3 }
  IF (N=1) THEN
    BEGIN
      S := 0.5*(B-A)*(COULELECS(A)+COULELECS(B));
      GLIT := 1;
    END
  ELSE
    BEGIN
     TNM := GLIT;
     DEL := (B-A)/TNM;
     X := A+0.5*DEL;
     SUM := 0.0;
     FOR J:=1 TO GLIT DO
       BEGIN
         SUM := SUM + COULELECS(X);
         X := X + DEL;
       END;
     S := 0.5*(S+(B-A)*SUM/TNM);
     GLIT := 2*GLIT;
    END;
END; { TRAPZD3 }



{----------------------------------------------------------------------}

BEGIN   { QROMB2 }
```

```
  H[1] := 1.0;
  FOR J := 1 TO JMAX DO
    BEGIN
      TRAPZD3(A,B,S[J],J);
      IF (J>=K) THEN
        BEGIN
          FOR I:=1 TO K DO
            BEGIN
              C[I] := H[J-K+I];
              D[I] := S[J-K+I];
            END;
          POLINT(C,D,K,0.0,SS,DSS);
          IF (ABS(DSS)<EPS*ABS(SS)) THEN GOTO 99
        END;
      S[J+1] := S[J];
      H[J+1] := 0.25*H[J]
    END;
  WRITELN('PAUSE IN QROMB2 - TOO MANY STEPS');
  READLN;
99: END; { QROMB2 }



{--------------------------------------------------------------------}

BEGIN    { COULOMB }
   QROMB2(6*-1/K2C[NUMC-1]-LZ/2,6*1/K2C[NUMC-1]+LZ/2,TERM1);

  {COULOMB := -TERM1*sqr(1.602e-19)/(2*pi)/lambda/K;}
  {COULOMB := -TERM1*SQR(ECHARGE)*4./SQR(LAMBDA)/K;

END;  { COULOMB }



{--------------------------------------------------------------------}
{--------------------------------------------------------------------}
FUNCTION HAMIL(LAMBDA:EXTENDED):EXTENDED;
{--------------------------------------------------------------------}
{ This function computes the expectation value of the hamiltonian given the  }
{    fitting parameter LAMBDA                                          }
{--------------------------------------------------------------------}
```

```
VAR

ATERM1,ATERM2,BTERM1,BTERM2,DTERM1,DTERM2,CTERM:EXTEND
ED;

BEGIN  { HAMIL }

{ NOW CALCULATE THE THIRD TERM }
BTERM1:=SQR(HBAR)/(2*MU)/SQR(LAMBDA);

{ THE FOURTH TERM IS THE COULOMBIC TERM WHICH IS A TRIPLE
INTEGRAL }
CTERM:=COULOMB(LAMBDA);

{ THE TOTAL TERM IS THE SUM OF THE INDIVIDUAL TERMS }
HAMIL := BTERM1+CTERM;
END; { HAMIL }



{-----------------------------------------------------------------------}
{-----------------------------------------------------------------------}
PROCEDURE MNBRAK(VAR AX,BX,CX,FA,FB,FC: EXTENDED);
{-----------------------------------------------------------------------}
{ This procedure brackets a minimum in the function HAMIL with the initial  }
{  values AX and BX it returns bracketing values AX, BX and CX.            }
{-----------------------------------------------------------------------}

LABEL 1;
CONST
   GOLD=1.618034;  { default magnification ratio }
   GLIMIT=100.0;   { maximum magnification }
   TINY=1.0E-200;
VAR
   ULIM,U,R,Q,FU,DUM:EXTENDED;

FUNCTION MAX(A,B:EXTENDED):EXTENDED;
BEGIN
   IF (A>B) THEN MAX:= A ELSE MAX:=B
END;

FUNCTION SIGN(A,B:EXTENDED):EXTENDED;
```

```
BEGIN
    IF (B>0.0) THEN SIGN := ABS(A) ELSE SIGN := -ABS(A)
END;

BEGIN
    FA := HAMIL(AX);  { calculate values at starting points }
    FB := HAMIL(BX);
    IF (FB>FA) THEN BEGIN   { switch to search in downhill dir }
      DUM := AX;
      AX:=BX;
      BX:=DUM;
      DUM :=FB;
      FB := FA;
      FA:=DUM;
      END;
    CX := BX+GOLD*(BX-AX);   { guess for C }
    FC := HAMIL(CX);
1:  IF (FB >= FC) THEN BEGIN   { do until bracketed }
      R:=(BX-AX)*(FB-FC);
      Q:=(BX-CX)*(FB-FA);
      { compute U by parabolic interpolation }

U:=BX-((BX-CX)*Q-(BX-AX)*R)/(2.0*SIGN(MAX(ABS(Q-R),TINY),Q-R));
      ULIM:=BX+GLIMIT*(CX-BX);     { limit on step size }
      IF ((BX-U)*(U-CX)>0.0) THEN BEGIN  { U is between B and C }
        FU:=HAMIL(U);
        IF (FU<FC) THEN BEGIN  { found a min between B and C }
          AX:=BX;
          FA:=FB;
          BX:=U;
          FB:=FU;
          GOTO 1 END   { exit }
        ELSE IF (FU>FB) THEN BEGIN  { found a min between A and U }
          CX:=U;
          FC:=FU;
          GOTO 1
        END;
        U := CX+GOLD*(CX-BX);  { parab. fit no good so use default mag. }
        FU := HAMIL(U);
        END
      ELSE IF ((CX-U)*(U-ULIM)>0.0) THEN BEGIN  { Try a fit bet. C and
Ulim}
```

```
         FU := HAMIL(U);
         IF (FU<FC) THEN BEGIN
            BX:=CX;
            CX:=U;
            U:=CX+GOLD*(CX-BX);
            FB:=FC;
            FC := FU;
            FU := HAMIL(U);
            END
            END
       ELSE IF ((U-ULIM)*(ULIM-CX)>=0.0) THEN BEGIN  {lim U to
allowed value}
            U:= ULIM;
            FU:=HAMIL(U);
            END
        ELSE BEGIN    { U no good, use default mag. }
            U:=CX+GOLD*(CX-BX);
            FU:=HAMIL(U)
            END;
        AX:=BX;  { eliminate oldest point }
        BX:=CX;
        CX:=U;
        FA:=FB;
        FB:=FC;
        FC:=FU;
        GOTO 1
END
END;



{-----------------------------------------------------------------------}
{-----------------------------------------------------------------------}
FUNCTION BRENT(AX,BX,CX,TOL:EXTENDED; VAR XMIN:
EXTENDED): EXTENDED;
{-----------------------------------------------------------------------}
{ This routine uses Brents method and the bracketing triplet AX, BX and CX   }
{  to find the minimum (XMIN) to a fractional tolerance (TOL).            }
{  BRENT returns the minimum value.                                     }
{-----------------------------------------------------------------------}

LABEL 1,2,3;
```

```
CONST
    ITMAX=100;     { max iterations }
    CGOLD=0.3819660; { ratio for golden section search }
    ZEPS=1.0E-200;    { smallest number greater than zero }
VAR
  A,B,D,E,ETEMP: EXTENDED;
  FU,FV,FW,FX: EXTENDED;
  ITER: INTEGER;
  P,Q,R,TOL1,TOL2: EXTENDED;
  U,V,W,X,XM: EXTENDED;

FUNCTION SIGN(A,B:EXTENDED): EXTENDED;
  BEGIN
    IF (B>0.0) THEN SIGN:=ABS(A) ELSE SIGN:=-ABS(A)
  END;

BEGIN
  IF AX<CX THEN A:=AX ELSE A:=CX;    { put A and B in ascending order
}
  IF AX>CX THEN B:=AX ELSE B:=CX;
  V:=BX;
  W:=V;
  X:=V;
  E:=0.0;
  FX:=HAMIL(X);
  FV:=FX;
  FW:=FX;
  FOR ITER:=1 TO ITMAX DO BEGIN  { main loop }
     XM:=0.5*(A+B);
     TOL1:=TOL*ABS(X)+ZEPS;
     TOL2:=2.0*TOL1;
     IF (ABS(X-XM)<=(TOL2-0.5*(B-A))) THEN GOTO 3; {test for end}
     IF (ABS(E)>TOL1) THEN BEGIN  { parabolic fit }
        R:=(X-W)*(FX-FV);
        Q:=(X-V)*(FX-FW);
        P:=(X-V)*Q-(X-W)*R;
        Q:=2.0*(Q-R);
        IF (Q>0.0) THEN P:=-P;
        Q:=ABS(Q);
        ETEMP:=E;
        E:=D;
        { test fit }
```

```
         IF((ABS(P)>=ABS(0.5*Q*ETEMP)) OR (P<=Q*(A-X))
                    OR (P>=Q*(B-X))) THEN GOTO 1;
         { parabolic fit OK }
         D:=P/Q;
         U:=X+D;
         IF (((U-A)<TOL2) OR ((B-U)< TOL2)) THEN
D:=SIGN(TOL1,XM-X);
         GOTO 2
      END;
      { fit not OK so take a golden step }
 1:   IF (X>=XM) THEN E:=A-X ELSE E:=B-X;
      D:=CGOLD*E;
 2:   IF (ABS(D)>=TOL1) THEN U:=X+D ELSE U:=X+SIGN(TOL1,D);
      FU:=HAMIL(U);
      IF (FU<=FX) THEN BEGIN  { switch around points, disp of old }
         IF (U>=X) THEN A:=X ELSE B:=X;
         V:=W;
         FV:=FW;
         W:=X;
         FW:=FX;
         X:=U;
         FX:=FU;
         END
      ELSE BEGIN
         IF (U<X) THEN A:=U ELSE B:=U;
         IF ((FU<=FW) OR (W=X)) THEN BEGIN
            V:=W;
            FV:=FW;
            W:=U;
            FW:=FU;
            END
         ELSE IF ((FU<=FV) OR (V=X) OR (V=2)) THEN BEGIN
            V:=U;
            FV:=FU;
            END
            END
            END;
      WRITELN('PAUSE IN ROUTINE BRENT - TOO MANY
ITERATIONS');
3:    XMIN:=X;
      BRENT:=FX;
END; { BRENT }
```

```
{----------------------------------------------------------------------}

BEGIN { MAIN PROGRAM - EXCITON }

  { assign structure parameters }

  WRITELN(’INPUT THE ALUMINUM FRACTION IN THE BARRIERS’);
  READLN(XAL);
  WRITELN(’INPUT THE WELL WIDTH IN METRES’);
  READLN(LZ);
  WRITELN(’INPUT THE FRACTION OF THE BAND DISCONTINUITY
WHICH ’);
  WRITELN(’APPEARS IN THE CONDUCTION BAND ’);
  READLN(BDC);

  { open output file }
  ASSIGN(OUTFILE,’C:EXCITON.DAT’);
  REWRITE(OUTFILE);

  { output structure data }
  WRITELN(OUTFILE,’THE AlGaAs BARRIERS CONTAIN ’,XAL*100:4:1,
   ’ PERCENT       ALUMINUM’);
  WRITELN(OUTFILE,’THE GaAs WELL IS ’,LZ*1E10:5:1,’ ANGSTROMS
WIDE’);
  WRITELN(OUTFILE,’THE CONDUCTION BAND HAS ’,BDC*100:4:1,
  ’ PERCENT OF THE BAND DISC.’);

  { calculate permittivities }
  KW:=13.18;            {WELL}
  KB:=(13.18-3.12*XAL);  {BARRIER}
  K:=SQRT(KW*KB)*EPS0;  {RADIAL - COULOMB}

  DELTAE := 1.247 * XAl * ECHARGE;    { ENERGY BAND
DISCONTINUITY }
  DELEEL := BDC * DELTAE;  { CONDUCTION BAND DISCONTINUITY
}
  DELEHOL := (1-BDC) * DELTAE; { VALENCE BAND DISCONTINUITY
}
  MBELEC := 0.0665 + 0.0835*XAL; { ELECTRON EFFECTIVE MASS -
BARRIER }
```

```
 MWELEC := 0.0665; { ELECTRON EFFECTIVE MASS - WELL }
 MBHOLE := 0.34 + 0.42 * XAL;  { HOLE EFFECTIVE MASS - BARRIER
}
 MWHOLE := 0.34  { HOLE EFFECTIVE MASS - WELL };

 { effective mass parameters for bind. energy }
 ME:= MWELEC*M0;
 MH := MWHOLE*M0;
{ MU := 1/(1/ME+1/(4*MH)+3/(4*0.087*M0));}
 MU := 1/(1/ME+1/(0.087*M0));  { EXCITON REDUCED MASS }

 { Calculate the unperturbed energy values for the square well.}
 {   The C's denote the conduction band and the V's the valence band}
 {   The 1's denote inside the welland the 2's outside}
 {   The K's are the wave numbers and the A's the norm. constants.}
 { They are arrays which go from 0 to NUMC(V)-1}
 WAVEFUNCTION(K1C,K2C,A1C,A2C,EC,K1V,K2V,A1V,A2V,EV,NUMC,NU
MV);


 { output results }
 SP:='          ';
 WRITELN(OUTFILE,'THERE ARE ',NUMC,' CONDUCTION BAND
STATES');
 WRITELN(OUTFILE);
 WRITELN(OUTFILE,'     K1',SP,'K2',SP,'A1',SP,'A2',SP,'E(eV)');
 WRITELN(OUTFILE);
 FOR I:=0 TO NUMC-1 DO
 BEGIN
  WRITELN(OUTFILE,K1C[I]:11,'  ',K2C[I]:11,'  ',A1C[I]:11,'  ',A2C[I]:11,
          '  ',EC[I]/1.602E-19:14);
 END;

 WRITELN(OUTFILE);

 WRITELN(OUTFILE,'THERE ARE ',NUMV,' VALENCE BAND STATES');
 WRITELN(OUTFILE);
 WRITELN(OUTFILE,'     K1',SP,'K2',SP,'A1',SP,'A2',SP,'E(eV)');
 WRITELN(OUTFILE);
 FOR I:=0 TO NUMV-1 DO
 BEGIN
  WRITELN(OUTFILE,K1V[I]:11,'  ',K2V[I]:11,'  ',A1V[I]:11,'  ',A2V[I]:11,
```

```
          ' ',-EV[I]/1.602E-19:14);
  END;
  WRITELN(OUTFILE);



  { now we apply the field }
  { the perturbed values are calculated for five applied fields and 0 }

  STEP := 1.2E7;  { FIELD INCREMENT in kV/m }

  { SET FUNCTION FOR QROMB TO INTEGRATE }
  FUNC3:=EXPECTVAL;

  FOR FIELD:=1 TO 10 DO  { do 10 field values }
  BEGIN
   EFIELD := STEP * ECHARGE * FIELD;

   { calculate the overlap integrals necessary for the eigenvalue problem}
   { VARRAYC(V) is square from 1 to NUMC(V) and is the matrix containing}
   { the overlap integrals of the field perturbation. }

GAMMA(NUMC,NUMV,K1C,K2C,K1V,K2V,A1C,A2C,A1V,A2V,VARRAYC,V
ARRAYV);

   { Add in the energies to get the full eigenvalue matrix.}
   FOR I:=1 TO NUMC DO
   BEGIN
    VARRAYC[I,I]:=VARRAYC[I,I]+EC[I-1];
   END;

   FOR I:=1 TO NUMV DO
   BEGIN
    VARRAYV[I,I]:=VARRAYV[I,I]+EV[I-1];
   END;

   { calculate eigenvalues and eigenvectors and sort the eigenvectors }
   { and eigenvalues to allow the ground states to be picked out. }

   { the relevant mixing coefficients will appear in column 1 of VC(V) }
   { and the energy will appear in element 1 of the DC(V) array.}
   JACOBI(VARRAYC,NUMC,DC,VC,NROTC);
```

```
  EIGSRT(DC,VC,NUMC);
  JACOBI(VARRAYV,NUMV,DV,VV,NROTV);
  EIGSRT(DV,VV,NUMV);

  { output mixing coefficients and energy values }
  WRITELN(OUTFILE);
  WRITELN(OUTFILE,’ WITH A FIELD OF ’,EFIELD/1.602E-19:11,
             ’ IN THE CONDUCTION BAND’);
  WRITELN(OUTFILE,’ THE ENERGY LOWEST ENERGY VALUE IS
’,DC[1]/1.602E-19:11);
  WRITELN(OUTFILE,’ THIS IS A DIFFERENCE OF
’,(DC[1]-EC[0])/1.602E-19:11);
  WRITELN(OUTFILE);
  WRITELN(OUTFILE,’ THE MIXING COEFFICIENTS ARE ’);

  FOR I:=1 TO NUMC DO
  BEGIN
   WRITELN(OUTFILE,’A’,I-1,’        ’,VC[I,1]:12);
  END;

  WRITELN(OUTFILE);
  WRITELN(OUTFILE,’ WITH A FIELD OF ’,EFIELD/1.602E-19:11,
             ’ IN THE VALENCE BAND’);
  WRITELN(OUTFILE,’ THE ENERGY LOWEST ENERGY VALUE
IS’,-DV[1]/1.602E-19:11);
  WRITELN(OUTFILE,’ THIS IS A DIFFERENCE OF
’,(-DV[1]+EV[0])/1.602E-19:11);
  WRITELN(OUTFILE);
  WRITELN(OUTFILE,’ THE MIXING COEFFICIENTS ARE ’);

  FOR I:=1 TO NUMV DO
  BEGIN
   WRITELN(OUTFILE,’A’,I-1,’        ’,VV[I,1]:12);
  END;

  {now store the coefficients in an array}
  { which has all the mixing coef. For all the fields}
  { array of 1..NUMC(V) 0..5}

  FOR I:=0 TO NUMC-1 DO
  BEGIN
   VVC[I,FIELD]:=VC[I+1,1];
```

```
    END;

    FOR I:=0 TO NUMV-1 DO
    BEGIN
      VVV[I,FIELD]:=VV[I+1,1];
    END;

  END; { FIELD LOOP }

  {assign values for the array for 0 field}

  FOR I:=1 TO NUMC-1 DO
  BEGIN
    VVC[I,0]:=0.0;
  END;
  VVC[0,0]:=1.0;

  FOR I:=1 TO NUMV-1 DO
  BEGIN
    VVV[I,0]:=0.0;
  END;
  VVV[0,0]:=1.0;

  WRITELN(OUTFILE);
  WRITELN(OUTFILE);
  WRITELN(OUTFILE,' FIELD (V/M)      BINDING ENERGY (meV)');
  WRITELN(OUTFILE);
  { set field loop to calculate the binding energy wrt field }
  FOR FIELD := 1 TO 10 DO
  BEGIN  { FIELD LOOP }
    EFIELD := STEP*FIELD;
    AX:=1.E-8;
    BX:=1.2E-8;
    MNBRAK(AX,BX,CX,FA,FB,FC);
    ANS:=BRENT(AX,BX,CX,1.E-4,XMIN);
    WRITELN(OUTFILE,EFIELD:11,'        ',ANS/ECHARGE:8:3);
    END; { FIELD LOOP }

  CLOSE(OUTFILE);

END. {MAIN PROGRAM - EXCITON}
```

APPENDIX C

SAMPLE OUTPUT FROM PROGRAM EXCITON

C.1 Sample Output

```
THE AlGaAs BARRIERS CONTAIN  3.00000000000000E+0001 PERCENT ALUMINUM
THE GaAs WELL IS  1.00000000000000E+0002 ANGSTROMS WIDE
THE CONDUCTION BAND HAS  6.00000000000000E+0001 PERCENT OF THE BAND DISC.
MU= 3.43323254071661E-0032
THERE ARE 2 CONDUCTION BAND STATES

    K1          K2          A1          A2          E(eV)

 2.28E+0008  6.84E+0008  1.20E+0004  1.53E+0005  2.98244E-0002
 4.51E+0008  5.08E+0008  1.17E+0004  1.15E+0005  1.16806E-0001

THERE ARE 4 VALENCE BAND STATES

    K1          K2          A1          A2          E(eV)

 2.61E+0008  1.32E+0009  1.29E+0004  2.45E+0006 -7.64693E-0003
 5.21E+0008  1.21E+0009  1.28E+0004  2.73E+0006 -3.04910E-0002
 7.79E+0008  9.99E+0008  1.27E+0004 -1.37E+0006 -6.80235E-0002
 1.03E+0009  6.22E+0008  1.22E+0004 -2.50E+0005 -1.18016E-0001


 WITH A FIELD OF  2.00000E+0006 IN THE CONDUCTION BAND
 THE ENERGY LOWEST ENERGY VALUE IS  2.95311E-0002
 THIS IS A DIFFERENCE OF -2.93300E-0004

 THE MIXING COEFFICIENTS ARE
A0        9.98324E-0001
A1       -5.78738E-0002

 WITH A FIELD OF  2.00000E+0006 IN THE VALENCE BAND
 THE ENERGY LOWEST ENERGY VALUE IS -6.83299E-0003
 THIS IS A DIFFERENCE OF  8.13942E-0004
```

```
 THE MIXING COEFFICIENTS ARE
A0       9.82881E-0001
A1       1.83625E-0001
A2      -1.45559E-0002
A3      -3.75572E-0003

 WITH A FIELD OF  4.00000E+0006 IN THE CONDUCTION BAND
 THE ENERGY LOWEST ENERGY VALUE IS  2.86628E-0002
 THIS IS A DIFFERENCE OF -1.16164E-0003

 THE MIXING COEFFICIENTS ARE
A0       9.93475E-0001
A1      -1.14051E-0001

 WITH A FIELD OF  4.00000E+0006 IN THE VALENCE BAND
 THE ENERGY LOWEST ENERGY VALUE IS -4.54745E-0003
 THIS IS A DIFFERENCE OF  3.09948E-0003

 THE MIXING COEFFICIENTS ARE
A0       9.40949E-0001
A1       3.34421E-0001
A2      -5.16673E-0002
A3      -1.03753E-0002

 WITH A FIELD OF  6.00000E+0006 IN THE CONDUCTION BAND
 THE ENERGY LOWEST ENERGY VALUE IS  2.72519E-0002
 THIS IS A DIFFERENCE OF -2.57252E-0003

 THE MIXING COEFFICIENTS ARE
A0       9.85939E-0001
A1      -1.67104E-0001

 WITH A FIELD OF  6.00000E+0006 IN THE VALENCE BAND
 THE ENERGY LOWEST ENERGY VALUE IS -1.12065E-0003
 THIS IS A DIFFERENCE OF  6.52628E-0003

 THE MIXING COEFFICIENTS ARE
A0       8.90444E-0001
A1       4.43681E-0001
A2      -9.91224E-0002
A3      -2.07484E-0002
```

```
 WITH A FIELD OF  8.00000E+0006 IN THE CONDUCTION BAND
 THE ENERGY LOWEST ENERGY VALUE IS  2.53463E-0002
 THIS IS A DIFFERENCE OF -4.47808E-0003

 THE MIXING COEFFICIENTS ARE
A0        9.76383E-0001
A1       -2.16048E-0001

 WITH A FIELD OF  8.00000E+0006 IN THE VALENCE BAND
 THE ENERGY LOWEST ENERGY VALUE IS  3.14031E-0003
 THIS IS A DIFFERENCE OF  1.07872E-0002

 THE MIXING COEFFICIENTS ARE
A0        8.41254E-0001
A1        5.18834E-0001
A2       -1.48096E-0001
A3       -3.42156E-0002

 WITH A FIELD OF  1.00000E+0007 IN THE CONDUCTION BAND
 THE ENERGY LOWEST ENERGY VALUE IS  2.30022E-0002
 THIS IS A DIFFERENCE OF -6.82216E-0003

 THE MIXING COEFFICIENTS ARE
A0        9.65507E-0001
A1       -2.60378E-0001

 WITH A FIELD OF  1.00000E+0007 IN THE VALENCE BAND
 THE ENERGY LOWEST ENERGY VALUE IS  8.01441E-0003
 THIS IS A DIFFERENCE OF  1.56613E-0002

 THE MIXING COEFFICIENTS ARE
A0        7.96896E-0001
A1        5.69866E-0001
A2       -1.94274E-0001
A3       -4.96686E-0002

 WITH A FIELD OF  1.20000E+0007 IN THE CONDUCTION BAND
 THE ENERGY LOWEST ENERGY VALUE IS  2.02778E-0002
 THIS IS A DIFFERENCE OF -9.54663E-0003

 THE MIXING COEFFICIENTS ARE
A0        9.53940E-0001
```

```
A1      -2.99998E-0001

 WITH A FIELD OF  1.20000E+0007 IN THE VALENCE BAND
 THE ENERGY LOWEST ENERGY VALUE IS  1.33521E-0002
 THIS IS A DIFFERENCE OF  2.09990E-0002

 THE MIXING COEFFICIENTS ARE
A0       7.57930E-0001
A1       6.04531E-0001
A2      -2.36039E-0001
A3      -6.61050E-0002

 WITH A FIELD OF  1.40000E+0007 IN THE CONDUCTION BAND
 THE ENERGY LOWEST ENERGY VALUE IS  1.72283E-0002
 THIS IS A DIFFERENCE OF -1.25961E-0002

 THE MIXING COEFFICIENTS ARE
A0       9.42183E-0001
A1      -3.35098E-0001

 WITH A FIELD OF  1.40000E+0007 IN THE VALENCE BAND
 THE ENERGY LOWEST ENERGY VALUE IS  1.90505E-0002
 THIS IS A DIFFERENCE OF  2.66974E-0002

 THE MIXING COEFFICIENTS ARE
A0       7.23929E-0001
A1       6.28103E-0001
A2      -2.73062E-0001
A3      -8.27717E-0002

 WITH A FIELD OF  1.60000E+0007 IN THE CONDUCTION BAND
 THE ENERGY LOWEST ENERGY VALUE IS  1.39039E-0002
 THIS IS A DIFFERENCE OF -1.59205E-0002

 THE MIXING COEFFICIENTS ARE
A0       9.30599E-0001
A1      -3.66040E-0001

 WITH A FIELD OF  1.60000E+0007 IN THE VALENCE BAND
 THE ENERGY LOWEST ENERGY VALUE IS  2.50364E-0002
 THIS IS A DIFFERENCE OF  3.26833E-0002
```

```
 THE MIXING COEFFICIENTS ARE
A0        6.94234E-0001
A1        6.44078E-0001
A2       -3.05568E-0001
A3       -9.91550E-0002

 WITH A FIELD OF  1.80000E+0007 IN THE CONDUCTION BAND
 THE ENERGY LOWEST ENERGY VALUE IS  1.03480E-0002
 THIS IS A DIFFERENCE OF -1.94764E-0002

 THE MIXING COEFFICIENTS ARE
A0        9.19427E-0001
A1       -3.93262E-0001

 WITH A FIELD OF  1.80000E+0007 IN THE VALENCE BAND
 THE ENERGY LOWEST ENERGY VALUE IS  3.12555E-0002
 THIS IS A DIFFERENCE OF  3.89024E-0002

 THE MIXING COEFFICIENTS ARE
A0        6.68207E-0001
A1        6.54781E-0001
A2       -3.33995E-0001
A3       -1.14931E-0001

 WITH A FIELD OF  2.00000E+0007 IN THE CONDUCTION BAND
 THE ENERGY LOWEST ENERGY VALUE IS  6.59769E-0003
 THIS IS A DIFFERENCE OF -2.32267E-0002

 THE MIXING COEFFICIENTS ARE
A0        9.08809E-0001
A1       -4.17213E-0001

 WITH A FIELD OF  2.00000E+0007 IN THE VALENCE BAND
 THE ENERGY LOWEST ENERGY VALUE IS  3.76665E-0002
 THIS IS A DIFFERENCE OF  4.53134E-0002

 THE MIXING COEFFICIENTS ARE
A0        6.45291E-0001
A1        6.61783E-0001
A2       -3.58837E-0001
A3       -1.29914E-0001
```

FIELD (V/M)	BINDING ENERGY (eV)
0.00000000000000E+0000	-7.32118707503040E-0003
2.00000000000000E+0006	-7.22247011585211E-0003
4.00000000000000E+0006	-6.97910745502927E-0003
6.00000000000000E+0006	-6.69030097860335E-0003
8.00000000000000E+0006	-6.41651075999507E-0003
1.00000000000000E+0007	-6.17766378459452E-0003
1.20000000000000E+0007	-5.97647711179242E-0003
1.40000000000000E+0007	-5.80910312002930E-0003
1.60000000000000E+0007	-5.67094494300163E-0003
1.80000000000000E+0007	-5.55678957459123E-0003
2.00000000000000E+0007	-5.44481281140715E-0003

REFERENCES

1. R.G. Hunsperger, *Integrated Optics: Theory and Technology* (Springer-Verlag, New York, 1985), Chapter 1.

2. R.A. Bergh, H.C. Lefevre, and H.J. Shaw, "An Overview of Fiber-Optic Gyroscopes," J. of Light. Tech. **LT-2**, 91 (1984).

3. R.G. Walker, "High-Speed Electrooptic Modulation in GaAs/GaAlAs Waveguide Devices," J. of Light. Tech. **LT-5**, 1444 (1987).

4. L. Friedman, R.A. Soref, and J.P. Lorenzo, "Silicon double-injection electro-optic modulator with junction gate control," J. Appl. Phys. **63**, 1831 (1988).

5. D.A. Holm and H.F. Taylor, "Infrared Phase Modulators with Multiple Quantum Wells," IEEE J. of Quan. Elec. **25**, 2266 (1989).

6. R.G. Hunsperger, *Integrated Optics: Theory and Technology* (Springer-Verlag, New York 1985), p61.

7. T. Tamir, *Integrated Optics* (Springer-Verlag, New York 1979), p244.

8. J.H. Weaver, C. Krafka, D.W. Lynch and E.E. Koch, *Physik Daten: Optical Properties of Metals* (Fachinformationszentrum Energie, Physik, Mathematik GMBH, Karlsruhe, 1981).

9. M. J. Adams, *An Introduction to Optical Waveguides* (John Wiley and Sons, Toronto, 1981), p188.

10. R.M. Knox and P.P. Toulios, "Integrated circuits for the millimetre through optical frequency range," in *Proceedings of the MRI*

Symposium on Submillimetre Waves (Polytechnic Press, Brooklyn, 1970), p497.

11. E.A.J. Marcatili, "Slab-Coupled Waveguides," The Bell System Technical Journal **53**, 645 (1974).

12. M.J. Adams, *An Introduction to Optical Waveguides* (John Wiley and Sons, Toronto 1981) p61.

13. E.M. Garmire, and H. Stoll, "Propagation losses in metal-film-substrate optical waveguides," IEEE J. Quant. Elec. **QE-8**, 763 (1972).

14. I.P. Kaminow, W.L. Mammel, and H.P. Weber, "Metal-clad optical waveguides: analytical and experimental study," Appl. Opt. **13**, 396 (1974).

15. M.J. Adams, *An Introduction to Optical Waveguides* (Wiley, Toronto, 1981).

16. D. Hall, A. Yariv, and E. Garmire, Optical Guiding and Electro-optic Modulation In GaAs Epitaxial Layers, Optics Communications **1**, April 1970, p403.

17. S. Adachi and K. Oe, "Chemical Etching Characteristics of (001) GaAs," J. Electrochem. Soc. **130**, 2427 (1983).

18. T.M. Benson, "Strain-induced effects in GaAs directional coupler switches," J. Appl. Phys. **54**, 6221 (1983).

19. D.N. MacFadyen, "On the Preferential Etching of GaAs by H_2SO_4-H_2O_2-H_2O," J. Electrochem. Soc. **130**, 1934 (1983).

20. T.E. Walsh, "Gallium arsenide electrooptic modulators," RCA Review **27**, 323 (1966).

21. L. Esaki and R. Tsu, "Superlattices and negative conductivity in semiconductors," IBM Research Note **RC-2418** (1969).

22. D.A. Wharam, T.J. Thornton, R. Newbury, M. Pepper, H. Ahmed, J.E.F. Frost, D.G. Hasko, D.C. Peacock, D.A. Ritchie, and G.A.C. Jones, "One-dimensional transport and the quantization of the ballistic resistance," J. Phys. C: Solid State Physics **21**, L209-1214 (1988).

23. H. Kroemer, "Theory of the Gunn effect," Proc. IEEE **52**, 1736 (1964).

24. L. Esaki, "New phenomenon in narrow germanium p-n junction," Physical Review **109**, 603 (1959).

25. B. Ricco and M. Azbel, "Physics of resonant tunnelling. The one dimensional double barrier case," Physical Review B **29**, 1970 (1984).

26. E.R. Brown, W.D. Goodhue, and T.C.L.G. Sollner, "Fundamental oscillations up to 200 GHz in resonant tunnelling diodes and new estimates of their maximum oscillation frequency from stationary state tunnelling theory," J. Appl. Phys. **64**, 1519 (1988).

27. R.S. Knox, "Theory of Excitons," *Solid State Physics*, ed. F. Seitz and D. Turnbull, Academic Press (1963).

28. S. Adachi, "GaAs, AlAs, and $Al_xGa_{1-x}As$: Material parameters for use in research and device applications," J. of Appl. Phys. **58**, R1 (1985).

29. D.A.B. Miller, D.S. Chemla, D.J. Eilenberger, P.W. Smith, A.C. Gossard, W.T. Tsang, "Large room temperature optical nonlinearity in $GaAs/Ga_{1-x}Al_xAs$ multiple quantum well structures," Appl. Phys

Lett. **41**, 679 (1982).

30. D.A.B. Miller, D.S. Chemla, T.C. Damen, A.C. Gossard, W. Wiegmann, T.H. Wood, and C.A. Burrus, "Electric field dependence of optical absorption near the bandgap of quantum-well structures," Phys. Rev. B. **32**, 1043 (1985).

31. T.H. Wood, C.A. Burrus, D.A.B. Miller, D.S. Chemla, T.C. Damen, A.C. Gossard, and W. Wiegmann, "High-speed optical modulation with GaAs/GaAlAs quantum wells in a p-i-n diode structure," Appl. Phys. Lett. **44**, 16 (1984).

32. A. Larsson, P.A. Andrekson, S.T. Eng and A. Yariv, "Tunable Superlattice p-i-n Photodetectors: Characteristics, Theory, and Applications," IEEE J. of Quant. Elect. **24**, 787 (1988).

33. D.A. Holm and H.F. Taylor, "Infrared Phase Modulators with Multiple Quantum Wells," IEEE J. of Quan. Elec. **25**, 2266 (1989).

34. G. Lengyel, K.W. Jelley and R.W.H. Engelmann, "A Semi-Empirical Model for Electroabsorption in GaAs/AlGaAs Multiple Quantum Well Modulator Structures," J. of Quan. Elec. **26**, 296 (1990).

35. R. Eisberg and R. Resnick, *Quantum Physics of Atoms, Molecules, Solids, Nuclei, and Particles* (John Wiley and Sons, Toronto 1985).

36. W. Stolz, J.C. Maan, M. Altarelli, L.Tapfer, and K. Ploog, "Absorption spectroscopy on $Ga_{0.47}In_{0.53}As/Al_{0.48}In_{0.52}As$ multi-quantum-well heterostructures. II. Subband structure," Phys. Rev. B **36**, 4310 (1987).

37. S.M. Sze, *Physics of Semiconductor Devices* (John Wiley and Sons, Toronto 1981).

38. J.I. Pankove, *Optical Processes in Semiconductors* (Dover, New York 1975), p29.

39. H. Fouckhardt, K.J. Ebeling, "Strong optical non-linearities for efficient all optical switching in GaAlAs waveguides," Optics and Laser Technology, 203 (Aug 1986).

40. J.C. Dyment, F.P. Kapron and A.J. SpringThorpe, "Devices based on electroabsorption effects in reverse bias GaAs-GaAlAs double heterostructures," Inst. Phys. Conf. Ser. **24**, 200 (1975).

41. D.A.B. Miller, D.S. Chemla, T.C. Damen, A.C. Gossard, W. Wiegmann, T.H. Wood, and C.A. Burrus, "Band-edge electroabsorption in quantum well structures: the quantum-confined Stark effect," Phys. Rev. Lett. **53**, 2173 (1984).

42. I.J. Fritz, "Energy levels of finite depth quantum wells in an electric field," J. Appl. Phys. **60**, 916 (1987).

43. H. Yamamoto, M. Asuda, and Y. Suematsu, "Theory of refractive index variation in QW structures and related intersectional optical switch," J. Lightwave Tech. **6**, 1831 (1988).

44. N.E.J. Hunt, Private communication: to appear in PhD thesis, Dept. of Engineering Physics, McMaster University.

45. W.H. Press, B.P. Flannery, S.A. Teukolsky, and W.T. Vetterling, *Numerical Recipes: The Art of Scientific Computing*, (Cambridge University Press, New York 1986).